The (Mis)Allocation Channel of Climate Change

Evidence from Global Firm-level Microdata *

Tianzi Liu †
Cornell University

Zebang Xu ‡
Cornell University

Job Market Paper, 2026-2027

December 2025, Updated Regularly

Abstract

Macroeconomic estimates of climate damages are large, yet firm-level micro estimates often appear modest. We reconcile this gap by uncovering a powerful channel—*the impact of extreme temperatures on capital misallocation*—as the major driver of aggregate climate damage. Using global firm-level microdata from 32 countries, we provide causal evidence that a day of extreme heat ($>$ 30°C) increases the dispersion of returns to capital across firms by 0.31 log points, implying a 0.11% annual aggregate TFP loss for the average region–sector. The effect is more pronounced in hotter and more economically developed regions. To explain these mechanisms, we develop a tractable general-equilibrium model of firm dynamics with heterogeneous temperature sensitivities, endogenous adaptation, and time-to-build capital. The model shows that higher climate volatility increases regional dispersion in returns to capital, with amplification driven by heterogeneity in firms' temperature exposure, adaptation, and capital wedges. When estimated by the microdata, climate-induced misallocation lowers global TFP by 12% and accounts for 9% of cross-country productivity differences. Our results shift the focus of climate damage from direct physical productivity losses to *allocative efficiency losses in the cross-section*, highlighting firm heterogeneity as central for measuring aggregate damages and designing effective mitigation and adaptation policy.

*We thank Ryan Chahrour, Kristoffer Nimark, Ivan Rudik, Ezra Oberfield and Mathieu Taschereau-Dumouchel for their continued guidance and support. This paper has also benefited from discussions with Doug Almond, Levon Barseghyan, Johannes Boehm, Tamma Carleton, Julieta Caunedo, Luming Chen, Tomás Domínguez-Iino, Caroline Flammer, Todd Gerarden, Cathy Kling, Kyle Meng, Pablo Ottonello, Will Rafey, Diego Restuccia, Jeffrey Shrader, and seminar participants at Columbia Climate School, Cornell Macro Lunch and Cornell SEERE Seminar, the 2024 Econometric Society NASM, CU Environmental & Resource Economics Workshop, the 2025 NBER Climate Finance PhD Workshop and ASSA 2026. We thank the Structural Transformation and Economic Growth (STEG) Research programme for supporting this research. First draft was circulated on February 16th, 2024.

†Department of Applied Economics and Management, Cornell University (email:tl567@cornell.edu).

‡Department of Economics, Cornell University (email:zx88@cornell.edu).

1 Introduction

Macroeconomic estimates of climate damages are large. By 2100, projected losses range from roughly 23 percent of global GDP in Burke, Hsiang, and Miguel (2015) to about 50 percent in Bilal and Känzig (2024). These costs are typically summarized as declines in aggregate productivity, often modeled as losses in aggregate TFP since the early climate-macro literature (Nordhaus 1992). Yet direct estimates of firm- and plant-level productivity damage from temperature are much smaller. Addoum, Ng, and Ortiz-Bobea (2020) and Ponticelli, Xu, and Zeume (2023) estimate losses below 2 percent in U.S. plants, while the more recent global manufacturing evidence in Nath (2025) suggests average losses on the order of 1–2 percent once adaptation is taken into account. This gap raises a basic question: if average within-firm productivity damage is modest, what microeconomic channel generates large aggregate productivity losses?

This paper identifies and quantifies one important answer: climate-induced *across-firm* capital misallocation. Temperature shocks need not mainly operate by shifting down the average firm's production frontier. They can also lower aggregate TFP by widening dispersion in firms' marginal revenue products of capital (MRPK), even within narrowly defined region–sector cells. The intuition is simple. Suppose one firm benefits from heat while another is harmed by it, either because their products differ in temperature sensitivity (for example, an ice cream parlor versus a ski resort) or because they differ in their endogenous adaptation choices. When an unexpected heat shock arrives, both firms enter the period with predetermined capital that takes time to build and cannot adjust on impact. The heat-favored firm becomes capital-scarce and its MRPK rises, while the heat-exposed firm becomes capital-abundant and its MRPK falls. Aggregate output is then lower than it would be if capital could be reallocated immediately toward the firm with the higher realized return. Climate damage, in this view, is partly allocative.

We begin by developing a climate–TFP accounting framework that decomposes region–sector-level aggregate TFP into an efficient frontier component (i.e., technology) and a loss component due to capital misallocation (i.e., allocative inefficiency). We then show formally that climate-induced changes in within-cell MRPK dispersion provide a sufficient statistic for the misallocation channel. Guided by this framework, we estimate the causal effect of temperature shocks on capital misallocation using firm-level data from 30 European countries, China, and India, matched to ERA5-Land daily weather data. Identification comes from year-to-year changes in local temperature distributions within region–sector cells, relative to other cells within the same country-year.

Our reduced-form estimates show a clear U-shaped relationship between temperature and capital misallocation: both extreme heat and extreme cold raise MRPK dispersion. Quantitatively, an additional day above $30°$C relative to a day in the $5°$C–$10°$C range increases MRPK dispersion by about 0.31 log points, implying a 0.11 percent decline in annual aggregate TFP. By contrast, the direct technology effect is much smaller: for heat shocks, the implied reduction in physical productivity is only about one-fifth as large as the loss operating through misallocation. The main empirical message is therefore not simply that temperature lowers average productivity, but that it also makes the cross-sectional allocation of capital less efficient. This distinction also helps clarify the paper's relationship to the existing literature: previous *micro* estimates typically isolate, at best, the technology channel and miss the misallocation channel entirely, while previous

macro estimates measure the sum of the two.

A second empirical result is that the misallocation effect of heat is substantially larger in hotter and more economically developed regions. This pattern is important for interpreting climate damages over the long run. It implies that the allocative consequences of warming do not automatically fade with development, and it suggests that market-based adaptation may protect the average firm without eliminating cross-firm differences in exposure and adjustment. These heterogeneous effects also help bridge the micro–macro disconnect in the climate damages literature: once the misallocation channel is incorporated, our micro-based estimates line up closely with corresponding macro estimates across countries, whereas without misallocation the micro estimates are essentially flat.

Using our causal estimates to project the effect of global warming on misallocation-induced TFP losses by the end of the century, we find that the same heterogeneity leads to large increases in losses as more regions become both hotter and richer over time. Under a moderate warming scenario, our estimates imply that, relative to current income and climate conditions, the global cost of climate-induced misallocation will amount to 36.73% of aggregate TFP by the end of the century.

To explain these facts, we build a tractable firm-dynamics model with heterogeneous firms, time-to-build capital, pre-existing capital wedges, and costly endogenous adaptation. Firms differ persistently in productivity, product exposure to climate, and capital wedges, and they choose capital and adaptation under risk before temperature is realized. We model adaptation in reduced form as a quasi-fixed cost that lowers the loading of TFP on climate, implying that adaptation is complementary to scale: firms with a larger expected profit base or a lower risk premium adapt more and invest more capital. Because firms differ in exposure, the same temperature surprise generates heterogeneous realized productivities and returns to capital.

The model highlights two mechanisms. A *level* effect implies that climates farther from the bliss point magnify idiosyncratic climate damages (e.g. a sudden blizzard or fire on the plant) and hence the scope for misallocation. A *forecast-and-risk* effect implies that forecast errors and forecast uncertainty translate into cross-firm dispersion in realized returns because firms differ in effective exposure to temperature. As a result, hotter and richer economies may adapt more on average, yet still exhibit greater dispersion in adaptation across firms, which widens the distribution of effective exposure and makes the misallocation channel stronger.

The data support these mechanisms. Using Indian plant-level air-conditioning adoption as a proxy for adaptation, we show that larger firms and firms with higher lagged MRPK adapt more. We also show that heat shocks shift MRPK differentially across firms depending on size and distortions, that TFP volatility is U-shaped in long-run temperature, and that larger forecast errors and forecast uncertainty are associated with greater MRPK dispersion. These patterns line up with the model's central implication that common temperature realizations generate dispersed returns because firms differ in exposure, adaptation, and adjustment capacity.

We then estimate the model on micro data from the EU, China, and India and use it to quantify the aggregate importance of the channel. The estimated model implies that climate-induced misallocation lowers global TFP by about 12.5 percent in an average year over 1981–2019, and that this channel accounts for about 9 percent of cross-country TFP differences. Most of this global cost

comes from persistent climate differences rather than from short-run forecast errors. The broader implication is that measuring climate damages through average firm-level productivity losses alone misses an important aggregate margin. Climate policy and adaptation policy affect allocative efficiency not only by protecting the representative firm, but also by shaping the dispersion of firms' exposure and adjustment across the cross section.

Contributions to the Literature. This paper contributes to three literatures. First, it relates to the large literature estimating the economic effects of temperature shocks and climate change, both at the aggregate level (Dell, Jones, and Olken 2012; Burke, Hsiang, and Miguel 2015; Lemoine 2018; Carleton et al. 2022; Nath, Ramey, and Klenow 2023; Bilal and Känzig 2024) and at the firm or worker level (Zhang et al. 2018; Somanathan et al. 2021; Tarsia 2023; Ponticelli, Xu, and Zeume 2023). Most of this work interprets climate damages as reductions in physical productivity or output. We complement it by identifying a distinct *allocative* channel: climate shocks can lower aggregate productivity by widening dispersion in returns to capital across firms.

Second, the paper speaks to the climate-macro literature that embeds climate change in workhorse macro and trade models (Nath 2025; Cruz and Rossi-Hansberg 2023; Bakkensen and Barrage 2021; Casey, Fried, and Gibson 2022; Rudik et al. 2021). These models typically abstract from within-region distortions and therefore from climate-induced factor misallocation. We contribute a sufficient-statistics framework that measures this channel in the data and a tractable dynamic model with endogenous adaptation that rationalizes the reduced-form evidence. Closest to our paper is Caggese et al. (2023). Relative to that work, we provide direct causal evidence on within-region dispersion in marginal products using historical temperature variation and firm-level data from 32 countries.

Third, the paper contributes to the literature on misallocation (Restuccia and Rogerson 2008; Hsieh and Klenow 2009; Gopinath et al. 2017; David and Zeke 2021; Asker, Collard-Wexler, and De Loecker 2014; David and Venkateswaran 2019; Baqaee and Farhi 2019) and to the growing literature that uses quasi-experimental variation to identify its drivers (Sraer and Thesmar 2023; Bau and Matray 2023). We add environmental shocks—and climate change more broadly—to the set of forces that can generate economically meaningful capital misallocation.

The rest of the paper proceeds as follows. Section 2 develops the climate–TFP accounting framework. Sections 3 and 4 describe the data and present the reduced-form evidence. Sections 5, 6, and 7 develop, test, and estimate the dynamic model. Section 8 concludes.

2 A Framework for Climate TFP Accounting

This section develops a measurement framework that links firm-level climate exposure to region-sector aggregate TFP. We extend Hsieh and Klenow (2009)'s distorted closed-economy model of heterogeneous firms to allow climate to affect firm-specific productivity, demand, and wedges. In this framework, climate affects aggregate productivity through two conceptually distinct channels: changes in firm-level productivity, which we call *technology*, and changes in the dispersion of marginal products induced by wedges, which we call *misallocation*. Beyond the demand and production functional forms, we allow for *arbitrary* climate-impact heterogeneity. This allows the

empirical strategy to capture the total contribution of all mechanisms through which climate affects aggregate TFP without committing to a specific microfoundation for climate-related wedges. The goal of this section is therefore not to explain the origin of those wedges, but to derive the sufficient statistics that guide the empirical strategy in Section 4. Section 5 then turns to the question of *why* climate changes these objects.

2.1 Model preliminaries

Consider an economy with many regions r and sectors s. We study the aggregation of firm-level activity within a region-sector pair $n = (r, s)$. We allow the fundamentals of firm i in market n to be arbitrary (smooth) functions of current and past regional climate conditions, $\tilde{\mathbf{T}}_{rt}$, aggregate states, $\tilde{\mathbf{X}}_{nt}$, and idiosyncratic firm states, $\tilde{\mathbf{Z}}_{nit}$.[1] This general formulation accommodates a wide range of structural models within our accounting framework.

2.2 Environment

Region-sector output is a CES aggregate of differentiated firm varieties of measure J_n:[2]

$$Y_{nt} = \left(\int_0^{J_n} B_{nit}^{\frac{1}{\sigma_n}} Y_{nit}^{\frac{\sigma_n - 1}{\sigma_n}} \, di \right)^{\frac{\sigma_n}{\sigma_n - 1}}, \tag{1}$$

where $\sigma_n > 1$ is the elasticity of substitution across varieties. The implied inverse demand for firm i is $Y_{nit} = B_{nit} Y_{nt} \left(\frac{P_{nit}}{P_{nt}} \right)^{-\sigma_n}$, where $P_{nt} = \left(\int_0^{J_n} B_{nit} P_{nit}^{1-\sigma_n} \, di \right)^{\frac{1}{1-\sigma_n}}$ is the region-sector price index. The demand shifter $B_{nit} \equiv B_{ni}(\tilde{\mathbf{T}}_{rt}, \tilde{\mathbf{X}}_{nt}, \tilde{\mathbf{Z}}_{nit})$ is a firm-specific function of climate and economic conditions, capturing how certain goods or services may be less desirable in hotter climates.[3]

Each firm produces with a constant-returns-to-scale Cobb-Douglas technology,

$$Y_{nit} = A_{nit} K_{nit}^{\alpha_{Kn}} L_{nit}^{\alpha_{Ln}}, \tag{2}$$

where $\alpha_{Kn} + \alpha_{Ln} = 1$. Physical productivity is firm specific and given by $A_{nit} \equiv A_{ni}(\tilde{\mathbf{T}}_{rt}, \tilde{\mathbf{X}}_{nt}, \tilde{\mathbf{Z}}_{nit})$, allowing climate conditions to affect firms differently within and across region-sectors. This heterogeneity may reflect differences in production technologies and climate adaptation, such as rainfed versus irrigated farms in agriculture, or outdoor versus indoor air-conditioned workplaces in manufacturing and services.[4]

1. For concreteness, $\mathbf{T}_{rt}$ may include realizations of daily temperature, precipitation, and other extreme-weather events. The vectors $\mathbf{X}_{nt}$ and $\mathbf{Z}_{nit}$ may be interpreted as other aggregate and firm-specific productivity or demand shocks. Their joint data-generating process may be stochastic. Throughout, a tilde denotes the history of realizations up to date t. We do not impose any restriction on whether $\mathbf{X}_{nt}$ and $\mathbf{Z}_{nit}$ depend on $\mathbf{T}_{rt}$.

2. In theory, J_n, the local variety, could also vary over time to capture how climate might affect firm entry and exit. However, accurately measuring these dynamics within a granular region-sector pair over time is challenging due to data limitations, particularly for cross-country analysis. Therefore, the model does not address this aspect.

3. This is particularly evident in service industries where climate can sharply affect consumer behavior. For example, Zivin and Neidell (2014) find that heat shocks shift Americans from outdoor to indoor recreational activities (e.g., away from recreational fishing as found by Dundas and Haefen 2020). Anecdotal examples in food services include ice-cream parlors versus hot tea shops.

4. In agriculture, rainfed farms are more exposed to heat stress than irrigated farms (Piao et al. 2010). In manufacturing, workers in plants with air conditioning are less vulnerable to heat than those in plants without it (Somanathan

Each firm faces a variety of frictions, including climate-related ones, which we represent as reduced-form, tax-like wedges. Firm i chooses its price and inputs to solve

$$\begin{aligned} \max_{P_{nit},K_{nit},L_{nit}} \quad & (1-\tau_{nit}^{Y})P_{nit}A_{nit}K_{nit}^{\alpha_{Kn}}L_{nit}^{\alpha_{Ln}} - (1+\tau_{nit}^{K})R_{nt}K_{nit} - (1+\tau_{nit}^{L})W_{nt}L_{nit} \\ \text{s.t.} \quad & Y_{nit} = B_{nit}Y_{nt}\left(\frac{P_{nit}}{P_{nt}}\right)^{-\sigma_n}. \end{aligned} \tag{3}$$

Here, R_{nt} is the user cost of capital and W_{nt} is the wage. The output wedge, $\tau_{nit}^{Y} \equiv \tau_{ni}^{Y}(\tilde{\mathbf{T}}_{rt}, \tilde{\mathbf{X}}_{nt}, \tilde{\mathbf{Z}}_{nit})$, captures firm-specific distortions to effective output prices, including revenue taxes and markups relative to the Dixit-Stiglitz benchmark. These distortions may vary with climate conditions, for example if temperature shocks affect local market structure (Ponticelli, Xu, and Zeume 2023). Similarly, the input wedges, $\tau_{nit}^{F} \equiv \tau_{ni}^{F}(\tilde{\mathbf{T}}_{rt}, \tilde{\mathbf{X}}_{nt}, \tilde{\mathbf{Z}}_{nit})$ for $F \in \{K, L\}$, capture distortions to effective input costs. These may reflect, for instance, tighter financing frictions for firms more exposed to adverse climate conditions (Ginglinger and Moreau 2023). For dynamic input choices with adjustment frictions, such as capital, they may also capture ex post investment mistakes generated by unanticipated temperature-related productivity shocks, in the spirit of Asker, Collard-Wexler, and De Loecker (2014) and David, Hopenhayn, and Venkateswaran (2016).

Within each period, total factor supplies are taken as given: $K_{nt} = \sum_i K_{nit}$ and $L_{nt} = \sum_i L_{nit}$. We call the allocation with wedges the *distorted equilibrium*, and the allocation that sets all wedges to zero while holding $\{A_{nit}, B_{nit}, K_{nt}, L_{nt}\}$ fixed the *efficient equilibrium*.[5]

Firm optimality implies that, for any input $F \in \{K, L\}$, its marginal revenue product (MRPF) satisfies:

$$\text{MRPF}_{nit} = \alpha_{Fn}\frac{\sigma_n - 1}{\sigma_n}\frac{P_{nit}Y_{nit}}{F_{nit}} = \frac{1+\tau_{nit}^{F}}{1-\tau_{nit}^{Y}}P_{nt}^{F}, \tag{4}$$

where $P_{nt}^{K} = R_{nt}$ and $P_{nt}^{L} = W_{nt}$. This is the key measurement result. In the efficient equilibrium, marginal revenue products are equalized within a region-sector. With wedges, cross-firm dispersion in marginal revenue products reveals input misallocation. A higher input wedge raises MRPF by discouraging input use, while a lower output wedge lowers MRPF by encouraging input use.

To focus on the main margin in the paper, the next lemma specializes to how capital wedges affect equilibrium (mis-)allocation. Let $\theta_{nit} \equiv \frac{P_{nit}Y_{nit}}{\int_0^{J_n} P_{njt}Y_{njt}\,dj}$ denote firm i's sales share, and let θ_{nit}^{*} denote its efficient-equilibrium counterpart.

Lemma 1 (Equilibrium (mis-)allocation of capital) *With capital distortions τ_{nit}^{K} only, the log ratio of firm i's distorted and efficient capital allocations satisfies*

$$\log\left(\frac{K_{nit}}{K_{nit}^{*}}\right) = \underbrace{-\log\left(\frac{1+\tau_{nit}^{K}}{1+\tau_{nt}^{K}}\right)}_{\textit{relative wedge effect}} + \underbrace{\log\left(\frac{\theta_{nit}}{\theta_{nit}^{*}}\right)}_{\textit{size effect}}, \tag{5}$$

et al. 2021). For evidence on cross-region heterogeneity in productivity damages due to adaptation, see Nath (2025).

5. Efficiency here is static and conditional on the period-t aggregate factor supplies.

where the efficient capital allocation is pinned down entirely by demand-adjusted productivity:

$$\frac{K^*_{nit}}{K_{nt}} = \theta^*_{nit} = \frac{B_{nit}A_{nit}^{\sigma_n-1}}{\int_0^{J_n} B_{njt}A_{njt}^{\sigma_n-1}\,dj}.$$

Proof. See Appendix A.2. ■

Lemma 1 shows that wedges distort capital allocation through two margins. The first is a *relative wedge effect*: firms facing a higher capital wedge than the region-sector average hold too little capital relative to the efficient benchmark. The second is a *size effect*: wedges can also make a firm inefficiently small, reducing its capital demand relative to its efficient counterfactual. By contrast, in the efficient equilibrium, capital is allocated entirely according to firms' relative demand-adjusted productivity. This benchmark is implicit in much of the empirical literature, but it is precisely what climate-related distortions can break. We next derive the aggregate implications of these distortions.

2.3 Aggregation and TFP decomposition

We now aggregate across firms. With a continuum of firms in each region-sector, we adopt the aggregation notion of Krusell and Smith (1998) and treat the cross-sectional distribution of firm states $\tilde{\mathbf{Z}}_{nit}$ as summarized by a finite set of moments contained in $\tilde{\mathbf{X}}_{nt}$. Using a second-order approximation, we show how dispersion in micro wedges maps into aggregate productivity losses through a set of sufficient statistics.

Proposition 1 (Aggregation and TFP Decomposition.) *Each region-sector n admits an aggregate production function of the form*

$$Y_{nt} = TFP_{nt}K_{nt}^{\alpha_{Kn}}L_{nt}^{\alpha_{Ln}}, \tag{6}$$

where, up to a second-order approximation, the region-sectoral aggregate total factor productivity $TFP_{nt} := TFP_n\left(\tilde{\mathbf{T}}_{rt}, \tilde{\mathbf{X}}_{nt}\right)$ can be decomposed as follows:

$$\begin{aligned}\log TFP_n(\tilde{\mathbf{T}}_{rt},\cdot) = {} & \underbrace{\frac{1}{\sigma_n-1}\log\left[\mathbb{E}_i\left[B_{ni}(\tilde{\mathbf{T}}_{rt},\cdot)\left(A_{ni}(\tilde{\mathbf{T}}_{rt},\cdot)\right)^{\sigma_n-1}\right]\right]}_{\textit{Technology}(\log TFP^E_{nt})} + \frac{1}{\sigma_n-1}\log J_n \\ & \textit{Misallocation Loss} \begin{cases} -\underbrace{\frac{\sigma_n}{2}\operatorname{var}_{\log\left(1-\tau^Y_{ni}\right)}(\tilde{\mathbf{T}}_{rt},\cdot)}_{\textit{Output Wedge Dispersion}} - \underbrace{\sum_{F\in\{K,L\}}\frac{\alpha_{Fn}+\alpha_{Fn}^2(\sigma_n-1)}{2}\operatorname{var}_{\log\left(1+\tau^F_{ni}\right)}(\tilde{\mathbf{T}}_{rt},\cdot)}_{\textit{Factor Wedge Dispersion}} \\ \underbrace{+\sigma_n\sum_{F\in\{K,L\}}\alpha_{Fn}\operatorname{cov}_{\log\left(1-\tau^Y_{ni}\right),\log\left(1+\tau^F_{ni}\right)}\left(\tilde{\mathbf{T}}_{rt},\cdot\right)}_{\textit{Output-Factor Mixed Distortion}} \\ \underbrace{-(\sigma_n-1)\alpha_{Kn}\alpha_{Ln}\operatorname{cov}_{\log\left(1+\tau^K_{ni}\right),\log\left(1+\tau^L_{ni}\right)}\left(\tilde{\mathbf{T}}_{rt},\cdot\right)}_{\textit{Factor Mixed Distortion}}. \end{cases}\end{aligned} \tag{7}$$

Here, expectations, variances, and covariances are taken across firms within region-sector n at

date t. Holding variety fixed, Proposition 1 decomposes aggregate TFP into two terms: *technology* and *misallocation loss*. The technology component, $\log \text{TFP}^E_{nt}$, represents the production possibility frontier. It is a CES aggregation of demand-adjusted physical productivity across firms. We label this term *technology* in the spirit of Basu and Fernald (2002) and Baqaee and Farhi (2019).

The remaining variance and covariance terms summarize the *misallocation loss*, that is, the TFP cost of wedges. These moments are themselves smooth functions of climate. Greater dispersion in output or factor wedges, captured by $\text{var}_{\log(1-\tau^Y_{ni})}$ and $\text{var}_{\log(1+\tau^F_{ni})}$, lowers TFP by widening marginal products across firms and thereby increasing misallocation. The resulting losses are larger when products are more substitutable (higher σ_n) and when the distorted factor has a larger cost share (higher α_{Fn}). The covariance terms capture whether different wedges reinforce or offset each other. In particular, productivity losses are larger when (i) firms facing higher taxes on output also face higher input prices, so that $\text{cov}_{\log\left(1-\tau^Y_{ni}\right),\log\left(1+\tau^F_{ni}\right)} < 0$, and (ii) firms facing larger capital distortions also face larger labor distortions, so that $\text{cov}_{\log\left(1+\tau^K_{ni}\right),\log\left(1+\tau^L_{ni}\right)} > 0$.

2.4 Decomposing the Impact of Climate Change on Aggregate TFP

Because all moments in Equation 7 are smooth functions of climate conditions $\tilde{\mathbf{T}}_{rt}$, the first-order effect of climate change on TFP can be written in terms of a set of measurable derivatives. We illustrate this in the benchmark case with capital wedges only.

Benchmark case: only capital wedges are present. We focus on the case with capital wedges only, following a large misallocation literature (Asker, Collard-Wexler, and De Loecker 2014; David and Venkateswaran 2019; Sraer and Thesmar 2023). This benchmark is natural because capital is a dynamic input: it is often externally financed, costly to adjust, and hard to reallocate on short notice. As a result, distortions in capital use—such as those arising from credit frictions or investment irreversibility—can be larger and more persistent than distortions in labor use (Gorodnichenko et al. 2018). This focus is therefore motivated ex ante by economic structure and tractability; later sections show empirically that capital is the quantitatively dominant margin, while other channels are comparatively small.

When only the capital wedge is present, the MRPK of each firm i satisfies that: $\text{MRPK}_{nit} = \alpha_{Kn}\frac{\sigma_n-1}{\sigma_n}\frac{P_{it}Y_{it}}{K_{it}} \propto (1+\tau^K_{nit})R_{nt}$. Hence, dispersion in capital wedges is directly measurable from the cross-sectional dispersion of MRPK:

$$\text{var}_i\left[\log(1+\tau^K_{nit})\right] = \text{var}_i(mrpk_{nit}) = \text{var}_i\left(\log\frac{P_{nit}Y_{nit}}{K_{nit}}\right), \tag{8}$$

where $mrpk_{nit} \equiv \log(\text{MRPK}_{nit})$. The last equality shows that given a common technology within the region-sector-year , the cross-sectional variance of log MRPK is simply the variance of log sales over capital stock. We can now formalize how climate conditions affect aggregate TFP via the following Lemma:

Lemma 2 *With only capital wedges, the first-order effect of climate conditions on region-sector TFP can*

be written as

$$\frac{d\log TFP_{nt}}{d\tilde{\mathbf{T}}_{rt}} = \underbrace{\frac{1}{\sigma_n - 1}\frac{d\log \mathbb{E}_i\left[B_{ni}(\tilde{\mathbf{T}}_{rt},\cdot)\left(A_{ni}(\tilde{\mathbf{T}}_{rt},\cdot)\right)^{\sigma_n-1}\right]}{d\tilde{\mathbf{T}}_{rt}}}_{\textit{Technology channel}} \underbrace{- \frac{\alpha_{Kn} + \alpha_{Kn}^2(\sigma_n - 1)}{2}\frac{d\,\mathrm{var}_{mrpk_{ni}}(\tilde{\mathbf{T}}_{rt},\cdot)}{d\tilde{\mathbf{T}}_{rt}}}_{\textit{Misallocation Channel}}, \tag{9}$$

Lemma 2 gives the empirical content of the framework. The first term in (9) captures the direct technology channel, while the second captures the misallocation channel. In the capital-wedge benchmark, measuring climate-induced misallocation reduces to estimating how climate changes within-cell MRPK dispersion. This is the key reduced-form object in Section 4. In practice, the paper estimates local semi-elasticities around the observed $\tilde{\mathbf{T}}_{rt}$ and $\tilde{\mathbf{X}}_{nt}$. Section 4.4 therefore allows these local effects to vary with long-run climate and development.

3 Data

3.1 Global Firm-level Microdata

We compile firm-level microdata from 30 European countries, China, and India, collectively covering 38.6% of world GDP. European firm data come from Bureau van Dijk's (BvD) Orbis database; Chinese data from the National Bureau of Statistics (NBS) Annual Survey of Industrial Firms; and Indian data from the Annual Survey of Industries (ASI). All three sources are widely used in the literature and provide nationally representative coverage of the formal sector.[6] Table B.1 lists countries, sample periods, and sources.

Key variables and measurement. The central object in our empirical analysis is the cross-firm dispersion of the marginal revenue product of capital, $\mathrm{var}(\log \mathrm{MRPK})$, within each region–sector–year cell. Constructing this sufficient statistic requires firm-level revenue $P_{it}Y_{it}$ and capital stock K_{it}. We measure revenue as reported operating revenue in Orbis and China NBS, and as total sales in India ASI. Capital is measured as the book value of gross fixed assets, with one exception: India ASI reports net fixed assets more consistently, so we use net values for India.[7] The ASI also records whether a plant has computerized air-conditioning (available 2001–2014), which we exploit as a plant-level adaptation proxy in Section 6. All three datasets additionally report wage bills, employment, and (with varying coverage) material costs, which we use in robustness exercises and in the technology-channel estimation of Section 4.3. We harmonize sectoral classifications into eight USSIC major divisions and define regions as NUTS 3 areas in Europe,

6. Orbis coverage is regulatory across Europe, extending to small private firms. The China NBS surveys cover all industrial firms with annual sales above CNY 5 million (1998–2007), representing over 90.7% of total output. The India ASI censuses plants with 100+ workers and samples smaller registered plants, ensuring representativeness at the state–industry level.

7. Gross fixed-asset values in ASI contain substantial missing data. In Appendix B we show that our results are not sensitive to this choice.

prefectures in China, and districts in India—units roughly comparable to U.S. counties.[8]

Sample construction. We retain all firm-year observations with non-missing revenue and capital stock, and trim the top and bottom 0.1% of MRPK within each country.[9] For region–sector–year level analysis, we further restrict to cells containing at least 30 firm-year observations, so that within-cell variance estimates are not dominated by sampling noise.[10] The resulting panel is an unbalanced sample of 124,567 region–sector–year observations covering 76,826,956 firm-years. For firm-level regressions, we use the full sample after trimming. Appendix B provides details on cleaning, variable construction, and sample selection for each dataset.

3.2 Weather and Forecast Data

Temperature. We obtain daily temperature from ERA5-Land (Sabater 2019), a reanalysis product from ECMWF that provides hourly surface variables at $0.1° \times 0.1°$ resolution (approximately 9 km) with global coverage. We compute daily mean temperature as the geometric average of the daily maximum and minimum, then construct annual temperature bins at 5°C intervals from below -5°C to above 30°C. Each bin counts the number of days per year a region's average temperature falls within that range.

Temperature bins capture the distributional shifts that define climate change—in particular, the increasing frequency of extreme heat events (Oudin Åström et al. 2013; Christidis, Mitchell, and Stott 2023)—more accurately than changes in annual means alone. Figure 1a documents that hot days (above 25°C) have increased substantially across all three sample regions relative to 1951–1980 baselines, with the shift accelerating in the most recent decade. Figure 1b shows the corresponding rightward shift in the full daily temperature distribution, including projections for 2100.

Climate projections. End-of-century temperature distributions come from the GFDL-ESM4 model under CMIP6's SSP3-4.5 scenario, which represents intermediate emissions with modest mitigation—a pathway widely regarded as among the more plausible (O'Neill et al. 2016).[11]

Weather forecasts. We use ECMWF's long-range (seasonal) forecasts (Copernicus Climate Change Service and Climate Data Store 2018), which provide daily maximum and minimum 2 m temperature forecasts up to seven months ahead at $1° \times 1°$ resolution. We extract 30-day-ahead forecasts issued on the first day of each month.[12] Details on how we map these forecasts to annual forecast errors and perceived forecast uncertainty are in Section 7 and Appendix B.

8. Industries are: agriculture, mining, construction, manufacturing, transportation & utilities, wholesale trade, retail trade, FIRE, and services. We adopt USSIC for cross-country comparability, following its availability in Orbis.

9. Trimming extreme log revenue-to-capital ratios is standard in the misallocation literature: Hsieh and Klenow (2009) trim at 1% and Gopinath et al. (2017) apply similar filters, as tail values in administrative data typically reflect reporting errors, dormant firms, or asset revaluations. Our 0.1% threshold is conservative relative to these precedents.

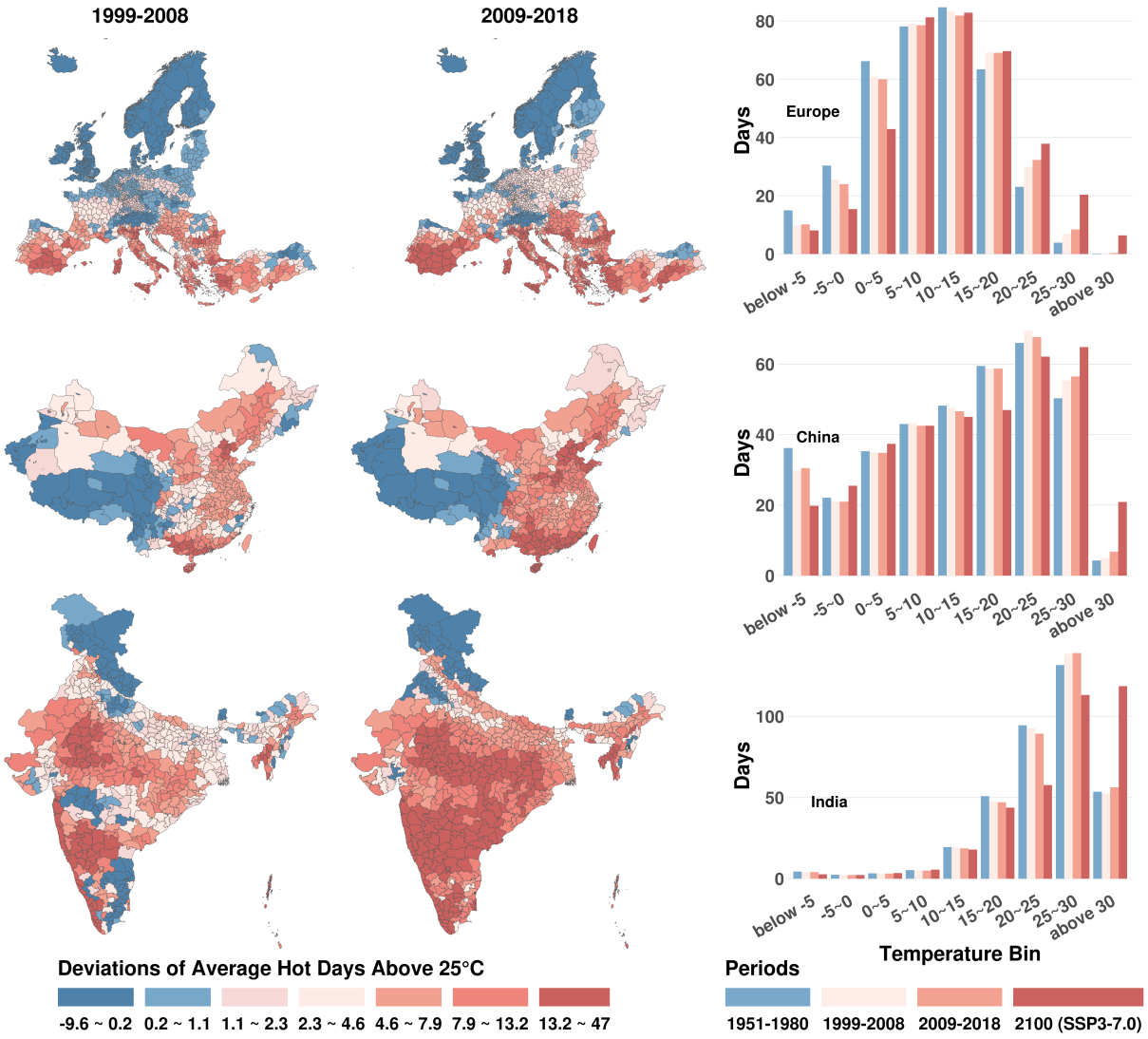
10. We also drop cells exhibiting discontinuous jumps in firm counts or aggregate sales, which likely reflect changes in reporting requirements rather than economic activity.

11. GFDL-ESM4 has a 1-degree nominal horizontal resolution, produced by NOAA's Geophysical Fluid Dynamics Laboratory.

12. Pre-2017 values are hindcasts from a 25-member ensemble; from 2017 onward, forecasts are produced monthly with a 51-member ensemble.

Figure 1: Climates of our sample regions

(a) Number of Hot Days Deviation Relative to 1951–1980 (b) Average Daily Temperature Distribution



Notes: Panel (a) plots the change in annual days above 25°C between each sample decade (1999–2008 and 2009–2018) and the 1951–1980 baseline. Panel (b) shows average daily temperature distributions for the baseline, two sample periods, and 2100 under SSP3-7.0.

3.3 Other Data

Regional GDP. We obtain sub-national GDP per capita (PPP-adjusted, 2017 international dollars) from the DOSE dataset (Wenz et al. 2023), matched to our regional definitions via spatial coordinates. Using sub-national rather than country-level income is important because countries like India and China exhibit large within-country income variation across districts and prefectures. We compute long-run regional averages over our sample period and use them in two ways: as a time-invariant moderator interacted with temperature bins in the heterogeneous-effects specification (Section 4.4), and as the key input to the adaptation-cost parameterization in the structural model (Section 7).

Income projections. National income per capita projections under the SSP scenarios are from the OECD EnvGrowth model (Dellink et al. 2017), hosted by the International Institute for Applied Systems Analysis. These projections enter the end-of-century decomposition (Section 4.6), where projected income growth drives the "income effect" component of future misallocation losses.

4 Estimating the Misallocation Channel of Climate Change

This section documents the paper's central empirical fact: temperature shocks increase capital misallocation within region–sector cells. Section 4.1 describes the empirical design. Section 4.2 reports the average effect of temperature on MRPK dispersion, showing a U-shaped relationship that is robust across specifications. Section 4.3 decomposes aggregate TFP into technology and misallocation channels, finding that misallocation accounts for roughly five times the loss from the technology channel alone. Section 4.4 documents that misallocation losses are larger in hotter and richer regions, a pattern that sharply distinguishes this channel from conventional climate damages. Section 4.5 shows that incorporating the misallocation channel reconciles micro-based and macro-based climate damage estimates. Section 4.6 projects end-of-century TFP losses under SSP3-4.5. Appendix C reports additional robustness checks.

4.1 Empirical design

We estimate how annual temperature realizations affect capital misallocation within region–sector cells, measured by the cross-firm variance of log MRPK. Following Deschênes and Greenstone (2011) and Carleton et al. (2022), we summarize each region-year temperature realization by the number of days in 5°C bins. Specifically, we define current climate conditions as the vector $\mathbf{T}_{r,t} = \left\{\text{Tbin}_{r,t}^{<-5^\circ\text{C}}, \text{Tbin}_{r,t}^{-5\sim0^\circ\text{C}}, ..., \text{Tbin}_{r,t}^{>30^\circ\text{C}}\right\}$, where each element $\text{Tbin}_{r,t}^{b}$ counts the number of days in year t for which region r's average temperature falls within bin b. This approach uses detailed daily temperature data while allowing for flexible nonlinear climate effects in a linear regression framework.

Our baseline specification is

$$\sigma^2_{mrpk_{(s,r),t}} = \sum_{b \in B/\{5\sim10^\circ\text{C}\}} \lambda^{b}_{\sigma^2_{mrpk}} \times \text{Tbin}^{b}_{r,t} + \boldsymbol{\delta}_{\sigma^2_{mrpk}} \mathbf{X}_{s,r,t} + \alpha_{c(r),t} + \eta_{s,r} + \varepsilon_{r,s,t}, \tag{10}$$

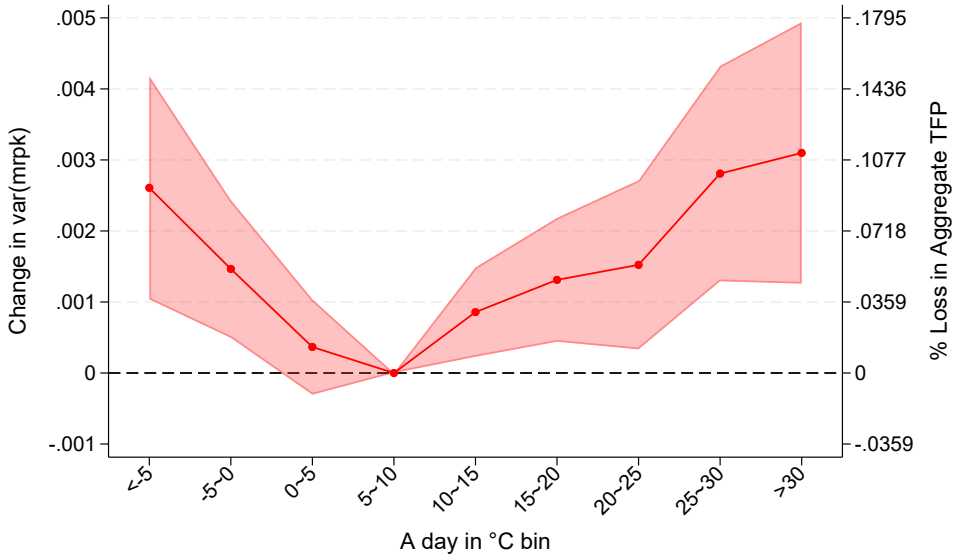
where $\sigma^2_{mrpk_{(s,r),t}}$ denotes the variance of log MRPK across firms within region–sector (s, r) in year t. Region–sector fixed effects $\eta_{s,r}$ absorb time-invariant differences across cells, while country–year fixed effects $\alpha_{c(r),t}$ absorb national shocks common to all regions within a country-year. The coefficients on the temperature bins are therefore identified from year-to-year fluctuations in local temperature realizations within a region–sector, relative to other regions in the same country and year. Such climate variation is plausibly exogenous, and $\boldsymbol{\lambda}_{\sigma^2_{mrpk}} = \mathbb{E}\left[d\,\mathrm{var}_{mrpk_{ni}}(\tilde{\mathbf{T}}_{rt}, \cdot)/d\mathbf{T}_{r,t}\right]$ captures the average effect of climate on misallocation. Because the temperature bins sum to 365 days, coefficients are interpreted relative to the omitted 5°C–10°C bin. Standard errors are clustered at the region level.

In our preferred specification, we omit time-varying region–sector controls. Variables such as the number of firms, average sales, and average MRPK may themselves respond to temperature shocks, so conditioning on them risks absorbing part of the total effect. Table 1 shows that the results are very similar when these controls are added.

4.2 Average effects of temperature on capital misallocation

The baseline estimates of $\hat{\lambda}^b_{\sigma^2_{mrpk}}$ and the implied TFP losses are reported in columns (1) and (5) of Table 1 and shown in Figure 2. We convert $\hat{\lambda}^b_{\sigma^2_{mrpk}}$ into implied TFP losses using the relationship $-\frac{\alpha_{Kn}+\alpha^2_{Kn}(\sigma_n-1)}{2}\hat{\lambda}^b_{\sigma^2_{mrpk}}$ in Equation (9), adopting the standard parameter values of capital share $\alpha_{Kn} = 0.35$ and elasticity of demand $\sigma_n = 4$ (Redding and Weinstein 2020) for all region-sector n.

Figure 2: Estimated impact of daily temperature shocks on annual MRPK dispersion and implied TFP loss



Notes: This figure shows the aggregate impact linking annual MRPK dispersion and TFP loss to average daily temperatures. The formula for computing TFP loss from misallocation is $-\frac{\alpha_{Kn}+\alpha^2_{Kn}(\sigma_n-1)}{2}\hat{\lambda}^b_{\sigma^2_{mrpk}}$. The estimation is normalized by setting the range of 5°C - 10°C as the reference category. Therefore, each $\lambda^b_{\sigma^2_{mrpk}}$ represents the estimated effect of an additional day in temperature bin b on annual MRPK dispersion or TFP loss, relative to a day with temperatures between 5°C - 10°C. The figure also includes the 90% confidence interval for these estimates where standard errors are clustered at the region level.

Table 1: Effects of daily mean temperature bins on MRPK dispersion and TFP loss

	(1) σ^2_{mrpk}	(2) σ^2_{mrpk}	(3) σ^2_{mrpk}	(4) σ^2_{mrpk}	(5) Implied TFP Loss
< -5°C	0.0026***	0.0025***	0.0028***	0.0012	0.0935***
	(0.0010)	(0.0009)	(0.0009)	(0.0023)	(0.0342)
$-5 \sim 0$°C	0.0015**	0.0013**	0.0016***	0.0006	0.0526**
	(0.0006)	(0.0006)	(0.0006)	(0.0013)	(0.0212)
$0 \sim 5$°C	0.0004	0.0002	0.0005	-0.0019**	0.0131
	(0.0004)	(0.0004)	(0.0004)	(0.0009)	(0.0146)
$10 \sim 15$°C	0.0009**	0.0008**	0.0008**	0.0036***	0.0308**
	(0.0004)	(0.0004)	(0.0004)	(0.0010)	(0.0137)
$15 \sim 20$°C	0.0013**	0.0012**	0.0014***	0.0045***	0.0471**
	(0.0005)	(0.0005)	(0.0005)	(0.0013)	(0.0190)
$20 \sim 25$°C	0.0015**	0.0015**	0.0015**	0.0080***	0.0546**
	(0.0007)	(0.0007)	(0.0007)	(0.0020)	(0.0259)
$25 \sim 30$°C	0.0028***	0.0027***	0.0027***	0.0095***	0.1008***
	(0.0009)	(0.0009)	(0.0009)	(0.0021)	(0.0331)
> 30°C	0.0031***	0.0030***	0.0030***	0.0090***	0.1112***
	(0.0011)	(0.0011)	(0.0011)	(0.0021)	(0.0401)
Controls	No	No	Yes	No	No
Region-Sector FE	Yes	Yes	Yes	Yes	Yes
Country-Year FE	Yes	No	Yes	Yes	Yes
Country-Sector-Year FE	No	Yes	No	No	No
1995 VA Weighted	No	No	No	Yes	No
Observations	124,065	123,518	124,065	123,847	124,065
R^2	0.876	0.903	0.878	0.897	0.876

Notes: Standard errors in parentheses. We cluster standard errors at the regional level (NUTS3 level for European countries, prefecture level for China, and district level for India). Dependent variables in columns (1) to (4) represent the variance of log MRPK. Results from estimating Equation 10 are displayed in columns (1) to (4), with controls in column (3) and weighted OLS regression in column (4). Column (5) is the implied TFP loss calculated using the formula, $-\frac{\alpha_{Kn}+\alpha^2_{Kn}(\sigma_n-1)}{2}\hat{\lambda}^b_{\sigma^2_{mrpk}}$, and the regression estimates. Countries included are China, India, and 30 European countries.

$^{*}\ p < 0.10$, $^{**}\ p < 0.05$, $^{***}\ p < 0.01$

Our estimates show a clear U-shaped relationship between temperature and capital misallocation. Both extreme heat and extreme cold raise MRPK dispersion, with the largest effects at the tails of the temperature distribution. This pattern can be directly translated into an inverted U-shape pattern between TFP and temperature, a well known result in the climate econometrics literature (Burke, Hsiang, and Miguel 2015).

Relative to a day in the 5°C–10°C bin, an additional day above 30°C raises the MRPK dispersion by 0.31 log points and implies a 0.11% reduction in annual TFP, equivalent to roughly 40% of one day's GDP. An additional day below -5°C raises the MRPK dispersion by about 0.26 log points, corresponding to an annual TFP loss of 0.09%. These estimates are large: larger than the firm-level productivity effect in the worse-hitting countries in the global sample of Nath (2025) and orders of magnitude larger than the estimates by Ponticelli, Xu, and Zeume (2023) in the US.

Robustness. The estimates are stable across alternative fixed effects, the inclusion of controls, and value-added weighting (Table 1). Appendix C examines sensitivity to sectoral composition, the choice of input margin, alternative weather measures, inference procedures, region–sector definitions, and production-function assumptions. The U-shaped pattern is present across major sectors (agriculture, manufacturing, transportation, retail, services), robust to alternative temperature constructions (daily max, population-weighted, polynomial), and preserved under CES production. Importantly, MRPL and MRPM dispersion show little response to temperature, consistent with the model's timing: capital is committed before temperature is realized, whereas labor and materials can adjust ex post.

4.3 Technology vs. Misallocation

A natural question is how the magnitude of climate-induced misallocation compares with the well-documented technology channel—the direct impact of climate on the aggregate productivity frontier. Our decomposition in Equation (9) separately identifies these two channels. The technology channel is

$$\frac{d\,\text{Technology}_{nt}}{d\tilde{\mathbf{T}}_{rt}} = \frac{d\log \text{TFP}_n^E(\tilde{\mathbf{T}}_{r,t},\cdot)}{d\tilde{\mathbf{T}}_{r,t}} = \frac{1}{\sigma_n - 1}\frac{d\log\left[\mathbb{E}_i \text{TFP}_{ni}(\tilde{\mathbf{T}}_{r,t},\cdot)^{\sigma_n-1}\right]}{d\tilde{\mathbf{T}}_{r,t}},$$

where $\text{TFP}_{ni}\left(\tilde{\mathbf{T}}_{r,t},\cdot\right) := B_{ni}\left(\tilde{\mathbf{T}}_{r,t},\cdot\right)^{\frac{1}{\sigma_n-1}} A_{ni}\left(\tilde{\mathbf{T}}_{r,t},\cdot\right)$. This object is an "elasticity of the aggregate"—the effect on the CES productivity aggregate, which endogenously places greater weight on larger, more productive firms whose climate responses may differ from the average firm's.[13] An un-

13. The elasticity of the aggregate is a productivity-share-weighted average of firm-level elasticities, whereas the average elasticity gives equal weight to all firms:

$$\underbrace{\frac{d\log \mathbb{E}_i\left[\text{TFP}_{ni}(\tilde{\mathbf{T}}_{r,t},\cdot)^{\sigma_n-1}\right]}{d\tilde{\mathbf{T}}_{r,t}}}_{\text{Elasticity of the Average}} = \mathbb{E}_i\left[\frac{\text{TFP}_{nit}^{\sigma_n-1}}{\mathbb{E}_i[\text{TFP}_{nit}^{\sigma_n-1}]}\cdot\frac{d\log \text{TFP}_{ni}(\tilde{\mathbf{T}}_{r,t},\cdot)^{\sigma_n-1}}{d\mathbf{T}_{r,t}}\right] \neq \underbrace{\mathbb{E}_i\left[\frac{d\log \text{TFP}_{ni}(\tilde{\mathbf{T}}_{r,t},\cdot)^{\sigma_n-1}}{d\mathbf{T}_{r,t}}\right]}_{\text{Average Elasticity}}.$$

A simple OLS regression would recover the latter rather than the former, and could therefore bias the aggregate estimate downward for heat shocks if larger, more productive firms are more resilient to heat, i.e., $\text{cov}\left(\frac{\text{TFP}_{nit}^{\sigma_n-1}}{\mathbb{E}_i[\text{TFP}_{nit}^{\sigma_n-1}]}, \frac{d\log \text{TFP}_{ni}(\tilde{\mathbf{T}}_{r,t},\cdot)^{\sigma_n-1}}{d\text{Tbin}_{r,t}^{>30C}}\right) > 0$.

weighted firm-level OLS regression generally recovers the "average elasticity" rather than the "elasticity of the aggregate," and can therefore misstate the aggregate technology response.

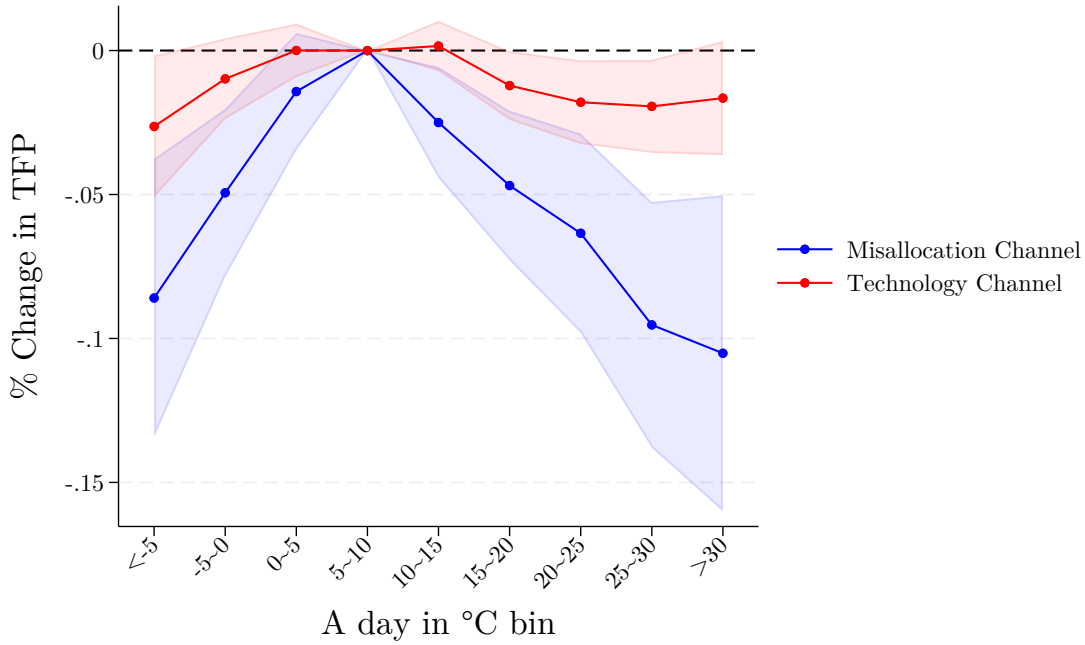
To estimate the elasticity of the aggregate, we use a Poisson Pseudo Maximum Likelihood (PPML) regression, which yields consistent estimates as shown by Tyazhelnikov, Zhou, and Shi (2024):

$$\mathrm{E}_i\left[\frac{1}{\sigma_n-1}\widetilde{\mathrm{TFP}}_{nit}^{\sigma_n-1} \mid \tilde{\mathbf{T}}_{rt}, \eta_i, \log(P_{nt}Y_{nt}), \kappa_{c(r)st}\right] = \exp\left[\boldsymbol{\beta}\tilde{\mathbf{T}}_{rt} + \eta_i + \delta\log(P_{nt}Y_{nt}) + \kappa_{c(r)st}\right], \tag{11}$$

where $\widetilde{\mathrm{TFP}}_{nit} := \frac{(P_{nit}Y_{nit})^{\frac{\sigma_n}{\sigma_n-1}}}{K_{nit}^{\alpha_{Kn}}L_{nit}^{\alpha_{Ln}}}$ is the model-consistent empirical measure of TFP, η_i denotes firm fixed effects, and $\log(P_{nt}Y_{nt})$ together with $\kappa_{c(r),s,t}$ captures differences between local and national price levels. Estimating Equation (11) by PPML yields a theory-consistent estimate of $\boldsymbol{\beta} = \mathbb{E}\left[\frac{1}{\sigma_n-1}\frac{d\log\mathbb{E}_i[\mathrm{TFP}_{nit}^{\sigma_n-1}|\cdot]}{d\tilde{\mathbf{T}}_{rt}}\right]$, which we plot alongside the misallocation channel in Figure 3.

The technology channel is noticeable but considerably smaller than the misallocation channel. An additional day below -5°C lowers annual aggregate physical productivity by about 0.03%, while an additional day above 25°C or 30°C lowers it by about 0.02%—roughly one-fifth of the corresponding misallocation loss.

Figure 3: Technology vs. Misallocation



Notes: The graphs include 90% confidence intervals, and standard errors are clustered at the regional level. The reference temperature is at 5∼10°C.

These results clarify the relationship between micro and macro approaches in the existing literature. Previous *micro* estimates typically recover an upper bound on the technology channel (by overweighting less-adapted small firms) while missing the misallocation channel entirely. Previous *macro* estimates capture the combined effect of both channels but cannot separate them.

Our framework identifies each channel individually.

4.4 Heterogeneous effects by long-run climate and development

The average effect masks substantial heterogeneity. We next ask whether the same temperature shock has different effects in places with different long-run climate conditions and levels of economic development. A priori, the answer is ambiguous: warmer or richer regions may be better adapted on average, but they may also exhibit greater cross-firm heterogeneity in exposure and adjustment capacity. In warmer climates, heat-averse firms may have already adapted, so additional heat shocks cause only limited disruption; alternatively, once temperatures exceed adaptation thresholds, limited adaptability (Moscona and Sastry 2023) and the convexity of heat damages (Burke, Hsiang, and Miguel 2015) may sharply widen cross-firm differences in marginal products. Likewise, richer regions tend to feature more specialized production and greater firm-size dispersion (Chen 2022; Poschke 2018), which can amplify MRPK divergence when some firms adjust quickly and others cannot.

Following Carleton et al. (2022) and Nath (2025), we interact time-invariant measures of long-run average temperature and GDP per capita with each temperature bin:

$$\begin{aligned}\sigma^2_{mrpk_{s,r,t}} = &\sum_{b \in B_{/(5\sim 10^\circ C)}} \lambda^b \times \text{Tbin}^b_{r,t} + \sum_{b \in B_{/(5\sim 10^\circ C)}} \lambda^b_{\overline{T}} \times \text{Tbin}^b_{r,t} \times \overline{T}_r \\ &+ \sum_{b \in B_{/(5\sim 10^\circ C)}} \lambda^b_{\text{GDP}_{\text{pc}}} \times \text{Tbin}^b_{r,t} \times \ln \overline{\text{GDP}_{\text{pc}}}_r + \boldsymbol{\delta} \tilde{\mathbf{X}}_{s,r,t} + \alpha_{c,t} + \eta_{s,r} + \varepsilon_{s,r,t}.\end{aligned} \tag{12}$$

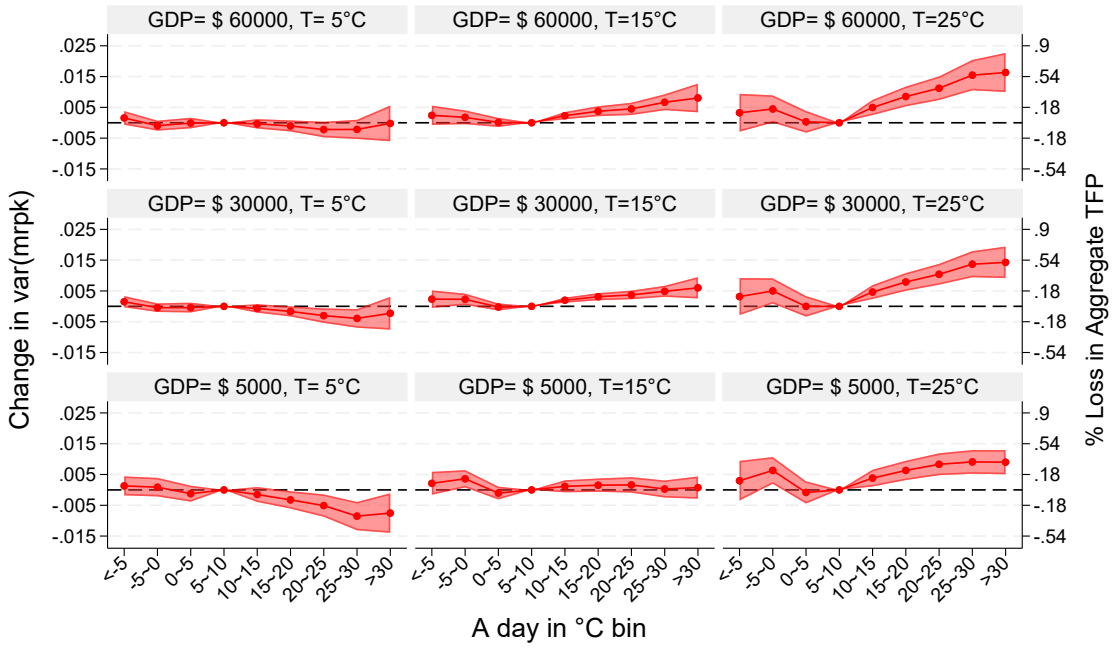
Here $\overline{T}_r$ and $\ln \overline{\text{GDP}_{pc,r}}$ are region-level averages over 1997–2018.[14] The interaction coefficients show how the effect of an additional day in bin b varies with long-run climate and development.

Figure 4 presents the results. Two facts stand out. First, extreme heat raises misallocation more in warmer regions: holding income fixed, the effect of a day above $30°$C is small in cold climates but large and positive in hot climates. For example, despite similar income levels of about \$60,000, an additional day above $30°$C lowers TFP by 0.27% in Arizona but raises it by 0.14% in Norway. Second, extreme heat raises misallocation more in richer regions: holding long-run climate fixed, the response becomes more U-shaped as GDP per capita rises. For example, although the Netherlands and Türkiye have similar average temperatures of about $9.9°$C, an additional day above $30°$C implies a TFP loss of 0.11% in the Netherlands but only 0.03% in Türkiye.

These heterogeneous effects distinguish the misallocation channel sharply from other climate channels, such as labor productivity (Nath 2025) and mortality risk (Carleton et al. 2022), where hotter and richer places often appear less vulnerable because of long-run adaptation. Here the opposite pattern emerges: hotter and richer regions suffer larger TFP losses through misallocation. As economies develop, production and adaptation become more sophisticated across firms, and achieving efficient allocations may itself become more difficult under climate stress.

14. The sub-national level (PPP-adjusted) GDP per capita data is from DOSE. It is important to use sub-national level data as countries like India and China admit large income heterogeneity across the districts or prefectures. The GDP per capita data is in 2017 International Dollars.

Figure 4: MRPK Dispersion and TFP Loss Across Climates and Income



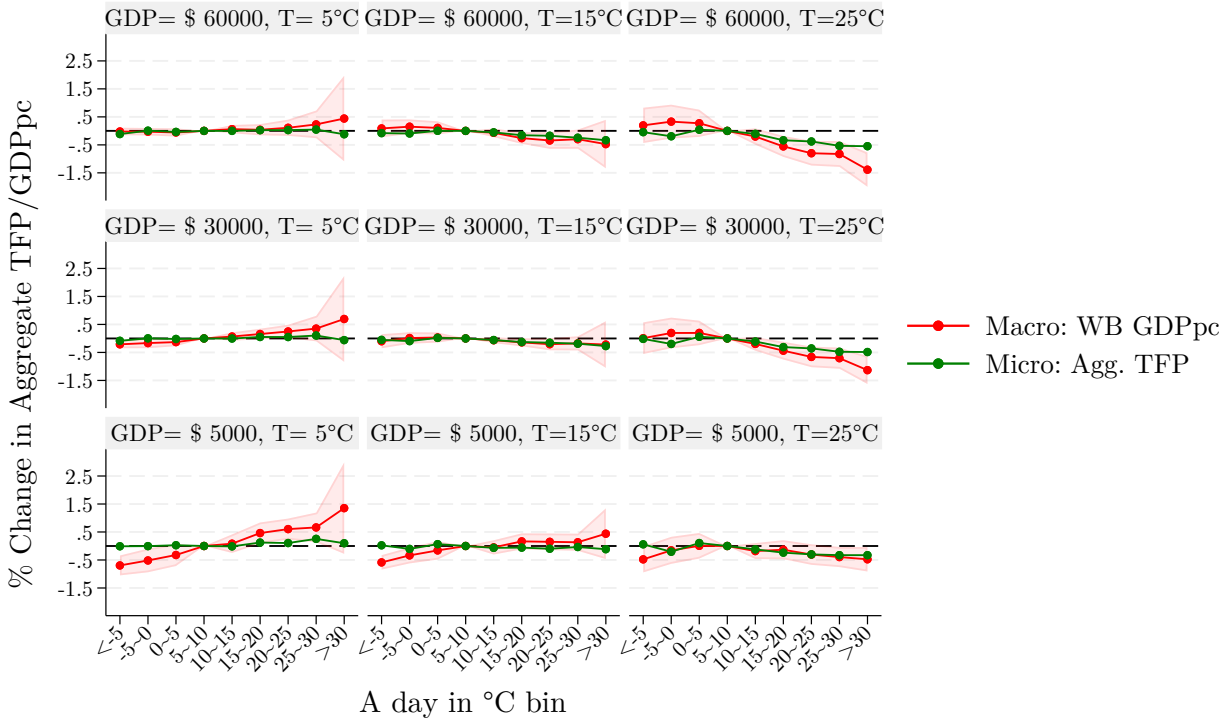
Notes: The graphs plot the predicted effect of exposure to daily mean temperature bins on MRPK dispersion and TFP loss at varying levels of income and climates. These predicted effects are derived from the interacted panel regression specified in Equation 12. The graphs include 90% confidence intervals, and standard errors are clustered at the regional level. The left y-axis indicates changes in MRPK dispersion, and the right y-axis shows the calculated TFP loss. The reference temperature is at 5∼10°C.

4.5 Micro estimates vs. macro estimates

To show that incorporating the misallocation channel quantitatively bridges the micro–macro disconnect, we compare *micro estimates*—derived from firm-level data and aggregation theory—with *macro estimates* obtained from country-level aggregate data. For the micro estimates, we estimate the technology channel using the PPML specification in Equation (11), augmented with the interaction terms from Equation (12), and combine the estimated technology effects with our misallocation estimates. If the misallocation channel is shut down, the resulting micro estimates are essentially flat, indicating that cross-country heterogeneity in the total effect is driven primarily by misallocation. For the macro estimates, we use annual GDP per capita data from the World Bank for 1990–2019 and estimate a country-level regression analogous to Equation (12), including country and year fixed effects.

Figure 5 plots the two sets of estimates. The micro-based estimates closely track the macro-based estimates, with two exceptions: they understate damages from extreme heat in regions with high income and high mean temperatures, and they overstate the benefits of heat shocks in colder, poorer regions. Both types of regions are rare in our sample. These results suggest that our micro estimates capture the same cross-country heterogeneity in temperature sensitivity as the macro estimates, making them informative for out-of-sample extrapolation.

Figure 5: Aggregate Impact of Climate Shocks: Micro vs. Macro Estimates



Notes: The graphs include 90% confidence intervals, and standard errors are clustered at the region level. The reference temperature is at 5∼10°C.

4.6 End-of-the-century projection

We use the estimates from Section 4.4 to project how climate-induced misallocation will affect aggregate TFP by the end of the 21st century (2081–2100) for 4,881 regions in 172 countries.[15]

Such projections require detailed region-level daily temperature distributions, average temperature levels, and GDP per capita projections. We use near-surface air temperature forecasts from the sixth phase of the Coupled Model Intercomparison Project (CMIP6) (Copernicus Climate Change Service 2021) under RCP 4.5, a scenario featuring moderate mitigation efforts. To project each region's daily temperature distribution, we calculate the average number of days in each temperature bin and the mean annual temperature for 2081–2100, taking a 20-year average to smooth over short-term climate fluctuations. Following Carleton et al. (2022), we obtain national per capita income projections from the OECD EnvGrowth model (Dellink et al. 2017) under the SSP3 scenario. For the average region, mean annual temperature is expected to rise by about 1.78°C between 2000–2014 and 2081–2100, while GDP per capita is projected to increase by approximately $20,748. Figure D.12 illustrates these projected changes.

We decompose the total effect of climate-induced misallocation into three components:

15. For our 32-country sample, regions are defined as in Section 3. For other countries, we use GADM1-level administrative units from the GADM dataset.

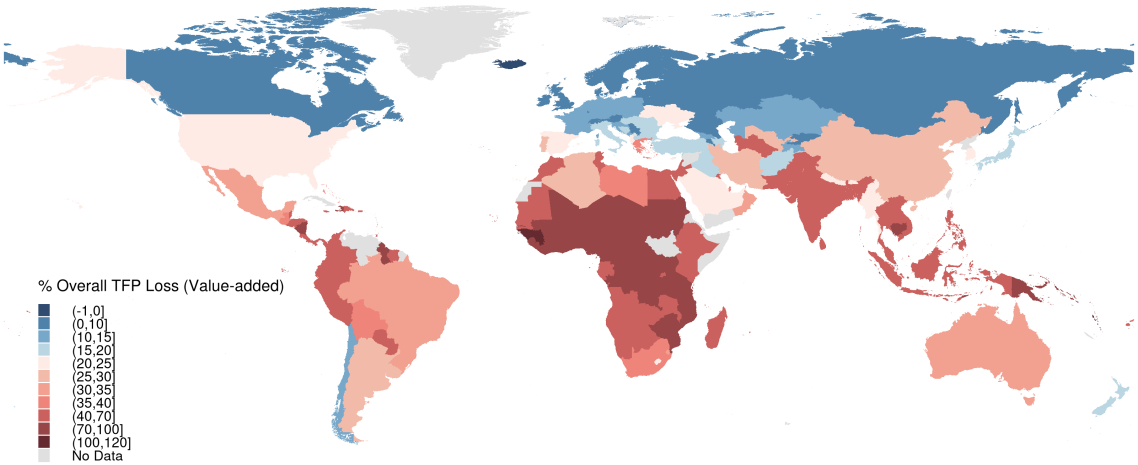
$$\underbrace{\Delta^{\text{Loss}} \ln \text{TFP}_r}_{\text{Total Effect}_r} = \frac{\alpha_{Kn} + \alpha_{Kn}^2(\sigma_n - 1)}{2} \Bigg[\underbrace{\sum_b \left(\lambda^b + \lambda^b_{\text{GDP}_{pc}} \ln \text{GDP}_{pc,r,\text{base}} + \lambda^b_{\bar{T}} \bar{T}_{r,\text{base}} \right) \times \Delta \text{Tbin}^b_r}_{\text{Shock Effect}_r}$$
$$+ \underbrace{\sum_b \lambda_{b,\bar{T}} \text{Tbin}^b_{r,\text{base}} \times \Delta T_r}_{\text{Level Effect}_r}$$
$$+ \underbrace{\sum_b \lambda^b_{\text{GDP}_{pc}} \text{Tbin}^b_{r,\text{base}} \times \Delta \ln \text{GDP}_{pc,r}}_{\text{Income Effect}_r} \Bigg] + \underbrace{\varepsilon_{rt}}_{\text{Residuals}_r}, \tag{13}$$

where Δ denotes the difference between end-of-century and baseline values. The *shock effect* captures the change in TFP losses due to shifts in daily temperature distributions ΔTbin^b_r, conditional on baseline income and long-run temperature; the *level effect* captures the change due to rising long-run temperature ΔT_r; and the *income effect* reflects the increasing misallocation arising from economic development $\Delta \ln \text{GDP}_{pc,r}$. We aggregate regional TFP losses to the country level using projected GDP shares under SSP3.[16]

Figure 6 displays each country's projected TFP loss. While most countries experience substantial losses, the magnitudes vary widely. The most severely affected are tropical and subtropical countries—Tanzania, Malaysia, Honduras, and India, where TFP losses exceed 40%—driven by sharp increases in days above 30°C combined with rising temperatures and incomes. Temperate high-income countries such as the United States (20.9%), Spain, and Argentina see losses of 20–30%, while maritime climates such as the United Kingdom (8.2%) and France are projected to lose less than 15%, reflecting the relatively low incidence of extreme heat even under warming.

16. Grid-level SSP3 GDP data from Wang and Sun (2022) provides projected GDP shares.

Figure 6: End-of-century Projected TFP Loss Due to the Misallocation Channel

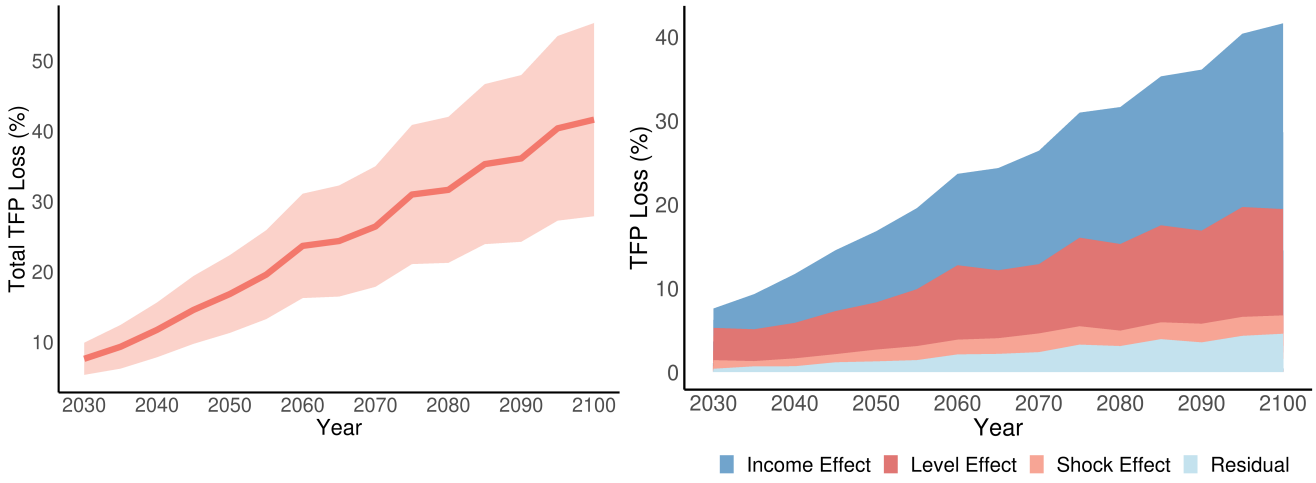


Notes: Figure shows the projected TFP losses from capital misallocation under SSP3-4.5 scenarios. The estimation follows Equation 13 where we estimate the total effect in MRPK dispersion and compute the equivalent value of TFP losses.

Figure 7: Projected Global TFP Loss and Its Decomposition: 2030-2100

(a) Total TFP Loss from the Misallocation Channel

(b) TFP Loss Decomposition



Notes: Figure 7a plots the total TFP loss across years. The dark red line plots the estimates and the shaded area is 90% confidence intervals from the parameter uncertainty. Figure 7b plots the three effects contributing to total TFP loss. All computations are under the SSP3-4.5 scenario and the percentage loss is compared to the baseline level.

Weighting each country's losses by its projected share of global GDP,[17] the worldwide cost of climate-induced misallocation is:

$$\underbrace{\Delta^{\text{Loss}} \ln \text{TFP}}_{\text{Total Effect}=36.73\%} = \underbrace{\text{Shock Effect}}_{2.13\%} + \underbrace{\text{Level Effect}}_{11.34\%} + \underbrace{\text{Income Effect}}_{19.46\%} + \underbrace{\text{Resid.}}_{3.8\%}.$$

17. Under this weighting scheme, the resulting TFP losses correspond to a model-implied global TFP loss based on a Cobb-Douglas aggregator of country-level value added. This also serves as a first-order approximation under any constant-returns-to-scale aggregator for global output.

Relative to baseline conditions, this translates into a 36.73% decline in aggregate TFP. Shifts in the daily temperature distribution (*shock effect*) contribute 2.13%, rising average temperature (*level effect*) accounts for 11.34%, and higher income per capita (*income effect*) explains 19.46%. Figure 7a depicts the projected evolution of misallocation-driven TFP losses from 7.60% in 2030 to 41.62% by 2100, with 90% confidence intervals accounting for parameter uncertainty. Figure 7b further separates these losses into the three components over time, highlighting the dominant roles of the level and income effects.

These estimates are substantial and comparable to the overall projected impacts reported by Burke, Hsiang, and Miguel (2015) and, more recently, Bilal and Känzig (2024). Much of the total projected effect arises from the sharp increase in the marginal effect of daily temperature shocks, driven by rising temperatures and incomes. As with any century-scale forecast, our projection is subject to caveats—most notably out-of-sample extrapolation, since end-of-century income and temperature levels lie well beyond historical experience. However, even if we only adjust the daily temperature distribution while keeping the first-order marginal effect at current levels, we still project a 2.14% global TFP loss from misallocation. Overall, these results underscore the quantitative importance of the misallocation channel, which may serve as one of the key forces driving up the social cost of carbon.

5 A Firm Dynamics Model of Climate and MRPK Dispersion

The reduced-form evidence establishes that both long-run climatic conditions and short-run temperature fluctuations raise capital misallocation, with stronger effects in hotter and more developed regions. Why does temperature disperse MRPK, and why does adaptation amplify rather than attenuate this effect? To answer these questions, we build a tractable general-equilibrium model with risk-averse households and heterogeneous firms, featuring time-to-build capital, pre-existing capital wedges, and costly endogenous climate adaptation. A novel feature is that adaptation is fully endogenous: firms choose their effective productivity process by selecting adaptation intensity in response to expected climate conditions and weather risk, building on Kopytov, Taschereau-Dumouchel, and Xu (2024).

The model's demand and production structure mirrors the structure of our accounting framework and is defined at the region-year level. For expositional clarity, we suppress the region-year notation here and introduce regional heterogeneity later.

5.1 Model Structure

5.1.1 Household

In each region, a representative household with King-Plosser-Rebelo preferences consumes C_t, inelastically supplies a mass N of unskilled labor to production, and elastically supplies skilled labor $\mathcal{R}_t$ to an adaptation sector. The household chooses $\{C_t, \mathcal{R}_t\}_{t\geq 0}$ to maximize

$$\max_{\{C_t,\mathcal{R}_t\}} \mathbb{E}_0 \sum_{t=0}^{\infty} \left(\frac{1}{1+r}\right)^t \frac{\left(C_t \exp\left(-\mathcal{R}_t\right)\right)^{1-\gamma}}{1-\gamma},$$

where r is the discount rate and $\gamma \geq 1$ governs relative risk aversion. The adaptation sector converts skilled labor into adaptation resources (e.g., air conditioning, building insulation) via $R_t = \frac{1}{\eta}\mathcal{R}_t$, where $\eta > 0$ governs the unit cost. We expect η to be lower in more developed regions (Carleton et al. 2022).

Households have Dixit-Stiglitz preferences over differentiated goods and consume the bundle $C_t = Y_t = \left(\int_0^1 B_{it}^{\frac{1}{\sigma}} Y_{it}^{\frac{\sigma-1}{\sigma}} di\right)^{\frac{\sigma}{\sigma-1}}$ where $\sigma > 1$ is the elasticity of substitution across varieties i and B_{it} is a preference shifter. We assume markets are complete with respect to aggregate risk, so firms discount future cash flows using the household's stochastic discount factor (SDF),

$$\Lambda_{t+1} = \frac{1}{1+r}\left(\frac{C_{t+1}}{C_t}\right)^{-\gamma} \exp\left[(\gamma-1)\eta\left(R_{t+1} - R_t\right)\right].$$

The household's optimality implies $w_{t+1}^R = \eta \frac{\mathbb{E}_t[\Lambda_{t+1}C_{t+1}]}{\mathbb{E}_t[\Lambda_{t+1}]}$.[18]

5.1.2 Firms

Each firm i produces a differentiated variety with Cobb-Douglas technology, $Y_{it} = \tilde{A}_{it} K_{it}^{\tilde{\alpha}_K} N_{it}^{\tilde{\alpha}_N}$, where $\tilde{A}_{it}$ is physical productivity, K_{it} is capital, N_{it} is labor, and $\tilde{\alpha}_K + \tilde{\alpha}_N = 1$. Firms compete monopolistically à la Dixit-Stiglitz. Combining the production function with the demand system implies an equilibrium revenue function of the form

$$P_{it}Y_{it} = Y_t^{\frac{1}{\sigma}} B_{it}^{\frac{1}{\sigma}} \tilde{A}_{it}^{\frac{\sigma-1}{\sigma}} K_{it}^{\alpha_K} N_{it}^{\alpha_N},$$

where $\alpha_F = \left(1 - \frac{1}{\sigma}\right)\tilde{\alpha}_F$ for $F \in \{K, N\}$, and $B_{it}^{\frac{1}{\sigma}} \tilde{A}_{it}^{\frac{\sigma-1}{\sigma}}$ captures the firm's demand-adjusted revenue productivity. Since the market structure is identical to Section 2, an aggregate production function $Y_t = A_t K_t^{\tilde{\alpha}_K} N^{\tilde{\alpha}_N}$ exists for aggregate productivity A_t and capital $K_t = \int_i K_{it}$.

Flexible Inputs and Profits At the beginning of period t, after capital and adaptation decisions are made and all shocks are realized, firms choose labor from a competitive market to maximize profits: $\Pi_{it} = \max_{N_{it}} Y_t^{\frac{1}{\sigma}} B_{it}^{\frac{1}{\sigma}} \tilde{A}_{it}^{\frac{\sigma-1}{\sigma}} K_{it}^{\alpha_K} N_{it}^{\alpha_N} - W_t N_{it}$. Writing the competitive wage W_t as a function of aggregate output, $W_t = \tilde{\alpha}_N \frac{Y_t}{N}$, we can solve for the optimal labor choice and obtain the profit function:

$$\Pi_{it} = G(A_t K_t^{\tilde{\alpha}_K})^{\theta_A} A_{it} K_{it}^{\alpha} \tag{14}$$

where $G := (1-\alpha_N)N^{\tilde{\alpha}_N}$ and $\theta_A = \frac{1}{\sigma} - \left(\frac{\sigma-1}{\sigma}\right)\frac{\alpha_N}{1-\alpha_N}$ summarizes a positive aggregate demand effect and a negative wage effect in general equilibrium. We restrict to the empirically relevant case $\tilde{\alpha}_N > \frac{1}{\sigma-1}$, so $\theta_A < 0$. We define $A_{it} = \left(B_{it}^{\frac{1}{\sigma}} \tilde{A}_{it}^{\frac{\sigma-1}{\sigma}}\right)^{\frac{1}{1-\alpha_N}}$ as the effective productivity (profitability) and $\alpha = \frac{\alpha_K}{1-\alpha_N}$ as the profit curvature of capital.

18. The full budget constraint and derivation are in Appendix E.

5.1.3 Productivity Process and Endogenous Adaptation

We assume firm productivity takes the form

$$\log A_{it} \equiv a_{it} = \beta_{it}\big(T_t - T^*\big) + z_{it} + \bar{a}_i,$$

so that productivity depends on the firm's temperature sensitivity β_{it}, the deviation of climate conditions from the bliss-point temperature $(T_t - T^*)$,[19] a transitory idiosyncratic component z_{it}, and a permanent component $\bar{a}_i \sim \mathcal{N}(0, \sigma^2_{\bar{a}})$. We model the idiosyncratic component as an AR(1) process:

$$z_{i,t+1} = \rho_z z_{it} + \varepsilon^z_{i,t+1}, \qquad \varepsilon^z_{i,t+1} \sim \mathcal{N}(0, \sigma^2_{\varepsilon^z}).$$

The temperature sensitivity comprises three components:

$$\beta_{it} = \underbrace{\beta_i}_{\text{product sensitivity}} + \underbrace{\xi_{it}}_{\text{random sensitivity}} + \underbrace{\widetilde{\beta}_{it}}_{\text{endogeneous sensitivity}}.$$

The product sensitivity $\beta_i \sim \mathcal{N}\left(\bar{\beta}, \sigma^2_\beta\right)$ captures persistent product- or technology-level exposure (e.g., ice-cream versus ski resort) and is known to the firm. The random sensitivity $\xi_{it} \sim \mathcal{N}\left(0, \sigma^2_\xi\right)$ captures unpredictable firm-specific disruptions whose damage scales with distance from the bliss point. Finally, $\widetilde{\beta}_{it}$ is endogenous: achieving $\widetilde{\beta}_{i,t+1}$ costs the firm $\frac{1}{2}H\widetilde{\beta}^2_{i,t+1}$ units of adaptation resources at price w^R_{t+1}, so the marginal cost of resilience is increasing.

5.1.4 Temperature Dynamics and Mid-range Weather Forecasts

We assume local temperature follows a stationary AR(p) process:

$$T_t - \bar{T} = \sum_{\tau=1}^{p} \rho_\tau \left(T_{t-\tau} - \bar{T}\right) + \varepsilon^T_t.$$

Agents observe an unbiased one-step-ahead forecast $\mathbb{E}_{t-1}[T_t]$ and perceive forecast uncertainty $\mathbb{VAR}_{t-1}(T_t)$, which evolves as a smoothed ARCH(q) process:

$$\mathbb{VAR}_{t-1}(T_t) = \frac{1}{q}\sum_{\tau=1}^{q}\left(T_{t-\tau} - \mathbb{E}_{t-\tau-1}[T_{t-\tau}]\right)^2.$$

Thus, perceived uncertainty rises following periods of large forecast errors.

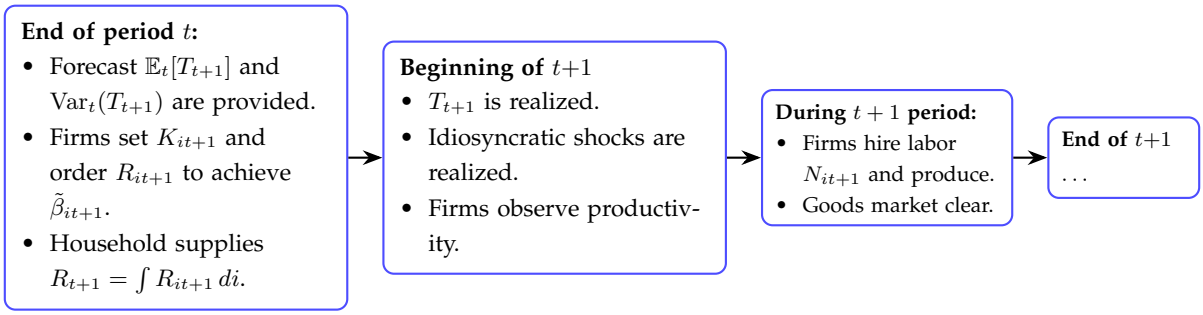
5.1.5 Timing and Dynamic Investment

At the end of period t, agents observe the forecast $\mathbb{E}_t[T_{t+1}]$ with perceived forecast uncertainty $\mathbb{VAR}_t(T_{t+1})$. Given this information, firms choose next-period capital $K_{i,t+1}$ and adaptation intensity $\widetilde{\beta}_{i,t+1}$; households supply aggregate adaptation resources $R_{t+1} = \int R_{i,t+1}\, di$. At the beginning of period $t+1$, temperature T_{t+1} and all idiosyncratic shocks are realized. Firms then

19. T^* denotes the bliss-point temperature emphasized in the climate-econometrics literature, typically estimated to lie around $10 - 13^\circ$C. For example, Burke, Hsiang, and Miguel (2015) estimate $T^* \approx 12^\circ$C.

observe realized productivity, choose flexible labor input $N_{i,t+1}$ to produce, and goods markets clear. Figure 8 illustrates the full timing of decisions in the model.

Figure 8: Timing of events in the model.



The firm's dynamic problem can be written as the Bellman equation

$$
\begin{aligned}
V(\mathbf{x}_t, \mathbf{x}_{it}, \mathbf{d}_t, \Gamma_{\text{micro},t}) = \max_{K_{i,t+1},\, \widetilde{\beta}_{i,t+1}} \Bigg\{ & G A_t^{\theta_A} K_t^{\theta_K} \underbrace{\exp\Big[\big(\beta_i + \xi_{it} + \widetilde{\beta}_{i,t+1}\big)\big(T_{t+1} - T^*\big) + z_{i,t+1} + \bar{a}_i\Big]}_{\equiv A_{i,t+1}} K_{it}^{\alpha} \\
& - \left(\frac{1}{2} H \widetilde{\beta}_{i,t+1}^2\right) w_{t+1}^R - K_{i,t+1} - \frac{r+\delta}{1+r} K_{i,t+1}\big(\mathcal{T}_{i,t+1} - 1\big) + (1-\delta) K_{it} \\
& + \mathbb{E}_t[\Lambda_{t+1}\, V(\mathbf{x}_{t+1}, \mathbf{x}_{i,t+1}, \mathbf{d}_{t+1}, \Gamma_{\text{micro},t+1})] \Bigg\}.
\end{aligned}
\tag{15}
$$

where

$$
\mathbf{x}_t \equiv \big(\mathbb{E}_t[T_{t+1}],\ \mathbb{VAR}_t(T_{t+1})\big), \qquad \mathbf{x}_{it} \equiv \big(K_{it},\ z_{it},\ \bar{a}_i,\ \beta_i,\ \xi_{it},\ \mathcal{T}_{i,t+1}\big), \qquad \mathbf{d}_t \equiv \big(A_t,\ K_t,\ R_t\big)
$$

collect the aggregate temperature moments, firm-level states, and aggregate endogenous variables, respectively; $\Gamma_{\text{micro},t}$ is the cross-sectional distribution of firm states, Λ_{t+1} is the stochastic discount factor, δ is the depreciation rate, and $\mathcal{T}_{i,t+1}$ is the firm-specific capital wedge.

Adaptation Costs Adaptation enters productivity multiplicatively: when $\widetilde{\beta}_{i,t+1}(T_{t+1} - T^*) > 0$, effective TFP rises by the factor $\exp\{\widetilde{\beta}_{i,t+1}(T_{t+1} - T^*)\}$. Because the payoff scales with the firm's operating scale while costs are convex in $\widetilde{\beta}_{i,t+1}$, adaptation is *non-homothetic*: scaling up the firm does not scale up optimal adaptation one-for-one. Heterogeneity in scale and fundamentals therefore translates directly into heterogeneity in endogenous adaptation choices.

Frictions in the Capital Market Firms face heterogeneous capital market distortions summarized by the (log) wedge $\tau_{i,t+1} \equiv \log \mathcal{T}_{i,t+1}$:

$$
\tau_{i,t+1} = \omega_{\bar{a}} \bar{a}_i + \phi_{i,t+1}^{\tau}, \qquad \omega_{\bar{a}} > 0.
$$

The first component captures *size-dependent* distortions: when $\omega_{\bar{a}} > 0$, firms with higher permanent productivity $\bar{a}_i$ (and hence larger scale) face systematically larger wedges, in the spirit of Restuccia and Rogerson (2008). The second component $\phi_{i,t+1}^{\tau}$ captures idiosyncratic distortions

and follows an AR(1) process,

$$\phi^{\tau}_{i,t+1} = \rho^{\tau}_{\phi}\,\phi^{\tau}_{i,t} + \varepsilon^{\phi^{\tau}}_{i,t+1}, \qquad \varepsilon^{\phi^{\tau}}_{i,t+1} \sim \mathcal{N}(0, \sigma^2_{\varepsilon^{\phi^{\tau}}}).$$

A firm with wedge $\mathcal{T}_{i,t+1}$ pays an additional $\mathcal{T}_{i,t+1} - 1$ on the risk-free user cost for each unit of installed capital.

Firm's Optimality Conditions The firm's optimal investment policies follow from the Bellman problem in (15). Optimal capital accumulation satisfies the Euler equation

$$\frac{1}{1+r}(r+\delta)\mathcal{T}_{i,t+1} = \alpha G\, K^{\theta_K}_{t+1} K^{\alpha-1}_{i,t+1}\, \mathbb{E}_t\Big[\Lambda_{t+1}\big(A^{\theta_A}_{t+1} e^{a_{i,t+1}}\big)\Big] + (1-\delta)\,\mathbb{E}_t\left[\Lambda_{t+1} - \frac{1}{1+r}\right].$$

Optimal adaptation satisfies

$$\widetilde{\beta}_{i,t+1} = \frac{G}{w^R_{t+1} H}\, K^{\theta_K}_{t+1} K^{\alpha}_{i,t+1}\, \mathbb{E}_t\Big[\Lambda_{t+1} A^{\theta_A}_{t+1} e^{a_{i,t+1}}\big(T_{t+1} - T^*\big)\Big].$$

Adaptation is increasing in expected scale and in distance from the bliss point, and decreasing in the resource cost $w^R_{t+1} H$.

The Homogeneous Deterministic Steady State To build intuition, consider a homogeneous deterministic steady state (HDSS) with no firm heterogeneity and no uncertainty.

$$\widetilde{\beta} = \kappa\,(\bar{T} - T^*), \qquad \kappa = \frac{1-\alpha_N}{(1+r)\eta H} > 0.$$

Steady-state adaptation is positive in warm regions ($\bar{T} > T^*$) and negative in cold regions ($\bar{T} < T^*$), with magnitude proportional to the distance from the bliss point.

5.2 Solving the Model

We solve the model in closed form using a risk-adjusted perturbation around the HDSS, following Coeurdacier, Rey, and Winant (2011) and David and Venkateswaran (2019). The approach proceeds in three steps: (i) we develop a second-order expansion of stochastic variables in conditional moments to approximate the risk-adjusted FOCs; (ii) we approximate firms' policy rules using an affine–bilinear expansion in firm-level and aggregate state vectors; and (iii) we substitute the approximated policy rules and aggregation equations into all equilibrium conditions and solve for the unknown coefficients by matching terms of equal order. This guess-and-verify procedure yields closed-form expressions for both micro policies and macro equilibrium objects, including MRPK dispersion and the resulting aggregate TFP losses. We provide the full derivation in Appendix E.

5.3 Investment and Adaptation in the Cross-section

We now analyze how cross-sectional differences in firms' capital and adaptation responses to climate shocks and climate risk generate dispersion in realized MRPK. We focus on the empiri-

cally relevant warm-region case in which heat remains productivity-reducing on average despite adaptation.

Definition 1 (A typical warm region.) *The climate is above the bliss point $\bar{T} > T^*$ where firms adapt positively $\tilde{\beta} > 0$, the average firm is heat-sensitive $\bar{\beta} < 0$, and adaptation is sufficiently costly $\eta H > \frac{(1-\alpha_N)(\bar{T}-T^*)}{(1+r)(-\bar{\beta})}$. Such world implies $\bar{\beta} + \widetilde{\beta} < 0$.*

Proposition 2 shows that cross-sectional differences in both adaptation and capital investment are driven by expected productivity and the covariance between firm profitability and temperature risk.

Proposition 2 (Investment and Adaptation) *Let $\Delta^i x_{it} \equiv x_{it} - \bar{x}_t$ denote firm i's deviation from the time-t cross-sectional mean. The expected profit is increasing in expected productivity but declining in wedges,*

$$\Delta^i \mathbb{E}_t \hat{\pi}_{it+1} \;=\; \Delta^i \mathbb{E}_t \hat{a}_{it+1} - \alpha\, \Delta^i \hat{\tau}_{it+1}.$$

In equilibrium, optimal policy decisions satisfy:

(i) ***Adaptation.***

$$\Delta^i \hat{\tilde{\beta}}_{it+1} = \frac{\tilde{\beta}}{1-\alpha}\left[\Delta^i \mathbb{E}_t \hat{\pi}_{it+1} + \Omega\, \mathrm{Cov}_t\Big(\hat{a}_{it+1}, \hat{T}_{t+1}\Big)\right] \tag{16}$$

(ii) ***Capital.***

$$\Delta^i \hat{k}_{it+1} = -\Delta^i \hat{\tau}_{it+1} + \frac{1}{1-\alpha}\,\Delta^i \mathbb{E}_t \hat{\pi}_{it+1} \;+\; \frac{\bar{\beta}+\tilde{\beta}}{1-\alpha}\,\Theta\,\Delta^i\,\mathrm{Cov}_t\Big(\hat{a}_{it+1}, \hat{T}_{t+1}\Big). \tag{17}$$

where $\Theta = \left(\frac{\sigma}{\sigma-1} - \tilde{\alpha}_N\right)(\theta_A - \gamma) + 1 < 0$, *and* $\Omega \equiv (\bar{\beta}+\tilde{\beta})\Theta + \frac{1-\alpha}{\bar{T}-T^*} > 0$.

Firms with higher expected productivity and lower wedges anticipate a larger profit base, and therefore adapt and invest more. A higher covariance $\mathbb{COV}_t(\hat{a}_{it+1}, \hat{T}_{t+1})$ raises risk-adjusted returns because the firm's productivity is high precisely in hot, high-marginal-utility states. In a typical warm region, firms whose productivity co-moves more positively with temperature invest and adapt more.

Corollary 1 shows that firms tilt toward adaptation relative to capital when facing larger capital wedges. Since the marginal payoff to adaptation is more state-contingent than that of capital, firms with higher temperature covariance also tilt further toward adaptation.

Corollary 1 (Within-firm Adaptation-capital Trade-off) *Combining part (i) and (ii) in Proposition 2 yields an expression for how a firm tilts its choices toward adaptation relative to capital:*

$$\frac{\Delta^i \widehat{\tilde{\beta}}_{it+1}}{\tilde{\beta}} - \Delta^i \hat{k}_{it+1} = \underbrace{\Delta^i \widehat{\tau}_{it+1}}_{\textit{relative price}} + \underbrace{\frac{\widetilde{\beta}}{\bar{T}-T^*}\,\Delta^i \mathbb{COV}_t\Big(\hat{a}_{it+1}, \widehat{T}_{t+1}\Big)}_{\textit{relative risk/curvature}}.$$

Proposition 2 and Corollary 1 characterize equilibrium forces but involve endogenous objects. We now solve the fixed-point problem and express firms' choices as functions of primitives and temperature forecasts. To ease interpretation, we introduce an endogenous sensitivity index.

Definition 2 (Endogenous Sensitivity Index) *Ψ_{it} collects the endogenous component of a firm's effective temperature sensitivity.*

$$\Psi_{it} = \Upsilon \left[\left(\bar{T} - T^* \right) \hat{\beta}_i + \bar{a}_i + \rho_z z_{it} - \alpha \tau_{it+1} \right], \tag{18}$$

where $\Upsilon = \frac{\tilde{\beta}}{1-\alpha-\tilde{\beta}\left(\bar{T}-T^*\right)}$ is the endogenous sensitivity multiplier with $\Upsilon > 0$ in the typical warm region.

The index increases with the firm's persistent and predictable productivity components ($\bar{a}_i$ and $\rho_z z_{it}$), intrinsic temperature exposure $\hat{\beta}_i(\bar{T} - T^*)$ and decreases with the effective user cost of capital (τ_{it+1}). Economically, Ψ_{it+1} summarizes the *aggregate-state-independent* profitability of a firm.

Proposition 3 (Policy Functions.) *(i) **Adaptation.***

$$\Delta^i \hat{\tilde{\beta}}_{it+1} = \Psi_{it+1} + \Upsilon \left(\hat{\beta}_i + \Psi_{it+1} \right) \left(\mathbb{E}_t(\hat{T}_{t+1}) + \Omega \mathbb{VAR}_t \left[\hat{T}_{t+1} \right] \right); \tag{19}$$

*(ii) **Capital.***

$$\Delta^i \hat{k}_{it+1} = -\tau_{it+1} + \frac{\Psi_{it+1}}{\tilde{\beta}} + \Upsilon \left(\hat{\beta}_i + \Psi_{it+1} \right) \left(\mathbb{E}_t(\hat{T}_{t+1}) + \left[\left(\bar{\beta} + \tilde{\beta} \right) \Theta + \tilde{\beta} \right] \mathbb{VAR}_t \left[\hat{T}_{t+1} \right] \right). \tag{20}$$

Both adaptation and capital investment increase with the endogenous sensitivity index and with aggregate temperature moments. Crucially, the effects of expected temperature and forecast uncertainty are multiplied by the firm's *effective exposure* $(\hat{\beta}_i + \Psi_{it+1})$, which combines intrinsic product sensitivity with endogenous adaptation. The mapping from expected scale to adaptation is governed by the *endogenous sensitivity multiplier*,

$$\Upsilon = \frac{\widetilde{\beta}}{1 - \alpha - \widetilde{\beta}(\bar{T} - T^*)} = \frac{\tilde{\beta}}{1-\alpha} \cdot \sum_{r=1}^{\infty} \left(\frac{\tilde{\beta}\left(\bar{T} - T^*\right)}{1-\alpha} \right)^r,$$

which captures the fixed-point feedback between scale and adaptation: higher profits raise the marginal value of adaptation, which raises productivity by $(\bar{T} - T^*)$, which raises profits again, generating a geometric series with loop gain $\frac{\tilde{\beta}(\bar{T}-T^*)}{1-\alpha}$.

Higher expected heat raises both adaptation and capital more for firms with greater effective exposure. In a typical warm region, expected warming therefore disproportionately increases investment and adaptation among firms already operating at larger scale (high Ψ) or with more temperature-exposed products (high $\hat{\beta}_i$), widening within-region dispersion. Forecast uncertainty further amplifies this heterogeneity. Endogenous adaptation is self-reinforcing: by raising effective productivity in hot states, it lowers risk premia, which further strengthens incentives to invest and adapt.

5.3.1 What Determines MRPK?

Using the profit function in Equation (14) and the constant markups implied by the Dixit-Stiglitz competition, log MRPK can be written (up to constants) as

$$\widehat{mrpk}_{it+1} = \hat{a}_{it+1} - (1-\alpha)\hat{k}_{it+1} + \theta_A \hat{y}_{t+1}. \tag{21}$$

Realized MRPK reflects ex post productivity surprises and ex ante capital choices. The aggregate term $\theta_A \hat{y}_{t+1}$ drops out of cross-sectional comparisons. Substituting the policy functions (19)–(20) into (21) yields:

Proposition 4 (Cross-sectional MRPK Differences.) *Comparing to the average firm, the cross-sectional differences in (log) MRPK of firm i can be written as*

$$\Delta^i \widehat{mrpk}_{it+1} = \underbrace{\left(\Delta^i a_{it+1} - \mathbb{E}_t \Delta^i \widehat{a}_{it+1}\right)}_{\textit{Unexpected Productivity}} + \underbrace{\widehat{\tau}_{it+1}}_{\textit{Distortions}} \underbrace{- (\bar{\beta} + \widetilde{\beta})\Theta \left[\widehat{\beta}_i + \Psi_{it+1}\right] \mathbb{VAR}_t \left(\widehat{T}_{t+1}\right)}_{\textit{Temperature Uncertainty}} \tag{22}$$

where the unexpected productivity can be expressed as

$$\Delta^i a_{it+1} - \mathbb{E}_t \Delta^i \widehat{a}_{it+1} = \underbrace{\left[\widehat{\beta}_i + \Psi_{it+1}\right]\left(\widehat{T}_{t+1} - \mathbb{E}_t\left(\widehat{T}_{t+1}\right)\right)}_{\textit{Temperature's Forecast Error}} + \underbrace{\xi_{it+1}\left(T_{t+1} - T^*\right)}_{\textit{Temperature's Random Damage}} + \varepsilon^z_{it+1} \tag{23}$$

Three forces drive cross-sectional MRPK heterogeneity. First, because capital is predetermined, productivity surprises translate directly into MRPK variation. A common heat surprise generates heterogeneous shocks through firm-specific effective exposure ($\widehat{\beta}_i + \Psi_{it+1}$), while idiosyncratic disruptions $\xi_{it+1}(T_{t+1} - T^*)$ grow more severe as climate deviates from the bliss point. Second, higher capital wedges depress investment, mechanically raising MRPK—the standard misallocation force. Third, higher temperature uncertainty lowers realized MRPK for firms with greater effective exposure, because such firms command more favorable risk premia and therefore accumulate more capital ex ante.

5.3.2 The Equilibrium MRPK Dispersion

This cross-sectional disparity in realized returns leads directly to the equilibrium misallocation of capital. Proposition 5 presents all the forces driving the dispersion.

Proposition 5 (Capital (Mis)Allocation in Equilibrium.) *The equilibrium MRPK dispersion admits the decomposition*

$$\begin{aligned}
\sigma^2_{mrpk,t+1} = \; & \underbrace{\mathbb{VAR}^i(\tau_{it+1})}_{\textit{baseline wedge dispersion}} + \underbrace{\sigma^2_{\varepsilon^z}}_{\textit{non-climate idiosyncratic productivity}} + \underbrace{\sigma^2_\xi \left(T_{t+1} - T^*\right)^2}_{\textit{random climate damages}} \\
& \underbrace{+ \mathbb{VAR}^i(\widehat{\beta}_i + \Psi_{i,t+1})\left(\widehat{T}_{t+1} - \mathbb{E}_t\left[\widehat{T}_{t+1}\right] - (\bar{\beta} + \widetilde{\beta})\Theta \mathbb{VAR}_t\left(\widehat{T}_{t+1}\right)\right)^2}_{\textit{exposure-amplified forecast error \& risk}} \\
& \underbrace{+ 2\,\mathbb{COV}^i(\tau_{it+1}, \widehat{\beta}_i + \Psi_{i,t+1})\left(\widehat{T}_{t+1} - \mathbb{E}_t\left[\widehat{T}_{t+1}\right] - (\bar{\beta} + \widetilde{\beta})\Theta \mathbb{VAR}_t\left(\widehat{T}_{t+1}\right)\right)}_{\textit{wedge–exposure interaction}},
\end{aligned} \tag{24}$$

where

$$\mathbb{VAR}^i(\tau_{it+1}) = \omega_{\tilde{a}}^2\sigma_{\tilde{a}}^2 + \sigma_{\phi^\tau}^2, \tag{25}$$

$$\mathbb{VAR}^i(\widehat{\beta}_i + \Psi_{i,t+1}) = \frac{(1-\alpha)^2\sigma_{\hat{\beta}}^2 + \widetilde{\beta}^2\Big((1-\alpha\omega_{\tilde{a}})^2\sigma_{\tilde{a}}^2 + \rho_z^2\sigma_z^2 + \alpha^2\sigma_{\phi^\tau}^2\Big)}{\big(1-\alpha-\widetilde{\beta}(\bar{T}-T^*)\big)^2}, \tag{26}$$

$$\mathbb{COV}^i(\tau_{it+1}, \widehat{\beta}_i + \Psi_{i,t+1}) = \frac{\widetilde{\beta}}{1-\alpha-\widetilde{\beta}(\bar{T}-T^*)}\left(\omega_{\tilde{a}}(1-\alpha\omega_{\tilde{a}})\sigma_{\tilde{a}}^2 - \alpha\sigma_{\phi^\tau}^2\right). \tag{27}$$

The first two terms of Proposition 5 capture baseline dispersion from wedges and non-climate productivity shocks, which would arise even without any temperature risk. The third term captures unpredictable climate damage that happens as temperature moves away from the bliss point. The magnitude of the impact is governed by idiosyncratic sensitivity dispersion σ_ξ^2. Importantly, this channel remains active even if all firms are well-adapted and aggregate temperature is perfectly forecasted.

The last two terms operate through aggregate weather—bundling forecast errors and risk-adjusted uncertainty—scaled by the cross-sectional dispersion of effective exposure and its covariance with capital wedges. Conditional on the same aggregate temperature moments, two regions differ in misallocation through $\mathbb{VAR}^i(\widehat{\beta}_i + \Psi_{i,t+1})$ and $\mathbb{COV}^i(\tau_{it+1}, \widehat{\beta}_i + \Psi_{i,t+1})$.

The variance term implies that greater dispersion of effective exposure—from heterogeneous product sensitivity or endogenous adaptation—amplifies misallocation. Crucially, better average adaptation need not reduce misallocation: lower adaptation costs raise steady-state adaptation $\tilde{\beta}$, which widens the differential response across firms and steepens the mapping from temperature risk to MRPK dispersion. The covariance term captures the interaction between distortions and exposure: misallocation rises when more distorted firms are also more temperature-exposed or more adapted. Together, these two channels show that cross-region differences in capital misallocation depend not only on aggregate temperature and forecast quality, but also on within-region heterogeneity in firm characteristics.

6 Reduced-Form Evidence for the Model Mechanisms

The model delivers two testable mechanisms linking temperature to MRPK dispersion: a *level channel* through which climate extremes raise damage volatility, and a *forecast-and-risk channel* through which temperature surprises and uncertainty are amplified by heterogeneous effective exposure. This section provides reduced-form evidence for both, first at the firm level, and then at the region-sector level.

6.1 Firm-Level Evidence

6.1.1 Adaptation Rises with Capital and Distortions

The linearized policy rules imply a within-firm capital–adaptation trade-off:

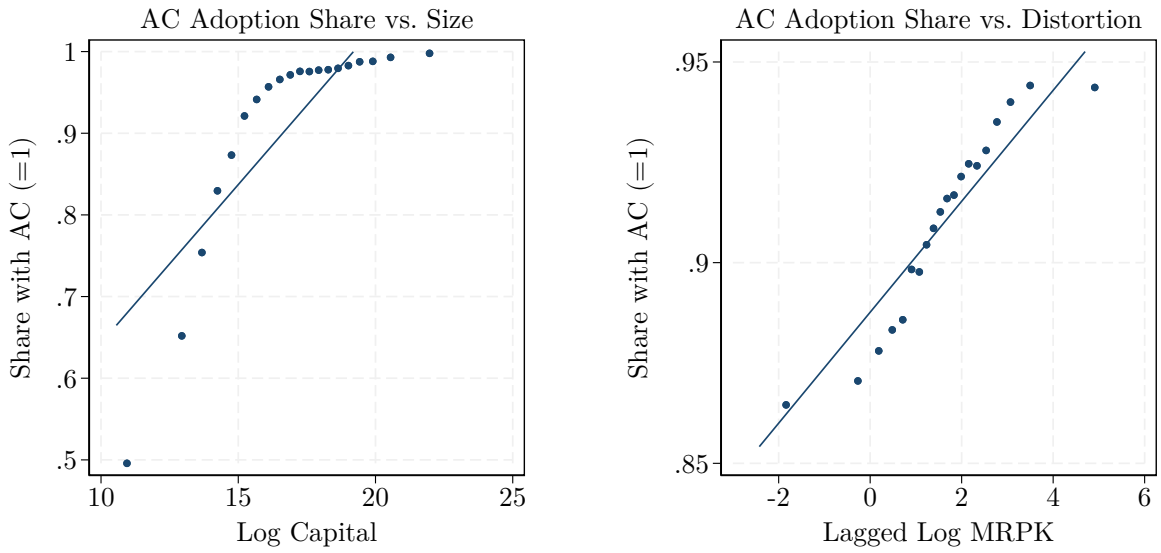
$$\frac{\Delta^i \widehat{\widetilde{\beta}}_{i,t+1}}{\widetilde{\beta}} = \Delta^i \hat{k}_{i,t+1} + \Delta^i \widehat{\tau}_{i,t+1} + \frac{1}{\bar{T} - T^*} \Delta^i \mathbb{COV}_t \left(\hat{a}_{i,t+1}, \widehat{T}_{t+1} \right), \tag{28}$$

where Δ^i denotes deviations from the region-year mean. In warm regions ($\widetilde{\beta} > 0$), larger firms choose higher adaptation, and firms facing higher capital wedges tilt toward adaptation relative to capital.[20] We test these predictions by estimating

$$\mathbf{1}\{AC_{it} = 1\} = \lambda_1 k_{it} + \lambda_2 mrpk_{i,t-1} + \eta_{r,s,t} + u_{it}, \tag{29}$$

where $\eta_{r,s,t}$ are region–sector–year fixed effects and lagged MRPK proxies for capital wedges.[21] Consistent with (28), AC adoption is increasing in firm capital and in lagged MRPK conditional on scale (Figure 9).

Figure 9: AC adoption, capital and wedges



Notes: Figure 9 is constructed using the `binsreg` while controlling for firm and region-sector-year fixed effects.

6.1.2 Heterogeneous MRPK Responses to Heat Shocks

The model predicts that a common temperature surprise generates heterogeneous MRPK responses proportional to firms' effective exposure. Since endogenous adaptation scales with capital and wedges, we can write $\Delta^i \widehat{mrpk}_{i,t} \propto \widetilde{\beta} \left(\Delta^i \hat{k}_{it} + \Delta^i \hat{\tau}_{it} \right) \left(\widehat{T}_t - \mathbb{E}_{t-1}[\widehat{T}_t] \right)$, conditional on intrinsic sensitivity. We test this by interacting temperature bins with lagged capital and lagged MRPK in

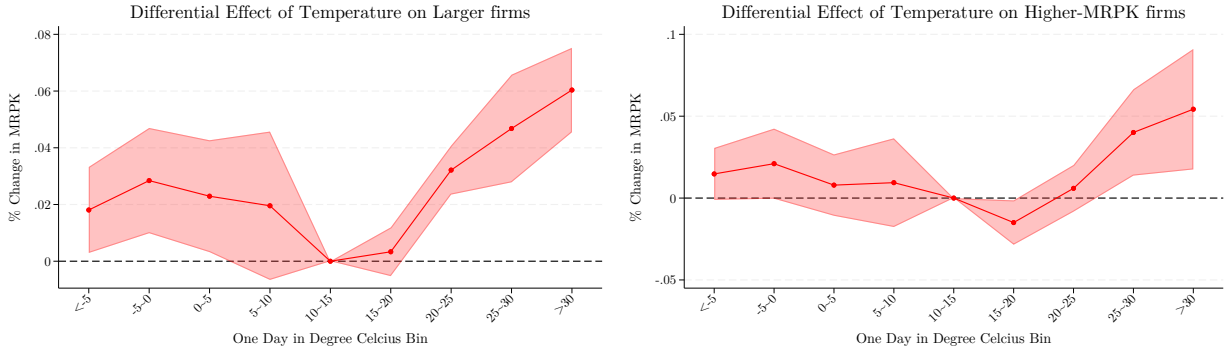
20. Direct measures of firm-level adaptation are rare. We proxy adaptation with computerized air-conditioning (AC) adoption from the Indian ASI, which records this variable for 2001–2014.

21. In the accounting framework, wedge-induced capital scarcity maps into systematically higher MRPK, making lagged MRPK a natural proxy for τ_{it}.

a firm-level panel regression with firm and country–sector–year fixed effects.[22]

Figure 10 confirms the prediction: conditional on distortions, extreme heat shifts MRPK more for firms with more capital; conditional on capital, extreme heat shifts MRPK more for more distorted firms.

Figure 10: Differential MRPK response to heat shocks interacted with capital and distortions



(a) Heterogeneous Effect with Capital

(b) Heterogeneous Effect with Distortion

6.2 Region–Sector Evidence

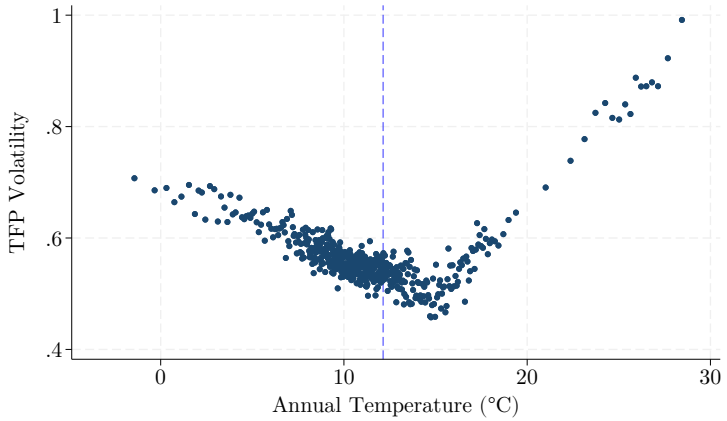
6.2.1 Mechanism 1: Climate Extremes Raise Damage Volatility

The level channel predicts that TFP volatility is minimized near T^* and rises as temperature departs from the bliss point. We measure TFP volatility as the within-cell variance of first-differenced firm productivity, $\mathrm{Var}_{(r,s)t}(\hat{a}_{it} - \hat{a}_{it-1})$, following Asker, Collard-Wexler, and De Loecker (2014).[23] Figure 11 plots this measure against annual average temperature after residualizing on region–sector and country–sector–year fixed effects. The U-shape is clear: volatility is minimized around 12–15°C and rises as temperature moves away from that range.

22. Specifically, we estimate $mrpk_{i,t} = \sum_b \lambda_b \, Tbin^b_{r,t} + \sum_b \lambda_{b,k} \, (Tbin^b_{r,t} \times \widetilde{k}_{i,t-1}) + \sum_b \lambda_{b,\tau} \, (Tbin^b_{r,t} \times \widetilde{mrpk}_{i,t-1}) + \boldsymbol{\delta} \boldsymbol{X}_{it} + \delta_i + \alpha_{s,c(r),t} + \varepsilon_{i,t}$, where $Tbin^b_{r,t}$ counts days in temperature bin b, $\widetilde{k}_{i,t-1}$ and $\widetilde{mrpk}_{i,t-1}$ are demeaned, and the omitted bin is 5–10°C. Using lagged variables aligns with the model's timing: capital and adaptation are chosen before temperature is realized.

23. We use first differences rather than innovations from the productivity law of motion to avoid sensitivity to specification of the AR process and agents' information set.

Figure 11: TFP volatility and average temperature.

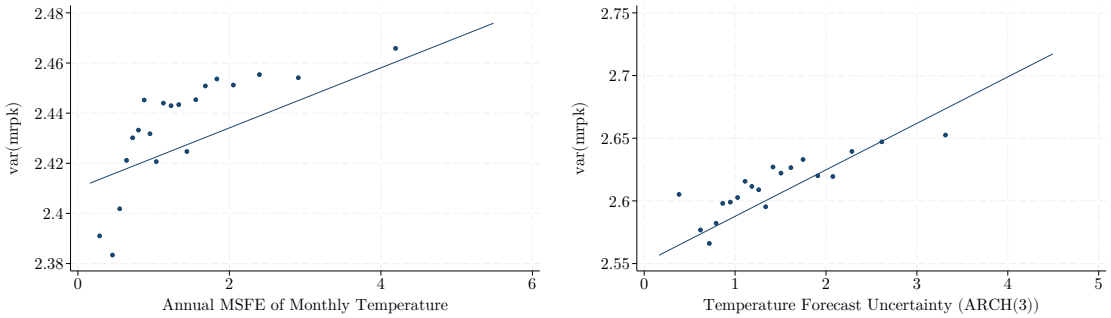


Notes: Figure 11 is constructed using the `binsreg` while controlling for region-sector and country-sector-year fixed effects.

6.2.2 Mechanism 2: Forecast Errors and Uncertainty Amplify MRPK Dispersion

Figure 12 shows that, after controlling for panel fixed effects, both larger forecast errors (annual MSFE of monthly temperature) and higher perceived forecast uncertainty (computed under ARCH(3)) are associated with greater MRPK dispersion. These patterns confirm the forecast-and-risk channel: when mid-range forecasts are less precise, temperature surprises and uncertainty translate more strongly into cross-firm dispersion in capital returns.

Figure 12: Forecast Accuracy, Uncertainty and Misallocation



(a) Contemporaneous Forecast Accuracy (b) ARCH(3) Forecast uncertainty

Notes: Figure 12 is constructed using the `binsreg` while controlling for region-sector and country-sector-year fixed effects.

7 Model Estimation and Quantitative Results

7.1 Estimation

This section describes how we bring the model in Section 5 to the data and quantify the contribution of temperature-driven misallocation to aggregate climate damages. We estimate the model parameters jointly using firm panels spanning 1,916 regions in the EU, China, and India. The closed-form solution delivers explicit policy rules and an accounting decomposition of realized

MRPK dispersion into (i) wedge-driven dispersion, (ii) idiosyncratic climate damages that scale with distance from the bliss point, and (iii) forecast-error and forecast-uncertainty components that are amplified by heterogeneity in firms' effective exposure. This structure yields a transparent mapping from primitives to observable moments, which we exploit in a Generalized Method of Moments (GMM) estimation of regional adaptation costs and climate-damage parameters.

The need for Joint Estimation Two features of the model make joint estimation essential. First, the temperature bliss point T^* is identified from how temperature affects volatility—TFP volatility and MRPK dispersion—but volatility is itself shaped by endogenous adaptation. Pinning down T^* therefore requires disciplining adaptation costs, because heterogeneity in adaptation contributes mechanically to measured volatility. Second, the firm-level fundamentals that drive the relevant cross-sectional moments are not directly observed. In the model, realized productivity and MRPK reflect not only permanent and transitory productivity components ($\bar{a}_i, z_{it}$) and wedges (τ_{it}) , but also heterogeneous temperature exposure through intrinsic product sensitivity ($\hat{\beta}_i$) and endogenous adaptation (Ψ_{it}). As a result, identification cannot proceed by simply inverting firm outcomes to recover primitives. Instead, bliss point T^*, product sensitivity $\hat{\beta}_i$ and the regional effective adaptation cost $\eta_r H_r$ governing the strength of Ψ_{it} must be jointly identified together with all micro-fundamentals in a model-consistent way under regional general equilibrium.

7.1.1 Parameterization and Measurement

We split parameters into (i) standard preference and technology parameters that we calibrate externally and impose to be common across regions, and (ii) climate- and region-specific objects that we discipline using moments from the data.

We take one model period to be one year and set the discount factor to $1/(1+r) = 0.96$. We set the CRRA coefficient to $\gamma = 5$, which lies within the median range commonly used in the macro literature (e.g., Mehra and Prescott (1985)). On the production side, we adopt the same demand elasticity as in the accounting exercise and set $\sigma = 4$. We set the Cobb–Douglas factor shares to $\hat{\alpha}_K = 0.35$ and $\hat{\alpha}_N = 0.65$. Under monopolistic competition, these imply revenue exponents $\alpha_F = (1 - 1/\sigma)\hat{\alpha}_F$ for $F \in \{K, N\}$, and hence the profit curvature $\alpha \equiv \frac{\alpha_K}{1-\alpha_N} = 0.51$. These parameters are held fixed across all regions in our baseline. With these parameters, we can map observables to model objects. Consistent with the model's profit function, we measure firm productivity as $a_{it} \equiv py_{it} - \alpha k_{it}$, where py_{it} and k_{it} are log sales and log capital, respectively. Similarly, up to constants common within a region-year (e.g., markups and aggregate price terms), log MRPK can be measured as $mrpk_{it} \equiv py_{it} - k_{it}$, which matches our reduced-form construction and is the sufficient statistic that enters the MRPK-dispersion moments.

As is standard in the literature, we assume the temperature bliss point T^* is common across regions, since it is identified from differential responses of TFP volatility to temperature variation across climates. We also impose that the volatility of random climate damages, σ^2_ξ, is common across regions, because all heterogeneity in product exposure and adaptation is captured by β_i and Ψ_i.[24] For product-level sensitivity, β_i, we assume it is common within each 3-digit USSIC

24. We also find limited heterogeneity in the TFP-volatility response to temperature across levels of economic devel-

sector.[25] For all other firm-level fundamentals (e.g., $\bar{a}_i$, z_{it}, and wedge components), we allow them to be firm-specific, with their cross-sectional moments varying by region.

Adaptation costs. The key regional object governing endogenous adaptation is the effective cost of adaptation resources, $\eta_r H_r$, which enters the model only through the product $\eta_r H_r$ and therefore cannot be separately identified. To allow adaptation costs to vary systematically with development, we parameterize the inverse cost as a flexible function of long-run income: $\frac{1}{\eta_r H_r} \equiv f\big(\overline{\ln \mathrm{GDP}_r}\big)$, where $f(\cdot)$ is a fourth-order polynomial in $\overline{\ln \mathrm{GDP}_r}$. Under this parameterization, steady-state adaptation intensity in region r can be written as $\widetilde{\beta}_r = \frac{1-\alpha_N}{1+r} f\big(\overline{\ln \mathrm{GDP}_r}\big)\ (\bar{T}_r - T^*)$. Moreover, the endogenous-sensitivity multiplier that appears in the policy rules and in the MRPK dispersion, $\widetilde{\beta}_r/\big(1-\alpha-\widetilde{\beta}_r(\bar{T}_r - T^*)\big)$, admits a convenient local approximation around $\bar{T}_r = T^*$ and $f = f^*$:

$$\frac{\widetilde{\beta}_r}{1-\alpha-\widetilde{\beta}_r(\bar{T}_r - T^*)} = \frac{1-\alpha_N}{(1+r)(1-\alpha)}\Big[\, f^*(\bar{T}_r - T^*) + (\bar{T}_r - T^*)\Big(f(\overline{\ln \mathrm{GDP}_r}) - f^*\Big)\Big] + O\big(\Delta f^3, \Delta \bar{T}_r^3\big), \tag{30}$$

so that, under the cubic specification for $f(\cdot)$, the multiplier becomes a simple polynomial function of long-run temperature and long-run GDP per capita.

Temperature and Forecasts. Lastly, we estimate the temperature process. Following Nath, Ramey, and Klenow (2023), we fit a climate-dependent autoregressive process for annual regional temperature with two-way fixed effects:

$$T_{rt} = \sum_{\tau=1}^{p} \Big(\rho_\tau^0 + \rho_\tau^{\bar{T}} \bar{T}_r^{1951\text{–}2018}\Big) T_{r,t-\tau} + \chi_r + \chi_t + \varepsilon_{rt}^T, \tag{31}$$

where the persistence coefficients vary flexibly with a region's long-run mean temperature $\bar{T}_r^{1951\text{–}2018}$. We set $p = 6$ as our baseline to capture medium-run temperature persistence while remaining parsimonious in annual data. The fitted values from (31) define the one-step-ahead statistical forecast $\widehat{\mathbb{E}}_{t-1}[T_{rt}]$, and we use the estimated innovations $\widehat{\varepsilon}_{rt}^T \equiv T_{rt} - \widehat{\mathbb{E}}_{t-1}[T_{rt}]$ as our empirical counterpart to the model's annual forecast error $T_{rt} - \mathbb{E}_{t-1}[T_{rt}]$.

To discipline squared forecast errors and hence forecast uncertainty, we use mid-range forecast data from ECMWF as in our reduced-form exercise. Let MSFE_{rt} denote the region-year mean squared error of monthly ECMWF forecasts, aggregated to the annual level. Because the ECMWF product is monthly (rather than year-ahead), we rescale the implied monthly forecast errors to be consistent with the unconditional variance of annual forecast innovations in our sample (1998–2018). Concretely, we map MSFE_{rt} into an annual forecast-error variance by preserving ECMWF's relative improvement over a monthly AR(6) benchmark:

$$\big(T_{rt} - \mathbb{E}_{t-1}T_{rt}\big)^2 = \frac{\mathrm{MSFE}_{rt}}{\frac{1}{12}\sum_{m=1}^{12} \mathbb{VAR}^{1998\text{–}2018}\big(\widehat{\varepsilon}_{rmt}^T\big)}\ \mathbb{VAR}^{1998\text{–}2018}\big(\widehat{\varepsilon}_{rt}^T\big), \tag{32}$$

opment.

25. To implement this in India and China, we harmonize the NIC-04 and GB-2002 classifications to USSIC at the 3-digit level.

where $\hat{\varepsilon}^T_{rmt}$ denotes the month-m AR(6) forecast error and $\hat{\varepsilon}^T_{rt}$ denotes the annual AR(6) forecast innovation. This scaling preserves time variation in forecast precision from ECMWF while matching the annual scale of temperature innovations in the estimation sample. Finally, we model perceived temperature uncertainty as a smoothed ARCH(3) process:

$$\mathbb{VAR}_{t-1}(T_{rt}) = \frac{1}{3}\sum_{\tau=1}^{3}\left(T_{r,t-\tau} - \mathbb{E}_{t-\tau-1}T_{r,t-\tau}\right)^2, \tag{33}$$

so that agents perceive temperature to be more volatile following periods with larger recent forecast errors.

7.1.2 Identification and Estimation

The model is identified from four sets of moment conditions, detailed in Appendix F. First, standard firm fixed-effect and Yule–Walker conditions recover the permanent and transitory components of productivity and wedges for each region, given temperature exposure parameters. Second, intrinsic product sensitivity β_i (common within 3-digit sectors) is identified from the orthogonality between residualized MRPK and temperature surprises, after netting out endogenous adaptation and region–year aggregates. Third, regional adaptation costs $(\eta_r H_r)^{-1}$, parameterized as a fourth-order polynomial in long-run income, are identified from how cross-firm variation in MRPK responses to temperature surprises covaries with model-implied drivers of endogenous adaptation. Fourth, the common bliss point T^* and random-damage dispersion σ^2_ξ are jointly identified from how residual TFP-growth volatility and MRPK dispersion scale with $(T_{rt} - T^*)^2$, after purging the components explained by heterogeneous exposure and forecast moments.

We implement the estimator via a fixed-point algorithm that iterates between inverting the model to recover firm-level latent objects (given current parameter guesses) and updating parameters using the moment conditions. The algorithm converges in fewer than 20 iterations across a wide range of initial conditions. Taken together, these moments jointly identify the common parameters $\{T^*, \sigma^2_\xi\}$ and the region-specific objects $\{\bar{\beta}_r,\ (\eta_r H_r)^{-1},\ \sigma^2_{\hat{\beta},r},\ \sigma^2_{\tilde{a},r},\ \sigma^2_{\varepsilon^z,r},\ \sigma^2_{\varepsilon^{\phi^\tau},r},\ \rho_{\phi^\tau,r},\ \rho_{z,r},\ \omega_{a,r}\}_r$.

7.1.3 Estimation Results

We briefly summarize the estimation results. Table 2 reports the common parameters and the coefficients governing the regional adaptation-cost shifter $f(\cdot)$. For region-specific moments and implied parameters, we report the cross-region distribution (p5, p50, p95) in Table 3.

The model-consistent temperature bliss point remains close to its reduced-form counterpart, at roughly $11°$C. We also identify substantial dispersion in idiosyncratic (random) climate damages, with $\sigma^2_\xi \simeq 0.0046$, implying that even conditional on the same (predictable) temperature realization, firms can experience materially different productivity impacts.

Regions' average intrinsic exposure $\bar{\beta}_r$ is tightly centered around zero and slightly negative: the 5th percentile is -0.0074, the median is essentially zero, and the 95th percentile is 0.006. This pattern suggests that, absent of endogenous adaptation, most regions exhibit a weakly negative response to temperature surprises, while a non-trivial right tail of regions responds positively.

Table 2: Estimated and Calibrated Parameters

Parameter	Description	Value
Panel A. Common estimated parameters		
T^*	Temperature bliss point (°C)	11.03
σ_ξ^2	Dispersion of random climate damages	0.0046
Panel B. Adaptation-cost shifter: $(\eta_r H_r)^{-1} = \sum_{j=0}^{4} c_j\, g_r^j,\ g_r \equiv \overline{\ln \mathrm{GDP}_r}$		
c_0	Constant	6.9462
c_1	Linear	−3.1359
c_2	Quadratic	0.5255
c_3	Cubic	−0.0387
c_4	Quartic	0.0011
Panel C. Calibrated parameters		
$\tilde{\alpha}_K$	Capital share	0.35
r	Interest rate	0.042
γ	CRRA risk aversion	5
σ	Demand elasticity of substitution	4

Table 3: Distribution of Region-Specific Estimates

Parameter	Description	p5	p50	p95
Climate exposure and adaptation				
$\bar{\beta}_r$	Avg. intrinsic product sensitivity	−0.0074	≈ 0	0.0060
$(\eta_r H_r)^{-1}$	Inverse effective adaptation cost	0.0006	0.0013	0.0063
$\sigma^2_{\hat{\beta},r}$	Within-region dispersion of $\hat{\beta}_i$	0.0001	0.0003	0.0007
Productivity and wedge dynamics				
$\sigma^2_{\bar{a},r}$	Permanent productivity dispersion	0.6516	1.5601	3.3667
$\sigma^2_{\varepsilon^z,r}$	Transitory productivity innovation var.	0.0925	0.1946	0.3019
$\sigma^2_{\varepsilon^{\phi^\tau},r}$	Wedge innovation variance	0.0327	0.1386	0.4110
$\rho_{z,r}$	Transitory productivity persistence	0.6401	0.7723	0.9086
$\rho_{\phi^\tau,r}$	Wedge persistence	0.6310	0.8103	0.9388
$\omega_{a,r}$	Size-dependent wedge coefficient	0.4713	0.9671	1.1840

Consistent with this interpretation, a sizeable share of regions in our sample have average temperatures below the bliss point.

At the product level, intrinsic sensitivities vary meaningfully across 3-digit categories, spanning roughly -0.11 to 0.09. Within a region, however, dispersion in intrinsic exposure is comparatively modest: $\sigma^2_{\hat{\beta},r}$ ranges from 10^{-4} to 7×10^{-4} (p5–p95). This stands in sharp contrast to the much larger dispersion in random climate damages captured by σ^2_ξ, highlighting that a substantial share of climate-induced heterogeneity operates through unpredictable firm-level disruptions rather than through persistent cross-product differences in exposure.

All regions exhibit positive adaptation responses. The inverse effective adaptation cost $(\eta_r H_r)^{-1}$ has a median of 0.0013 and spans 0.0006 to 0.0063 (p5–p95), implying nearly an order-of-magnitude variation in adaptation capacity across regions. Under the estimated income-based shifter $f(\overline{\ln \mathrm{GDP}_r})$, adaptation is cheaper in higher-income regions on average, which translates into stronger predicted endogenous adaptation—especially in climates farther from the bliss point, where the marginal value of adaptation is higher.

Turning to region-specific parameters governing firm dynamics, we find large dispersion in permanent productivity and substantial idiosyncratic volatility. Permanent productivity dispersion $\sigma^2_{\bar{a},r}$ is sizable (p5 $= 0.65$, p50 $= 1.56$, p95 $= 3.37$), and both transitory productivity and wedge components are highly persistent, with $\rho_{z,r}$ and $\rho_{\phi^\tau,r}$ typically between 0.6 and 0.95. Innovation variances in transitory productivity and idiosyncratic wedges are also economically large, indicating that both long-run heterogeneity and short-run shocks contribute meaningfully to within-region dispersion.

Finally, correlated distortions are strong. The size-dependent wedge coefficient $\omega_{a,r}$ is close to one at the median, implying that a 1% increase in permanent productivity (and hence scale) is associated with roughly a 1% higher effective user cost of capital. This magnitude is consistent with size-dependent distortion mechanisms recently estimated in Ayerst, Nguyen, and Restuccia (2024).

7.2 Quantitative Results

With the model estimated for regions spanning the EU, China, and India, we now quantify the aggregate importance of the misallocation channel. We use the estimated region-level moments to (i) measure the global productivity cost of climate-induced misallocation in an average year, (ii) track how this cost evolves from 1981–2019 as global warming unfolds and (iii) revisit the classic geography-development relationship by comparing the model-implied misallocation losses to cross-country productivity gaps in the macro data.

7.2.1 The Global Cost of Climate-Induced Misallocation

We first measure the total cost of climate-driven misallocation in our framework. We define the *global cost of climate-induced misallocation* as the aggregate TFP (or output) loss when comparing the observed economy to a counterfactual in which all within-region dispersion in climate sensitivities is eliminated. Operationally, for each region-year we shut down the three within-region dispersion objects that generate climate-driven MRPK dispersion: $\sigma^2_\xi = 0$, $\mathbb{VAR}^i_{rt}(\hat{\beta}_i + \Psi_{it}) = 0$ and

$\mathbb{COV}^i_{rt}\left(\tau_{it+1}, \widehat{\beta}_i + \Psi_{i,t+1}\right) = 0$. All other region-level fundamentals are held fixed. Intuitively, this counterfactual removes the within-region heterogeneity in (effective) temperature exposure and idiosyncratic climate damages, as well as its interaction with wedges, thereby isolating the allocative-efficiency losses that operate through dispersion in MRPK.

Global implementation. To implement this exercise at the global level, we pair our micro estimates with gridded climate data (ERA5) and seasonal forecast data (ECMWF) for all countries worldwide. We partition the globe into roughly 4,894 regions. For China, India, and EU countries, we adopt the same regional definitions used in our empirical analysis; for all other countries, we use GADM level-1 partitions.

For regions in our estimation sample, we use the estimated firm-level moments directly. For regions outside the sample, we extrapolate these moments using long-run GDP per capita, leveraging the fact that firm-level dispersion moments covary systematically with development.[26] We also impute regional adaptation costs using the estimated mapping $\eta_r H_r = f(\bar{T}_r, \overline{\ln \mathrm{GDP}}_r)$.

Aggregation. We aggregate the world economy using a Cobb–Douglas output index across countries and regions (see Appendix F for details). This implies

$$\log \mathrm{TFP}_t^{\mathrm{Global}} = \sum_r \omega_{rt} \log \mathrm{TFP}_{rt}, \qquad \omega_{rt} \equiv \omega_{ct}\omega^c_{rt},$$

where ω_{ct} is country c's global output share and ω^c_{rt} is region r's share of country c's output.

Sufficient-statistics decomposition. Under this aggregation, the global misallocation cost implied by the model can be written as a weighted average of three sufficient statistics: (i) squared deviations from the optimal (bliss) temperature $(T_{rt} - T^*)^2$; (ii) forecast errors and forecast uncertainty, amplified by within-region dispersion in effective exposure; and (iii) the interaction between wedges and exposure. Define the relevant temperature innovation (forecast error net of the risk adjustment) as:

26. For parameters governing climate sensitivity, we extrapolate using both long-run GDP per capita and long-run climate.

$$\underbrace{\overline{\Delta^{T,\text{Mis}} \log \text{TFP}_t^{\text{Global}}}}_{\approx -12.5\%} = -\frac{\tilde{\alpha}_K + \tilde{\alpha}_K^2(\sigma-1)}{2}\Bigg[\underbrace{\sigma_\xi^2\Big(\overline{\sum_r \omega_{rt}(T_{rt}-T^*)^2}\Big)}_{\substack{\text{Random Climate Damage}\\ \approx -10.38\%}}$$
$$+\underbrace{\Big(\overline{\sum_r \omega_{rt}\mathbb{VAR}^i_{rt}(\hat{\beta}_i+\Psi_{it})\cdot\Big(T_{rt}-\mathbb{E}_{t-1}[T_{rt}]-(\bar{\beta}_r+\widetilde{\beta}_r)\Theta\mathbb{VAR}_{t-1}[T_{r,t}]\Big)^2}\Big)}_{\substack{\text{Exposure-amplified Forecast Error \& Risk}\\ \approx -2.11\%}}$$
$$+\underbrace{\Big(2\overline{\sum_r \omega_{rt}\mathbb{COV}^i_{rt}(\tau_{it},\hat{\beta}_i+\Psi_{it})\cdot\Big(T_{rt}-\mathbb{E}_{t-1}[T_{rt}]-(\bar{\beta}_r+\widetilde{\beta}_r)\Theta\mathbb{VAR}_{t-1}[T_{r,t}]\Big)}\Big)}_{\substack{\text{Wedge–exposure Interaction}\\ \approx -0.01\%}}\Bigg]. \tag{34}$$

Here $\overline{(\cdot)}$ denotes the time average over 1981–2019. Averaging these output-weighted sufficient statistics over 1981–2019, we find that climate-induced misallocation lowers global TFP by about 12.5% in an average year. Of this total, 10.38% arises from the *random climate damage* channel (persistent displacement from the bliss point, which magnifies heterogeneous and unpredictable firm-level disruptions), while 2.11% comes from forecast errors and climate uncertainty amplified by dispersion in effective exposure. The wedge–exposure interaction, while heterogeneous in the cross-section of regions, is quantitatively negligible in the global aggregate (about 0.01%).

The quantitative message is clear: most climate-induced misallocation reflects persistent deviations of regional climates from the optimal temperature—which magnify heterogeneous, unpredictable firm-level disruptions—rather than short-run forecast errors or forecast uncertainty. In other words, long-run climate displacement dominates weather predictability as a driver of global allocative inefficiency in our estimates.

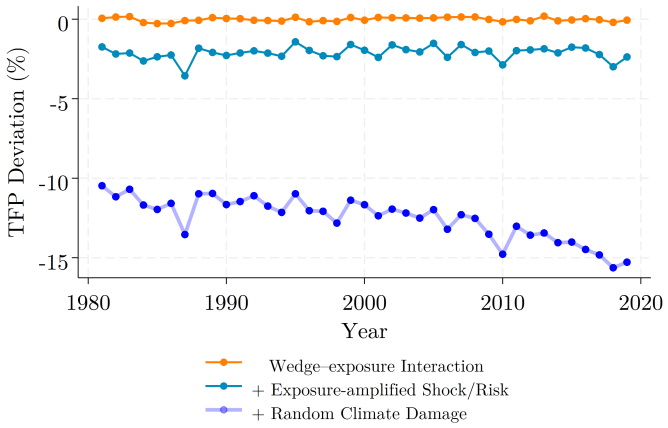
The Changing Cost with Global Warming. We next quantify how the global misallocation cost evolves over time, feeding the observed paths of regional temperatures and ECMWF forecasts into (34) from $t_0 = 1981$ to $t_1 = 2019$. Figure 13a plots the implied evolution of the three components. Over this period, climate-induced misallocation becomes more costly, lowering global TFP by an additional

$$\Delta^{T,\text{Mis}}_{t_1,t_0} \log \text{TFP}^{\text{Global}} \approx -4.81\%.$$

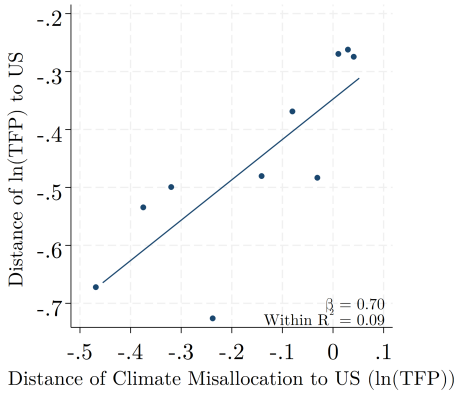
The dominant driver is again the level/random-damage channel: warming pushes many already-warm, high-output regions further away from T^*, more than it brings cooler regions closer, mechanically raising disruption-driven volatility and worsening allocative efficiency. The exposure-amplified forecast/risk component and the wedge–exposure interaction contribute little to the aggregate time trend.

Figure 13: The Cost of Climate-Induced Misallocation and Cross-country Development

(a) The Changing Cost of Climate-Induced Misallocation



(b) Cross-country TFP Dispersion: Model vs. Data



7.2.2 Climate and Productivity Differences Across Countries: Macro Data vs. Model Estimates

We next use our framework to revisit a central question in development economics: what explains large cross-country productivity gaps? Geography and climate have long been emphasized in comparative development (Montesquieu 1748; Sachs and Warner 1997; Gallup, Sachs, and Mellinger 1999; Nordhaus 2006; Dell, Jones, and Olken 2012), but the mechanisms linking climate to aggregate productivity remain debated. Here we focus on one mechanism—the misallocation channel—and ask how much of the observed cross-country TFP dispersion can be explained with the model-implied climate-misallocation losses.

We match our model-generated country-year misallocation costs to country-level TFP from the Penn World Table (PWT) 10.01 (Feenstra, Inklaar, and Timmer 2015). For each country-year, we compare the measured TFP gap relative to the United States, $\ln \mathrm{TFP}_{c,t} - \ln \mathrm{TFP}_{\mathrm{US},t}$, to the model-predicted climate-misallocation gap relative to the United States, $\Delta^{T,\mathrm{Mis}} \log \mathrm{TFP}_{c,t} - \Delta^{T,\mathrm{Mis}} \log \mathrm{TFP}_{\mathrm{US},t}$. The U.S. is a natural benchmark as a productivity frontier, and it is also close to the estimated temperature optimum ($T^* \approx 11.03°\mathrm{C}$), implying comparatively low climate-induced misallocation.

Figure 13b reports a binned scatter plot of macro TFP gaps against model-implied misallocation gaps, with both variables demeaned by year fixed effects to remove common global trends. The fitted relationship has a slope of about 0.7: when a country's predicted TFP distance to the U.S. due to climate misallocation rises by 1%, its measured TFP distance rises by about 0.7% on average. The corresponding R^2 of 0.094 implies that roughly 9% of observed cross-country TFP differences can be accounted for by climate through the misallocation channel. Notably, the model object is constructed solely from micro estimates combined with granular temperature and forecast data, yet it aligns well with the macro evidence.

8 Conclusion

This paper provides the first causal estimates of the misallocation effect from temperature shocks using firm-level microdata from 32 countries. On average, an additional hot day with > 30°C of temperature increases MRPK dispersion by 0.31 log points and contributes to a 0.11 % decline in annual aggregate TFP. Intriguingly, the detrimental impact of extreme heat on capital misallocation is more severe in regions with hotter climates and higher incomes, highlighting a significant productivity cost of climate change coupled with a limited capacity for market-based adaptation. A novel firm dynamics model of endogenous adaptation rationalizes these pattern and reveals the quantitative important of random climate damages on TFP volatility and undermining the allocative efficiency investment. Climate-induced misallocation explains 9% of cross-country aggregate productivity differences.

References

Addoum, Jawad M, David T Ng, and Ariel Ortiz-Bobea. 2020. "Temperature shocks and establishment sales." *The Review of Financial Studies* 33 (3): 1331–1366.

Allcott, Hunt, Allan Collard-Wexler, and Stephen D O'Connell. 2016. "How do electricity shortages affect industry? Evidence from India." *American Economic Review.*

Asker, John, Allan Collard-Wexler, and Jan De Loecker. 2014. "Dynamic Inputs and Resource (Mis)Allocation." *Journal of Political Economy* 122 (5): 1013–1063.

Ayerst, Stephen, Duc M Nguyen, and Diego Restuccia. 2024. *The micro and macro productivity of nations.* Technical report. National Bureau of Economic Research.

Bakkensen, Laura A, and Lint Barrage. 2021. "Going Underwater? Flood Risk Belief Heterogeneity and Coastal Home Price Dynamics." *The Review of Financial Studies* 35 (8): 3666–3709.

Baqaee, David Rezza, and Emmanuel Farhi. 2019. "The Macroeconomic Impact of Microeconomic Shocks: Beyond Hulten's Theorem." *Econometrica* 87 (4): 1155–1203.

Basu, Susanto, and John G. Fernald. 2002. "Aggregate productivity and aggregate technology." *European Economic Review* 46 (6): 963–991.

Bau, Natalie, and Adrien Matray. 2023. "Misallocation and Capital Market Integration: Evidence From India." *Econometrica* 91 (1): 67–106.

Bilal, Adrien, and Diego R Känzig. 2024. *The Macroeconomic Impact of Climate Change: Global vs. Local Temperature.* Technical report. National Bureau of Economic Research.

Bils, Mark, Peter J. Klenow, and Cian Ruane. 2021. "Misallocation or Mismeasurement?" *Journal of Monetary Economics* 124:S39–S56.

Brandt, Loren, Johannes Van Biesebroeck, and Yifan Zhang. 2014. "Challenges of working with the Chinese NBS firm-level data." *China Economic Review.*

Burke, Marshall, Solomon M. Hsiang, and Edward Miguel. 2015. "Global non-linear effect of temperature on economic production." *Nature* 527 (7577): 235–239.

Caggese, Andrea, Andrea Chiavari, Sampreet Goraya, and Carolina Villegas-Sanchez. 2023. "Climate Change, Firms, and the Aggregate Productivity." Working Paper.

Carleton, Tamma, Amir Jina, Michael Delgado, Michael Greenstone, Trevor Houser, Solomon Hsiang, Andrew Hultgren, et al. 2022. "Valuing the Global Mortality Consequences of Climate Change Accounting for Adaptation Costs and Benefits." *The Quarterly Journal of Economics* 137 (4): 2037–2105.

Casey, Gregory, Stephie Fried, and Matthew Gibson. 2022. "Understanding Climate Damages: Consumption versus Investment." Federal Reserve Bank of San Francisco Working Paper 2022-21.

Chen, Zhang. 2022. "Economic Growth and the Rise of Large Firms."

Christidis, Nikolaos, Dann Mitchell, and Peter A. Stott. 2023. "Rapidly increasing likelihood of exceeding 50°C in parts of the Mediterranean and the Middle East due to human influence." *npj Climate and Atmospheric Science* 6, no. 1 (May 26, 2023): 45.

Coeurdacier, Nicolas, Helene Rey, and Pablo Winant. 2011. "The risky steady state." *American Economic Review* 101 (3): 398–401.

Copernicus Climate Change Service. 2021. *CMIP6 climate projections.* Copernicus Climate Change Service (C3S) Climate Data Store (CDS).

Copernicus Climate Change Service and Climate Data Store. 2018. *Seasonal forecast daily and subdaily data on single levels.*

Cruz, José-Luis, and Esteban Rossi-Hansberg. 2023. *The Economic Geography of Global Warming.*

David, Joel M., Hugo A. Hopenhayn, and Venky Venkateswaran. 2016. "INFORMATION, MISALLOCATION, AND AGGREGATE PRODUCTIVITY." *The Quarterly Journal of Economics* 131 (2): 943–1006. Accessed November 27, 2023.

David, Joel M., and Venky Venkateswaran. 2019. "The Sources of Capital Misallocation." *American Economic Review* 109 (7): 2531–67.

David, Joel M., and David Zeke. 2021. *Risk-Taking, Capital Allocation and Optimal Monetary Policy.* Federal Reserve Bank of Chicago.

Dell, Melissa, Benjamin F Jones, and Benjamin A Olken. 2012. "Temperature Shocks and Economic Growth: Evidence from the Last Half Century." *American Economic Journal: Macroeconomics* 4 (3): 66–95.

Dellink, Rob, Jean Chateau, Elisa Lanzi, and Bertrand Magné. 2017. "Long-term economic growth projections in the Shared Socioeconomic Pathways." *Global Environmental Change.*

Deschênes, Olivier, and Michael Greenstone. 2011. "Climate Change, Mortality, and Adaptation: Evidence from Annual Fluctuations in Weather in the US." *American Economic Journal: Applied Economics* 3 (4): 152–185.

Dundas, Steven J., and Roger H. von Haefen. 2020. "The Effects of Weather on Recreational Fishing Demand and Adaptation: Implications for a Changing Climate." *Journal of the Association of Environmental and Resource Economists* 7 (2): 209–242.

Fan, Jingting. 2024. "Talent, Geography, and Offshore R
amp;D." *The Review of Economic Studies* (April): rdae044. ISSN: 0034-6527.

Feenstra, Robert C, Robert Inklaar, and Marcel P Timmer. 2015. "The next generation of the Penn World Table." *American economic review* 105 (10): 3150–3182.

Gallup, John Luke, Jeffrey D. Sachs, and Andrew D. Mellinger. 1999. "Geography and Economic Development." *International Regional Science Review* 22 (2): 179–232.

Ginglinger, Edith, and Quentin Moreau. 2023. "Climate risk and capital structure." *Management Science* 69 (12): 7492–7516.

Gopinath, Gita, Sebnem Kalemli-Ozcan, Loukas Karabarbounis, and Carolina Villegas-Sanchez. 2017. "Capital Allocation and Productivity in South Europe." *Quarterly Journal of Economics* 132 (4).

Gorodnichenko, Yuriy, Debora Revoltella, Jan Svejnar, and Christoph T Weiss. 2018. *Resource misallocation in European firms: The role of constraints, firm characteristics and managerial decisions.* Technical report. National Bureau of Economic Research.

Hsieh, Chang-Tai, and Peter J. Klenow. 2009. "Misallocation and Manufacturing TFP in China and India." *Quarterly Journal of Economics* 124 (4): 1403–1448.

Kalemli- Özcan, Şebnem, Bent E. Sørensen, Carolina Villegas-Sanchez, Vadym Volosovych, and Sevcan Yeşiltaş. 2024. "How to Construct Nationally Representative Firm-Level Data from the Orbis Global Database: New Facts on SMEs and Aggregate Implications for Industry Concentration." *American Economic Journal: Macroeconomics* 16, no. 2 (April): 353–74.

Kopytov, Alexandr, Mathieu Taschereau-Dumouchel, and Zebang Xu. 2024. "The Origin of Risk." *Available at SSRN.*

Krusell, Per, and Anthony A. Smith Jr. 1998. "Income and Wealth Heterogeneity in the Macroeconomy." *Journal of Political Economy* 106 (5): 867–896.

Lemoine, Derek. 2018. *Estimating the Consequences of Climate Change from Variation in Weather.* Working Paper, Working Paper Series 25008. National Bureau of Economic Research.

Mehra, Rajnish, and Edward C Prescott. 1985. "The equity premium: A puzzle." *Journal of monetary Economics* 15 (2): 145–161.

Montesquieu, Baron de, Charles de Secondat. 1748. *The Spirit of Laws.* Printed for T. Evans.

Moscona, Jacob, and Karthik A Sastry. 2023. "Does directed innovation mitigate climate damage? evidence from us agriculture." *The Quarterly Journal of Economics* 138 (2): 637–701.

Nath, Ishan. 2025. "Climate change, the food problem, and the challenge of adaptation through sectoral reallocation." *Journal of Political Economy.*

Nath, Ishan, Valerie Ramey, and Peter Klenow. 2023. "How Much Will Global Warming Cool Global Growth?"

Nordhaus, William D. 1992. "An optimal transition path for controlling greenhouse gases." *Science* 258 (5086): 1315–1319.

———. 2006. "Geography and Macroeconomics: New Data and New Findings." *Proceedings of the National Academy of Sciences* 103 (10): 3510–3517.

O'Neill, B. C., C. Tebaldi, D. P. van Vuuren, V. Eyring, P. Friedlingstein, G. Hurtt, R. Knutti, et al. 2016. "The Scenario Model Intercomparison Project (ScenarioMIP) for CMIP6." *Geosci. Model Dev.*

Oberfield, Ezra, and Devesh Raval. 2021. "Micro data and macro technology." *Econometrica.*

Oudin Åström, Daniel, Bertil Forsberg, Kristie L. Ebi, and Joacim Rocklöv. 2013. "Attributing mortality from extreme temperatures to climate change in Stockholm, Sweden." *Nature Climate Change* 3, no. 12 (December 1, 2013): 1050–1054.

Piao, Shilong, Philippe Ciais, Yao Huang, Zehao Shen, Shushi Peng, Junsheng Li, Liping Zhou, Hongyan Liu, Yuecun Ma, Yihui Ding, et al. 2010. "The impacts of climate change on water resources and agriculture in China." *Nature.*

Ponticelli, Jacopo, Qiping Xu, and Stefan Zeume. 2023. *Temperature and Local Industry Concentration.* Technical report w31533. National Bureau of Economic Research.

Poschke, Markus. 2018. "The Firm Size Distribution across Countries and Skill-Biased Change in Entrepreneurial Technology." *American Economic Journal: Macroeconomics* 10 (3): 1–41.

Redding, Stephen J, and David E Weinstein. 2020. "Measuring aggregate price indices with taste shocks: Theory and evidence for CES preferences." *The Quarterly Journal of Economics* 135 (1): 503–560.

Restuccia, Diego, and Richard Rogerson. 2008. "Policy distortions and aggregate productivity with heterogeneous establishments." *Review of Economic dynamics* 11 (4): 707–720.

Rudik, I., G. Lyn, W. Tan, and A. Ortiz-Bobea. 2021. *The Economic Effects of Climate Change in Dynamic Spatial Equilibrium.*

Sabater, Joaquin Muñoz. 2019. *ERA5-Land monthly averaged data from 1950 to present.* Copernicus Climate Change Service (C3S) Climate Data Store (CDS).

Sachs, Jeffrey D., and Andrew M. Warner. 1997. "Sources of Slow Growth in African Economies." *Journal of African Economies* 6 (3): 335–376.

Somanathan, E., Rohini Somanathan, Anant Sudarshan, and Meenu Tewari. 2021. "The Impact of Temperature on Productivity and Labor Supply: Evidence from Indian Manufacturing" [in en]. *Journal of Political Economy* 129 (6). Accessed November 27, 2023.

Sraer, David, and David Thesmar. 2023. "How to Use Natural Experiments to Estimate Misallocation." *American Economic Review* 113 (4): 906–38.

Tarsia, Romano. 2023. "Heterogeneous effects of weather shocks on firm economic performance." *Available at SSRN 4672552.*

Tyazhelnikov, Vladimir, Xinbei Zhou, and Xuetao Shi. 2024. *PPML, Gravity, and Heterogeneous Trade Elasticities.* Technical report.

Wang, Tingting, and Fubao Sun. 2022. "Global gridded GDP data set consistent with the shared socioeconomic pathways." *Scientific Data.*

Wenz, Leonie, Robert Devon Carr, Noah Kögel, Maximilian Kotz, and Matthias Kalkuhl. 2023. "DOSE – Global data set of reported sub-national economic output." *Scientific Data* 10 (1): 425.

Zhang, Peng, Olivier Deschenes, Kyle C Meng, and Junjie Zhang. 2018. "Temperature effects on productivity and factor reallocation: Evidence from a half million Chinese manufacturing plants." *Journal of Environmental Economics and Management* 88:1–17.

Zivin, Joshua Graff, and Matthew Neidell. 2014. "Temperature and the Allocation of Time: Implications for Climate Change." *Journal of Labor Economics* 32 (1): 1–26.

Online Appendix

A Additional Derivations for Section 2

This appendix provides the derivation of the expressions and propositions featured in Section 2.

A.1 Equilibrium Allocations in Distorted Equilibrium

In this appendix, we solve the firm's profit maximization problem in Equation 3 and derive Equation 4.

Subject to the inverse demand and wedges, each firm i in region-sector n engages in monopolistic competition and optimally chooses its quantity of inputs and price to maximize profits

$$\max_{P_{nit},K_{nit},L_{nit}} \left(1-\tau^Y_{nit}\right) P_{nit} \underbrace{A_{nit}K^{\alpha_{Kn}}_{nit}L^{\alpha_{Ln}}_{nit}}_{Y_{nit}} - \left(1+\tau^K_{nit}\right) R_{nt}K_{nit} - \left(1+\tau^L_{nit}\right) W_{nt}L_{nit}$$
$$\text{subject to : } Y_{nit} = B_{nit}Y_{nt}\left[\frac{P_{nit}}{P_{nt}}\right]^{-\sigma_n}.$$

After substituting the demand curve $P_{nit}Y_{nit} = P_{nt}Y^{\frac{1}{\sigma_n}}_{nt}B^{\frac{1}{\sigma_n}}_{nit}Y^{\frac{\sigma_n-1}{\sigma_n}}_{nit}$ into the objective function, we derive the first-order condition with respect to any factor input F_{nit} used (where F_{nit} can be either K_{nit} or L_{nit})

$$MRPF_{nit} = \frac{\partial P_{nit}Y_{nit}}{\partial F_{nit}} = \alpha_{F_n}\frac{\sigma_n-1}{\sigma_n}\frac{P_{nit}Y_{nit}}{F_{nit}} = \frac{1+\tau^F_{ni}(\tilde{\mathbf{T}}_{rt},\cdot)}{1-\tau^Y_{ni}(\tilde{\mathbf{T}}_{rt},\cdot)}P^F_{nt},$$

where P^F_{nt} denotes the factor price, specifically W_{nt} for labor and R_{nt} for capital. $\frac{\sigma_n-1}{\sigma_n}$ is the optimal CES markup. This is Equation 4 in the main text.

Equation 4 can be rearranged to yield the following:

$$K_{nit} = \alpha_{K_n}(1-\tau^Y_{ni}(\tilde{\mathbf{T}}_{rt},\cdot))\frac{\sigma_n-1}{\sigma_n}\frac{P_{nit}Y_{nit}}{(1+\tau^K_{ni}(\tilde{\mathbf{T}}_{rt},\cdot))P^K_{nt}}$$
$$L_{nit} = \alpha_{L_n}(1-\tau^Y_{ni}(\tilde{\mathbf{T}}_{rt},\cdot))\frac{\sigma_n-1}{\sigma_n}\frac{P_{nit}Y_{nit}}{(1+\tau^L_{ni}(\tilde{\mathbf{T}}_{rt},\cdot))P^L_{nt}}$$

Plugging the labor and capital first order conditions into the expression for production yields a relationship between output Y_{nit} and sale $P_{nit}Y_{nit}$

$$\begin{aligned} Y_{nit} &= A_{nit}K^{\alpha_{Kn}}_{nit}L^{\alpha_{Ln}}_{nit} \\ &= A_{nit}\alpha^{\alpha_{Kn}}_{K_n}\alpha^{\alpha_{Ln}}_{L_n}(1-\tau^Y_{ni}(\tilde{\mathbf{T}}_{rt},\cdot))\frac{\sigma_n-1}{\sigma_n}P_{nit}Y_{nit}\left[\frac{1}{(1+\tau^K_{ni}(\tilde{\mathbf{T}}_{rt},\cdot))P^K_{nt}}\right]^{\alpha_{Kn}}\left[\frac{1}{(1+\tau^L_{ni}(\tilde{\mathbf{T}}_{rt},\cdot))P^L_{nt}}\right]^{\alpha_{Ln}} \end{aligned} \tag{35}$$

Using demand curve once again solves for sales $P_{nit}Y_{nit}$

$$
\begin{aligned}
P_{nit}Y_{nit} &= P_{nt}Y_{nt}^{\frac{1}{\sigma_n}}B_{nit}^{\frac{1}{\sigma_n}}Y_{nit}^{\frac{\sigma_n-1}{\sigma_n}} \\
&= P_{nt}Y_{nt}^{\frac{1}{\sigma_n}}B_{nit}^{\frac{1}{\sigma_n}}\left\{A_{nit}\alpha_{K_n}^{\alpha_{K_n}}\alpha_{L_n}^{\alpha_{L_n}}(1-\tau_{ni}^{Y}(\tilde{\mathbf{T}}_{rt},\cdot))\frac{\sigma_n-1}{\sigma_n}P_{nit}Y_{nit}\left[\frac{1}{(1+\tau_{ni}^{K}(\tilde{\mathbf{T}}_{rt},\cdot))P_{nt}^{K}}\right]^{\alpha_{Kn}}\left[\frac{1}{(1+\tau_{ni}^{L}(\tilde{\mathbf{T}}_{rt},\cdot))P_{nt}^{L}}\right]^{\alpha_{Ln}}\right\}^{\frac{\sigma_n-1}{\sigma_n}} \\
(P_{nit}Y_{nit})^{\frac{1}{\sigma_n}} &= P_{nt}Y_{nt}^{\frac{1}{\sigma_n}}B_{nit}^{\frac{1}{\sigma_n}}\left\{A_{nit}\alpha_{K_n}^{\alpha_{K_n}}\alpha_{L_n}^{\alpha_{L_n}}(1-\tau_{ni}^{Y}(\tilde{\mathbf{T}}_{rt},\cdot))\frac{\sigma_n-1}{\sigma_n}\left[\frac{1}{(1+\tau_{ni}^{K}(\tilde{\mathbf{T}}_{rt},\cdot))P_{nt}^{K}}\right]^{\alpha_{Kn}}\left[\frac{1}{(1+\tau_{ni}^{L}(\tilde{\mathbf{T}}_{rt},\cdot))P_{nt}^{L}}\right]^{\alpha_{Ln}}\right\}^{\frac{\sigma_n-1}{\sigma_n}} \\
P_{nit}Y_{nit} &= P_{nt}^{\sigma_n}Y_{nt}B_{nit}\left\{A_{nit}\alpha_{K_n}^{\alpha_{K_n}}\alpha_{L_n}^{\alpha_{L_n}}(1-\tau_{ni}^{Y}(\tilde{\mathbf{T}}_{rt},\cdot))\frac{\sigma_n-1}{\sigma_n}\left[\frac{1}{(1+\tau_{ni}^{K}(\tilde{\mathbf{T}}_{rt},\cdot))P_{nt}^{K}}\right]^{\alpha_{Kn}}\left[\frac{1}{(1+\tau_{ni}^{L}(\tilde{\mathbf{T}}_{rt},\cdot))P_{nt}^{L}}\right]^{\alpha_{Ln}}\right\}^{\sigma_n-1}
\end{aligned}
\tag{36}
$$

We aggregate sales across all firms and obtain

$$
\begin{aligned}
\int_i P_{nit}Y_{nit} &= \int_i P_{nt}^{\sigma_n}Y_{nt}B_{nit}\left\{A_{nit}\alpha_{K_n}^{\alpha_{K_n}}\alpha_{L_n}^{\alpha_{L_n}}(1-\tau_{ni}^{Y}(\tilde{\mathbf{T}}_{rt},\cdot))\frac{\sigma_n-1}{\sigma_n}\left[\frac{1}{(1+\tau_{ni}^{K}(\tilde{\mathbf{T}}_{rt},\cdot))P_{nt}^{K}}\right]^{\alpha_{Kn}}\left[\frac{1}{(1+\tau_{ni}^{L}(\tilde{\mathbf{T}}_{rt},\cdot))P_{nt}^{L}}\right]^{\alpha_{Ln}}\right\}^{\sigma_n-1} \\
&= P_{nt}^{\sigma_n}Y_{nt}\left(\alpha_{K_n}^{\alpha_{K_n}}\alpha_{L_n}^{\alpha_{L_n}}\frac{\sigma_n-1}{\sigma_n}\left(P_{nt}^{K}\right)^{-\alpha_{K_n}}\left(P_{nt}^{L}\right)^{-\alpha_{L_n}}\right)^{\sigma_n-1}\int_i B_{nit}\left\{A_{nit}(1-\tau_{ni}^{Y}(\tilde{\mathbf{T}}_{rt},\cdot))\left[\frac{1}{(1+\tau_{ni}^{K}(\tilde{\mathbf{T}}_{rt},\cdot))}\right]^{\alpha_{Kn}}\left[\frac{1}{(1+\tau_{ni}^{L}(\tilde{\mathbf{T}}_{rt},\cdot))}\right]^{\alpha_{Ln}}\right\}^{\sigma_n-1}
\end{aligned}
\tag{37}
$$

Then the sales share of firm i in region-sector n, θ_{nit} can be expressed in closed form of the fundamentals and parameters as

$$
\begin{aligned}
\theta_{nit} &= \frac{P_{nit}Y_{nit}}{\int_i P_{nit}Y_{nit}} \\
&= \frac{B_{nit}\left\{A_{nit}(1-\tau_{ni}^{Y}(\tilde{\mathbf{T}}_{rt},\cdot))\left[\frac{1}{(1+\tau_{ni}^{K}(\tilde{\mathbf{T}}_{rt},\cdot))}\right]^{\alpha_{Kn}}\left[\frac{1}{(1+\tau_{ni}^{L}(\tilde{\mathbf{T}}_{rt},\cdot))}\right]^{\alpha_{Ln}}\right\}^{\sigma_n-1}}{\int_i B_{nit}\left\{A_{nit}(1-\tau_{ni}^{Y}(\tilde{\mathbf{T}}_{rt},\cdot))\left[\frac{1}{(1+\tau_{ni}^{K}(\tilde{\mathbf{T}}_{rt},\cdot))}\right]^{\alpha_{Kn}}\left[\frac{1}{(1+\tau_{ni}^{L}(\tilde{\mathbf{T}}_{rt},\cdot))}\right]^{\alpha_{Ln}}\right\}^{\sigma_n-1}},
\end{aligned}
$$

which is Equation 6 in the paper.

A.2 Proof of Proposition 1

Proposition 1. Equilibrium (Mis)Allocation. The (log) ratio of firm i's distorted and efficient equilibrium allocation of factor, $\frac{F_{nit}}{F_{nit}^*}$,

$$
\log(\frac{F_{nit}}{F_{nit}^*}) = -\underbrace{\log(\frac{1+\tau_{nit}^{F}}{1+\tau_{nt}^{F}})}_{\substack{\text{relative wedge}\\ \text{effect}}} + \underbrace{\log(\frac{\theta_{nit}}{\theta_{nit}^*})}_{\substack{\text{size}\\ \text{effect}}}
$$

is decreasing in the ratio of firm i's own factor wedge comparing to the aggregate factor wedge $1+\tau_{nt}^{F} \equiv \left(\int_0^{J_n}\frac{1}{(1+\tau_{nit}^{F})}\theta_{nit}di\right)^{-1}$, and increasing in the ratio of the firm's sales share θ_{nit} comparing to its efficient counterfactual θ_{nit}^*. Moreover, the efficient allocation of inputs, $\frac{F_{nit}^*}{F_{nt}} = \theta_{nit}^* = \frac{B_{nit}A_{nit}^{\sigma_n-1}}{\int_0^{J_n}B_{nit}A_{nit}^{\sigma_n-1}di}$, is entirely determined by firm i's relative preference shifter and physical productivity within the region-sector and aligns with sales share θ_{nit}^*.

Proof. We first re-write the expression for output Y_{nit} in Equation 35 by plugging in for P_{nit}

$$\begin{aligned}
Y_{nit} &= A_{nit} K_{nit}^{\alpha_{Kn}} L_{nit}^{\alpha_{Ln}} \\
&= A_{nit} \alpha_{K_n}^{\alpha_{Kn}} \alpha_{L_n}^{\alpha_{Ln}} (1 - \tau_{ni}^{Y}(\tilde{\mathbf{T}}_{rt}, \cdot)) \frac{\sigma_n - 1}{\sigma_n} \underbrace{P_{nit}}_{\left(\frac{Y_{nit}}{B_{nit} Y_{nt}}\right)^{-\frac{1}{\sigma_n}} P_{nt}} Y_{nit} \left[\frac{1}{(1 + \tau_{ni}^{K}(\tilde{\mathbf{T}}_{rt}, \cdot)) P_{nt}^{K}}\right]^{\alpha_{Kn}} \left[\frac{1}{(1 + \tau_{ni}^{L}(\tilde{\mathbf{T}}_{rt}, \cdot)) P_{nt}^{L}}\right]^{\alpha_{Ln}} \\
Y_{nit}^{\frac{1}{\sigma_n}} &= A_{nit} \alpha_{K_n}^{\alpha_{Kn}} \alpha_{L_n}^{\alpha_{Ln}} (1 - \tau_{ni}^{Y}(\tilde{\mathbf{T}}_{rt}, \cdot)) \frac{\sigma_n - 1}{\sigma_n} P_{nt} (B_{nit} Y_{nt})^{\frac{1}{\sigma_n}} \left[\frac{1}{(1 + \tau_{ni}^{K}(\tilde{\mathbf{T}}_{rt}, \cdot)) P_{nt}^{K}}\right]^{\alpha_{Kn}} \left[\frac{1}{(1 + \tau_{ni}^{L}(\tilde{\mathbf{T}}_{rt}, \cdot)) P_{nt}^{L}}\right]^{\alpha_{Ln}} \\
Y_{nit} &= B_{nit} Y_{nt} \left\{ A_{nit} \alpha_{K_n}^{\alpha_{Kn}} \alpha_{L_n}^{\alpha_{Ln}} (1 - \tau_{ni}^{Y}(\tilde{\mathbf{T}}_{rt}, \cdot)) \frac{\sigma_n - 1}{\sigma_n} P_{nt} \left[\frac{1}{(1 + \tau_{ni}^{K}(\tilde{\mathbf{T}}_{rt}, \cdot)) P_{nt}^{K}}\right]^{\alpha_{Kn}} \left[\frac{1}{(1 + \tau_{ni}^{L}(\tilde{\mathbf{T}}_{rt}, \cdot)) P_{nt}^{L}}\right]^{\alpha_{Ln}} \right\}^{\sigma_n}
\end{aligned} \tag{38}$$

Next we solve for factor allocation K_{nit} and L_{nit} and express them to be a function of the wedges, aggregate variables, prices and parameters. Plugging Equation 38 back to the first-order conditions of capital and labor, and rearranging terms in the FOCs to connect to sales share θ_{nit} yields

$$\begin{aligned}
F_{nit} = Z_{nt} \frac{(1 - \tau_{ni}^{Y}(\tilde{\mathbf{T}}_{rt}, \cdot))}{(1 + \tau_{ni}^{F}(\tilde{\mathbf{T}}_{rt}, \cdot))} \theta_{nit} \int_i B_{nit} \left\{ A_{nit} (1 - \tau_{ni}^{Y}(\tilde{\mathbf{T}}_{rt}, \cdot)) \left[\frac{1}{(1 + \tau_{ni}^{K}(\tilde{\mathbf{T}}_{rt}, \cdot))}\right]^{\alpha_{Kn}} \left[\frac{1}{(1 + \tau_{ni}^{L}(\tilde{\mathbf{T}}_{rt}, \cdot))}\right]^{\alpha_{Ln}} \right\}^{\sigma_n - 1} di \\
F \in (K, L),
\end{aligned} \tag{39}$$

where $Z_{nt} = \alpha_{Kn} \left[\frac{\sigma_n - 1}{\sigma_n} P_{nt}\right]^{\sigma_n} Y_{nt} \frac{1}{P_{nt}^{K}} \left[\left(\frac{\alpha_{Kn}}{P_{nt}^{K}}\right)^{\alpha_{Kn}} \left(\frac{\alpha_{Ln}}{P_{nt}^{L}}\right)^{\alpha_{Ln}}\right]^{\sigma_n - 1}$.

Aggregate across firms:

$$\begin{aligned}
F_{nt} &= \int_i F_{nit} di \\
&= Z_{nt} \int_i B_{nit} \left\{ A_{nit} (1 - \tau_{ni}^{Y}(\tilde{\mathbf{T}}_{rt}, \cdot)) \left[\frac{1}{(1 + \tau_{ni}^{K}(\tilde{\mathbf{T}}_{rt}, \cdot))}\right]^{\alpha_{Kn}} \left[\frac{1}{(1 + \tau_{ni}^{L}(\tilde{\mathbf{T}}_{rt}, \cdot))}\right]^{\alpha_{Ln}} \right\}^{\sigma_n - 1} di \\
&\cdot \int_i \frac{(1 - \tau_{ni}^{Y}(\tilde{\mathbf{T}}_{rt}, \cdot))}{(1 + \tau_{ni}^{F}(\tilde{\mathbf{T}}_{rt}, \cdot))} \theta_{nit} di
\end{aligned}$$

The ratio between firm and region allocation $\frac{F_{nit}}{F_{nt}}$ is

$$\frac{F_{nit}}{F_{nt}} = \frac{\frac{(1 - \tau_{ni}^{Y}(\tilde{\mathbf{T}}_{rt}, \cdot))}{(1 + \tau_{ni}^{F}(\tilde{\mathbf{T}}_{rt}, \cdot))} \theta_{nit}}{\int_i \frac{(1 - \tau_{ni}^{Y}(\tilde{\mathbf{T}}_{rt}, \cdot))}{(1 + \tau_{ni}^{F}(\tilde{\mathbf{T}}_{rt}, \cdot))} \theta_{nit} di}$$

We can evaluate the expression at the efficient equilibrium where all distortions are eliminated and obtain

$$\frac{F_{nit}^{*}}{F_{nt}^{*}} = \frac{\theta_{nit}^{*}}{\underbrace{\theta_{nt}^{*}}_{=1}} = \theta_{nit}^{*}$$

Finally, combining this with Equation (A.2) yields

$$\frac{F_{nit}/F_{nt}}{F_{nit}^{*}/F_{nt}^{*}} = \frac{F_{nit}}{F_{nit}^{*}} = \frac{\frac{(1 - \tau_{ni}^{Y}(\tilde{\mathbf{T}}_{rt}, \cdot))}{(1 + \tau_{ni}^{F}(\tilde{\mathbf{T}}_{rt}, \cdot))}}{\int_i \frac{(1 - \tau_{ni}^{Y}(\tilde{\mathbf{T}}_{rt}, \cdot))}{(1 + \tau_{ni}^{F}(\tilde{\mathbf{T}}_{rt}, \cdot))} \theta_{nit} di} \frac{\theta_{nit}}{\theta_{nit}^{*}},$$

where the aggregate factor is exogenously given and $K_{nt} = K^*_{nt}$. Taking log yields a more intuitive expression

$$\log \frac{F_{nit}}{F^*_{nit}} = \log \frac{\frac{(1-\tau^Y_{ni}(\tilde{\mathbf{T}}_{rt},\cdot))}{(1+\tau^F_{ni}(\tilde{\mathbf{T}}_{rt},\cdot))}}{\int_i \frac{(1-\tau^Y_{ni}(\tilde{\mathbf{T}}_{rt},\cdot))}{(1+\tau^F_{ni}(\tilde{\mathbf{T}}_{rt},\cdot))}\theta_{nit}di} + \log \frac{\theta_{nit}}{\theta^*_{nit}} = \log \frac{\frac{(1-\tau^Y_{ni}(\tilde{\mathbf{T}}_{rt},\cdot))}{(1+\tau^F_{ni}(\tilde{\mathbf{T}}_{rt},\cdot))}}{(1+\tau^F_{nt})} + \log \frac{\theta_{nit}}{\theta^*_{nit}}.$$

When factor-F distortions $(1+\tau^F_{nit})$ are the only sources of distortions present, we arrive at the exact expression as in (**??**) in Proposition 1.

■

A.3 Proof of Proposition 2

Proposition 2. Aggregation and TFP Decomposition. Each region–sector n admits an aggregate production function of the form

$$Y_{nt} = \text{TFP}_{nt} K_{nt}^{\alpha_{Kn}} L_{nt}^{\alpha_{Ln}},$$

where, under a second-order approximation, region–sectoral aggregate total factor productivity $\text{TFP}_{nt} := \text{TFP}_n\left(\tilde{\mathbf{T}}_{rt}, \tilde{\mathbf{X}}_{nt}\right)$ can be decomposed as follows:

$$\begin{aligned}
\log \text{TFP}_n(\tilde{\mathbf{T}}_{rt},\cdot) = {} & \underbrace{\frac{1}{\sigma_n - 1}\log\left[\mathbb{E}_i\left[B_{ni}(\tilde{\mathbf{T}}_{rt},\cdot)\left(A_{ni}(\tilde{\mathbf{T}}_{rt},\cdot)\right)^{\sigma_n-1}\right]\right]}_{\text{Technology}(\log \text{TFP}^E_n)} + \frac{1}{\sigma_n-1}\log J_n \\
& \underbrace{-\frac{\sigma_n}{2}\,\text{var}_{\log\left(1-\tau^Y_{ni}\right)}(\tilde{\mathbf{T}}_{rt},\cdot)}_{\text{Output Wedge Dispersion}} \\
& \underbrace{-\sum_{F\in\{K,L\}}\frac{\alpha_{Fn}+\alpha^2_{Fn}(\sigma_n-1)}{2}\,\text{var}_{\log\left(1+\tau^F_{ni}\right)}(\tilde{\mathbf{T}}_{rt},\cdot)}_{\text{Factor Wedge Dispersion}} \\
& \underbrace{+\sigma_n\sum_{F\in\{K,L\}}\alpha_{Fn}\,\text{cov}_{\log\left(1-\tau^Y_{ni}\right),\log\left(1+\tau^F_{ni}\right)}\left(\tilde{\mathbf{T}}_{rt},\cdot\right)}_{\text{Output-Factor Mixed Distortion}} \\
& \underbrace{-(\sigma_n-1)\alpha_{Kn}\alpha_{Ln}\,\text{cov}_{\log\left(1+\tau^K_{ni}\right),\log\left(1+\tau^L_{ni}\right)}\left(\tilde{\mathbf{T}}_{rt},\cdot\right)}_{\text{Factor Mixed Distortion}}
\end{aligned} \tag{40}$$

Proof. Note that $P_{nt} = 1$. Rearranging Equation 39 yields

$$\left(\frac{\alpha_{L_n}}{W_{nt}}\right)^{\alpha_{L_n}(\sigma_n-1)} = \frac{1}{\left(\frac{\sigma_n-1}{\sigma_n}\right)^{\sigma_n-1}\left(\frac{\alpha_{Kn}}{R_{nt}}\right)^{\alpha_{Kn}(\sigma_n-1)} I_{nt}},$$

where $I_{nt} = \int_i B_{nit}\left\{A_{nit}(1-\tau^Y_{ni}(\tilde{\mathbf{T}}_{rt},\cdot))\left[\frac{1}{(1+\tau^K_{ni}(\tilde{\mathbf{T}}_{rt},\cdot))}\right]^{\alpha_{Kn}}\left[\frac{1}{(1+\tau^L_{ni}(\tilde{\mathbf{T}}_{rt},\cdot))}\right]^{\alpha_{Ln}}\right\}^{\sigma_n-1}$. Plugging Equa-

tion A.3 to aggregate capital yields

$$K_{nt} = Y_{nt}\frac{\alpha_{K_n}}{R_{nt}}\left[\frac{\sigma_n-1}{\sigma_n}\right]^{\sigma_n}\left[\left(\frac{\alpha_{K_n}}{R_{nt}}\right)^{\alpha_{Kn}}\left(\frac{\alpha_{L_n}}{W_{nt}}\right)^{\alpha_{Ln}}\right]^{\sigma_n-1}J_{nt}$$
$$\frac{K_{nt}}{Y_{nt}} = \left(\frac{\alpha_{K_n}}{R_{nt}}\right)\frac{\sigma_n-1}{\sigma_n}\frac{J_{nt}}{I_{nt}},$$

where $J_{nt} = \int_i \left[(1-\tau^Y_{ni}(\tilde{\mathbf{T}}_{rt},\cdot))\right]^{\sigma_n} B_{nit}\frac{1}{(1+\tau^K_{ni}(\tilde{\mathbf{T}}_{rt},\cdot))}\left\{A_{nit}\left[\frac{1}{(1+\tau^K_{ni}(\tilde{\mathbf{T}}_{rt},\cdot))}\right]^{\alpha_{Kn}}\left[\frac{1}{(1+\tau^L_{ni}(\tilde{\mathbf{T}}_{rt},\cdot))}\right]^{\alpha_{Ln}}\right\}^{\sigma_n-1}$.
Taking logs yield

$$\log\frac{Y_{nt}}{K_{nt}} = \log I_{nt} - \log J_{nt} - \log\left(\frac{\sigma_n-1}{\sigma_n}\right)\frac{\alpha_{K_n}}{R_{nt}}.$$

Using Equation A.3 once again to obtain aggregate labor

$$L_{nt} = Y_{nt}\left(\frac{\sigma_n-1}{\sigma_n}\right)^{\frac{-\alpha_{K_n}}{1-\alpha_{K_n}}}\left(\frac{\alpha_{K_n}}{R_{nt}}\right)^{-\frac{\alpha_{K_n}}{1-\alpha_{K_n}}}Q_{nt}I_{nt}^{-1-\frac{1}{\alpha_{L_n}(\sigma_n-1)}},$$

where $Q_{nt} = \int_i \left[(1-\tau^Y_{ni}(\tilde{\mathbf{T}}_{rt},\cdot))\right]^{\sigma_n} B_{nit}\frac{1}{(1+\tau^L_{ni}(\tilde{\mathbf{T}}_{rt},\cdot))}\left\{A_{nit}\left[\frac{1}{(1+\tau^K_{ni}(\tilde{\mathbf{T}}_{rt},\cdot))}\right]^{\alpha_{Kn}}\left[\frac{1}{(1+\tau^L_{ni}(\tilde{\mathbf{T}}_{rt},\cdot))}\right]^{\alpha_{Ln}}\right\}^{\sigma_n-1}$.
Taking logs yield

$$\log\frac{Y_{nt}}{L_{nt}} = \left(1+\frac{1}{\alpha_{L_n}(\sigma_n-1)}\right)\log I_{nt} - \log Q_{nt} + \frac{\alpha_{K_n}}{1-\alpha_{K_n}}\log\frac{\sigma_n-1}{\sigma_n}\frac{\alpha_{K_n}}{R_{nt}}.$$

This allows to find aggregate TFP in the distorted economy:

$$\begin{aligned}\text{TFP}_{nt} &:= \frac{Y_{nt}}{K_{nt}^{\alpha_{Kn}}L_{nt}^{\alpha_{Ln}}}\\ \log TFP_{nt} &= \alpha_{K_n}\log\frac{Y_{nt}}{K_{nt}} + \alpha_{L_n}\log\frac{Y_{nt}}{L_{nt}}\\ &= \frac{\sigma_n}{\sigma_n-1}\log I_{nt} - \alpha_{K_n}\log J_{nt} - \alpha_{L_n}\log Q_{nt}\end{aligned}$$

where

$$\log I_{nt} = \log\int_i B_{nit}\left\{A_{nit}(1-\tau^Y_{ni}(\tilde{\mathbf{T}}_{rt},\cdot))\left[\frac{1}{(1+\tau^K_{ni}(\tilde{\mathbf{T}}_{rt},\cdot))}\right]^{\alpha_{Kn}}\left[\frac{1}{(1+\tau^L_{ni}(\tilde{\mathbf{T}}_{rt},\cdot))}\right]^{\alpha_{Ln}}\right\}^{\sigma_n-1}$$
$$\log J_{nt} = \log\int_i \left[(1-\tau^Y_{ni}(\tilde{\mathbf{T}}_{rt},\cdot))\right]^{\sigma_n} B_{nit}\frac{1}{(1+\tau^K_{ni}(\tilde{\mathbf{T}}_{rt},\cdot))}\left\{A_{nit}\left[\frac{1}{(1+\tau^K_{ni}(\tilde{\mathbf{T}}_{rt},\cdot))}\right]^{\alpha_{Kn}}\left[\frac{1}{(1+\tau^L_{ni}(\tilde{\mathbf{T}}_{rt},\cdot))}\right]^{\alpha_{Ln}}\right\}^{\sigma_n-1}$$
$$\log Q_{nt} = \log\int_i \left[(1-\tau^Y_{ni}(\tilde{\mathbf{T}}_{rt},\cdot))\right]^{\sigma_n} B_{nit}\frac{1}{(1+\tau^L_{ni}(\tilde{\mathbf{T}}_{rt},\cdot))}\left\{A_{nit}\left[\frac{1}{(1+\tau^K_{ni}(\tilde{\mathbf{T}}_{rt},\cdot))}\right]^{\alpha_{Kn}}\left[\frac{1}{(1+\tau^L_{ni}(\tilde{\mathbf{T}}_{rt},\cdot))}\right]^{\alpha_{Ln}}\right\}^{\sigma_n-1}$$

We use the following second-order approximation. Let x_i be any firm-level term and normalize the measure so that $\int di = 1$ (so $\int \cdot\, di = \mathbb{E}[\cdot]$). Define

$$\mu \equiv \mathbb{E}[x_i], \qquad \tilde{x}_i \equiv x_i - \mu, \qquad \mathbb{E}[\tilde{x}_i] = 0.$$

Then

$$\ln\left(\int e^{x_i}\,di\right) = \ln\left(\int e^{\mu+\tilde{x}_i}\,di\right) = \mu + \ln\left(\int e^{\tilde{x}_i}\,di\right).$$

A second-order expansion of $e^{\tilde{x}_i}$ around zero implies

$$\int e^{\tilde{x}_i}\, di \approx \int \left(1 + \tilde{x}_i + \frac{1}{2}\tilde{x}_i^2\right) di = 1 + \frac{1}{2}\mathbb{E}[\tilde{x}_i^2] = 1 + \frac{1}{2}\mathbb{VAR}(x_i).$$

Next, apply the second-order expansion of $\ln(1+u)$:

$$\ln(1+u) = u - \frac{u^2}{2} + O(u^3), \qquad u = \frac{1}{2}\mathbb{VAR}(x_i),$$

to obtain

$$\ln\left(\int e^{\tilde{x}_i}\, di\right) = \ln\left(1 + \frac{1}{2}\mathbb{VAR}(x_i)\right) = \frac{1}{2}\mathbb{VAR}(x_i) - \frac{1}{8}\mathbb{VAR}(x_i)^2 + O\big(\mathbb{VAR}(x_i)^3\big)\,.$$

Combining terms yields

$$\ln\left(\int e^{x_i}\, di\right) = \mathbb{E}[x_i] + \frac{1}{2}\mathbb{VAR}(x_i) - \frac{1}{8}\mathbb{VAR}(x_i)^2 + O\big(\mathbb{VAR}(x_i)^3\big)\,.$$

Writing $x_i = \mu + \varepsilon z_i$ with $\mathbb{E}[z_i] = 0$ and $\mathbb{VAR}(z_i) = 1$ implies $\mathbb{VAR}(x_i) = \varepsilon^2$, so $\mathbb{VAR}(x_i)^2 = O(\varepsilon^4)$. Hence, under a second-order approximation,

$$\ln\left(\int e^{x_i}\, di\right) = \mathbb{E}[x_i] + \frac{1}{2}\mathbb{VAR}(x_i) + O(\varepsilon^4),$$

For a multivariate case when x_i is a sum of logs, $x_i = \log A_i + \log B_i + \log C_i$, this implies

$$\begin{aligned}\ln\left(\int e^{\log A_i + \log B_i + \log C_i}\, di\right) \approx\ & \mathbb{E}[\log A_i] + \mathbb{E}[\log B_i] + \mathbb{E}[\log C_i] \\ & + \frac{1}{2}\mathbb{VAR}(\log A_i) + \frac{1}{2}\mathbb{VAR}(\log B_i) + \frac{1}{2}\mathbb{VAR}(\log C_i) \\ & + \mathbb{COV}(\log A_i, \log B_i) + \mathbb{COV}(\log A_i, \log C_i) + \mathbb{COV}(\log B_i, \log C_i).\end{aligned}$$

We apply this second-order approximation to all the $\log I_{nt}, \log J_{nt}, \log Q_{nt}$ to obtain

$$\begin{aligned}\log \mathrm{TFP}_n(\tilde{\mathbf{T}}_{rt}, \cdot) =\ & \underbrace{\frac{1}{\sigma_n - 1}\log \mathbb{E}_i\left[B_{ni}(\tilde{\mathbf{T}}_{rt}, \cdot)\left(A_{ni}(\tilde{\mathbf{T}}_{rt}, \cdot)\right)^{\sigma_n - 1}\right]}_{\text{Technology}(\log \mathrm{TFP}_n^E)} - \underbrace{\frac{\sigma_n}{2}\operatorname{var}_{\log\left(1-\tau_{ni}^Y\right)}(\tilde{\mathbf{T}}_{rt}, \cdot)}_{\text{Output Wedge Dispersion}} \\ & \underbrace{- \sum_{F \in \{K,L\}} \frac{\alpha_{Fn} + \alpha_{Fn}^2(\sigma_n - 1)}{2} \operatorname{var}_{\log\left(1+\tau_{ni}^F\right)}(\tilde{\mathbf{T}}_{rt}, \cdot)}_{\text{Factor Wedge Dispersion}} \\ & \underbrace{+ \sigma_n \sum_{F \in \{K,L\}} \alpha_{Fn} \operatorname{cov}_{\log\left(1-\tau_{ni}^Y\right), \log\left(1+\tau_{ni}^F\right)}\left(\tilde{\mathbf{T}}_{rt}, \cdot\right)}_{\text{Output-Factor Mixed Distortion}} \\ & \underbrace{- (\sigma_n - 1)\alpha_{Kn}\alpha_{Ln} \operatorname{cov}_{\log\left(1+\tau_{ni}^K\right), \log\left(1+\tau_{ni}^L\right)}\left(\tilde{\mathbf{T}}_{rt}, \cdot\right)}_{\text{Factor Mixed Distortion}}\end{aligned} \tag{41}$$

which is the Equation 7 in the text.

■

B Data Sources and Variable Construction

This appendix details the data sources, cleaning procedures, and variable construction that supplement Section 3.

B.1 Orbis Data (Europe)

Our European firm data come from the Orbis Historical Disk Product maintained by Bureau van Dijk (now Moody's). Orbis aggregates administrative filings from over 170 information providers across countries, including national business registries and regulatory bodies (Kalemli- Özcan et al. 2024). Under EU Directive 2013/34/EU, limited liability companies in all 30 countries in our sample are required to file financial statements, which gives Orbis broad coverage of the formal sector—approximately 99% of covered firms are private entities. Since our analysis centers on MRPK dispersion, we retain every firm-year observation with non-missing revenue and fixed assets, which maximizes coverage of the revenue-to-capital ratio.[27] The pooled sample spans 1998–2018; country-specific coverage periods are listed in Table B.1.

Sample cleaning. Following Kalemli- Özcan et al. (2024), we link multiple vintages of Orbis products over time and match each firm's descriptive information with its financial records via the unique BvD firm identifier (BVDID). We then apply the following cleaning steps:

1. We restrict to firms whose country of residence (latest address) matches the ISO-2 code embedded in their BVDID. Firms with mismatched codes are excluded.
2. For firms lacking address information but possessing postcodes, we manually map postcodes to NUTS 3 regions within each country.
3. We harmonize fiscal years with calendar years based on the closing date: if the closing date is on or after July 1, we assign the current calendar year; otherwise, the previous year.
4. Following Fan (2024), we use unconsolidated accounts to avoid double-counting that can arise with consolidated reporting. When a firm reports multiple sales figures from different sources (e.g., local registries, annual reports), we prioritize the unconsolidated entry.
5. We keep only observations with non-missing and positive sales (`operating_revenue_turnover`) and fixed assets (`fixed_assets`).
6. We compute firm-level log MRPK as

$$\log \text{MRPK}_{it} = \log\Big(\alpha_{Kn} \frac{\sigma_n - 1}{\sigma_n} \frac{P_{it}Y_{it}}{K_{it}}\Big),$$

   where $P_{it}Y_{it}$ is measured with sales and K_{it} with fixed assets.

27. This choice follows the same principle as Kalemli- Özcan et al. (2024), Gopinath et al. (2017), and Nath (2025), who each restrict their samples to the variables required by their respective analyses.

7. We winsorize MRPK, fixed assets, and sales at the top and bottom 0.1% of the distribution within each country to prevent outliers from distorting variance estimates.

B.2 China NBS Data

The NBS Annual Survey covers all industrial firms with annual sales above CNY 5 million (1998–2007). These "above-scale" firms account for over 90.7% of total industrial output when benchmarked against the 2004 NBS economic census (Brandt, Van Biesebroeck, and Zhang 2014). Manufacturing constitutes more than 90% of observations; the remaining firms are in mining and utilities. We restrict the sample to 1998–2007 because of well-documented reporting inconsistencies after 2008 (Brandt, Van Biesebroeck, and Zhang 2014; Nath 2025).

Sample cleaning. We follow Zhang et al. (2018). Sales are measured using "产品销售收入" (product sales revenue) and capital using "固定资产合计" (total fixed assets). Each firm is classified by its four-digit Chinese Industry Classification (CIC) code, which we harmonize to the USSIC division level. Firm locations are mapped to prefecture-level divisions. The remaining cleaning (variable construction and winsorization) follows items 5–7 of the Orbis procedure in Appendix B.1.

B.3 India ASI Data

The ASI is a census of large plants (100+ workers) combined with a probability sample of smaller registered plants under the Indian Factories Act (Allcott, Collard-Wexler, and O'Connell 2016).[28] Almost all sampled plants are in manufacturing. The sample period is 1998–2018.

Sample cleaning. We match plants to Indian districts following Somanathan et al. (2021) and harmonize industry codes first to NIC-04, then to USSIC divisions. Sales are measured using the gross sale value of all products; capital is measured as the average of opening and closing net book value of total fixed assets, following Bils, Klenow, and Ruane (2021).[29] The ASI also records whether a plant has computerized air-conditioning (2001–2014), which we exploit as an adaptation proxy in Section 6. The remaining cleaning follows items 5–7 of Appendix B.1.

B.4 Temperature Variable Construction

Starting from hourly ERA5-Land data at 0.1° resolution, we compute the daily maximum and minimum 2 m air temperature for each grid cell and take their geometric mean as the daily average.[30] We aggregate to the regional level using area-weighted averages over all grid cells intersecting each NUTS 3 region, prefecture, or district. Annual temperature bins are then constructed

28. The census threshold was 200 workers during 1997–2003. The sampling fraction for smaller plants was one-third until 2004 and one-fifth thereafter.

29. We use net rather than gross fixed assets because gross values in ASI contain substantial missing data. In Section 3 we note that results are not sensitive to this choice.

30. The daily maximum (minimum) is the highest (lowest) value among the 24 hourly readings within a grid cell.

by counting the number of days each region's daily average temperature falls within each 5°C interval: <-5, $[-5,0)$, $[0,5)$, $\ldots$, $[25,30)$, ≥ 30°C. Because the bins sum to 365 (or 366) days per year, we omit the $[5,10)$°C bin as the reference category in all regressions to avoid perfect collinearity.

B.5 Forecast Error and Uncertainty Construction

We construct three forecast-related objects from the ECMWF seasonal forecast data: monthly forecast errors, annual mean squared forecast errors (MSFE), and perceived forecast uncertainty. This subsection details each step.

Monthly forecast errors. For each region r and month m, we compute the raw forecast error as the difference between realized monthly mean temperature and the ensemble-mean ECMWF seasonal forecast issued on the first day of that month. We then remove a region-by-month fixed effect $\widehat{\text{Bias}}_{m,r}$, to correct for systematic biases in the forecast product that may reflect differences in forecast methodology across regions and seasons.

Annual MSFE. We aggregate monthly squared forecast errors to the annual level by averaging across all twelve months within each region-year:

$$\text{MSFE}_{\text{annual},r,t} = \frac{1}{12}\sum_{m=1}^{12}\left(T_{m,r,t} - \mathbb{E}_{m-1}[T_{m,r,t}] - \widehat{\text{Bias}}_{m,r}\right)^2.$$

We also construct seasonal variants (summer: April–September; winter: October–March) for robustness. Because the ECMWF product provides month-ahead forecasts rather than year-ahead forecasts, the monthly MSFE and the annual forecast-error variance from the AR(6) model in Section 7 operate at different horizons. To map the ECMWF-based MSFE into an annual-scale squared forecast error consistent with the model, we rescale by preserving the ECMWF forecast's relative improvement over a monthly AR(6) benchmark:

$$\left(T_{rt} - \mathbb{E}_{t-1}T_{rt}\right)^2 = \frac{\text{MSFE}_{rt}}{\frac{1}{12}\sum_{m=1}^{12}\mathbb{VAR}^{1998\text{–}2018}\left(\widehat{\varepsilon}^{T}_{rmt}\right)}\,\mathbb{VAR}^{1998\text{–}2018}\left(\widehat{\varepsilon}^{T}_{rt}\right),$$

where $\widehat{\varepsilon}^{T}_{rmt}$ is the month-m AR(6) forecast error and $\widehat{\varepsilon}^{T}_{rt}$ is the annual AR(6) innovation. This scaling preserves time variation in forecast precision from ECMWF while matching the annual scale of temperature innovations in the estimation sample.

Perceived forecast uncertainty. We model perceived temperature uncertainty as a smoothed ARCH(3) process:

$$\mathbb{VAR}_{t-1}(T_{rt}) = \frac{1}{3}\sum_{\tau=1}^{3}\left(T_{r,t-\tau} - \mathbb{E}_{t-\tau-1}T_{r,t-\tau}\right)^2,$$

so that agents perceive temperature to be more volatile following periods with larger recent forecast errors. This object enters the model's risk-adjustment channel through the households' stochastic discount factor.

B.6 Regional GDP Matching

The DOSE dataset (Wenz et al. 2023) provides sub-national GDP in PPP-adjusted 2017 international dollars. We match DOSE units to our regional definitions (NUTS 3, prefectures, districts) using spatial joins on administrative boundary shapefiles from GADM. Long-run averages of regional GDP per capita and mean temperature (computed over 1997–2018) serve as time-invariant moderators in the heterogeneity analysis of Section 4.4. For end-of-century projections, we use grid-level SSP3 GDP shares from Wang and Sun (2022) to construct projected regional output weights.

B.7 Descriptive Statistics

Table B.1 lists the countries, sample periods, number of regions, and total firm-year observations in the final sample used for empirical analysis.

Table B.1: Descriptive Table of Dataset by Country

Dataset	Country	Coverage	Number of Regions	Number of Firm-Year Obs
NBS China Industrial	China	1998-2007	325	2069100
India ASI	India	1998-2017	267	473646
BvD Orbis	Austria	2004-2018	34	185029
	Belgium	1998-2018	44	781322
	Bulgaria	1998-2018	28	1439871
	Switzerland	2003-2018	3	1701
	Cyprus	2005-2018	1	17356
	Czech Republic	1998-2018	14	1425901
	Germany	1998-2018	346	765981
	Denmark	1999-2018	11	392015
	Estonia	1998-2018	5	791340
	Greece	1998-2018	44	342636
	Spain	1998-2018	52	12210663
	Finland	1998-2018	19	1909080
	France	1998-2018	96	15151185
	Croatia	1998-2018	21	1202515
	Hungary	2004-2018	20	3095326
	Ireland	2000-2018	8	115344
	Italy	1998-2018	107	12083926
	Lithuania	1998-2018	10	129442
	Luxembourg	1998-2018	1	74287
	Latvia	2010-2018	6	533640
	Malta	2000-2018	1	21249
	Netherlands	1998-2018	36	201182
	Norway	1998-2018	12	2462277
	Poland	1998-2018	73	1207428
	Portugal	1998-2018	24	3882515
	Romania	1998-2018	42	4636047
	Sweden	1998-2018	21	3934403
	Slovenia	1998-2018	12	744495
	Slovakia	1998-2018	8	1008353
	United Kingdom	1998-2018	178	3537701

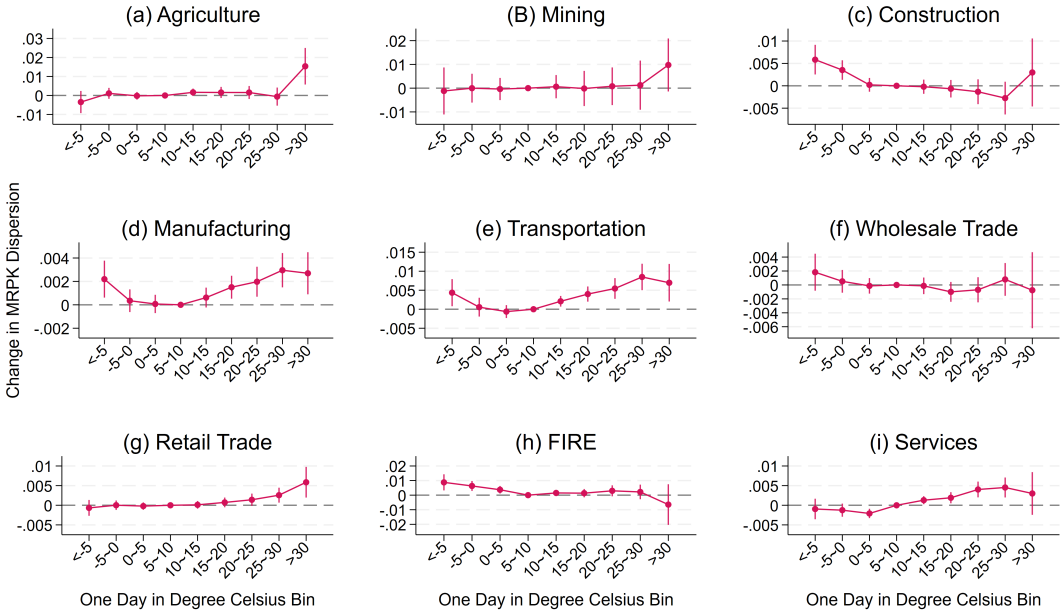
C Robustness for the Empirical Results in Section 4

This appendix examines the sensitivity of the main reduced-form results (Figure 2) to the choice of outcome variable, region–sector definition, weather measure, standard-error clustering, winsorization threshold, and production-function specification.

C.1 Sectoral Results

Figure C.1 reports the estimated effect of daily temperature shocks on regional MRPK dispersion separately for each SIC division. Extreme heat (above 25–30°C) significantly increases MRPK dispersion in agriculture, manufacturing, transportation, services, and retail trade, whereas the effects are modest in mining, construction, wholesale trade, and FIRE. This pattern is consistent with the model's prediction that sectors with greater heterogeneity in product-level climate sensitivity—and with production processes more directly exposed to ambient temperature—exhibit larger MRPK dispersion responses to heat.

Figure C.1: Estimated impact of daily temperature shocks on annual MRPK dispersion by SIC Divisions



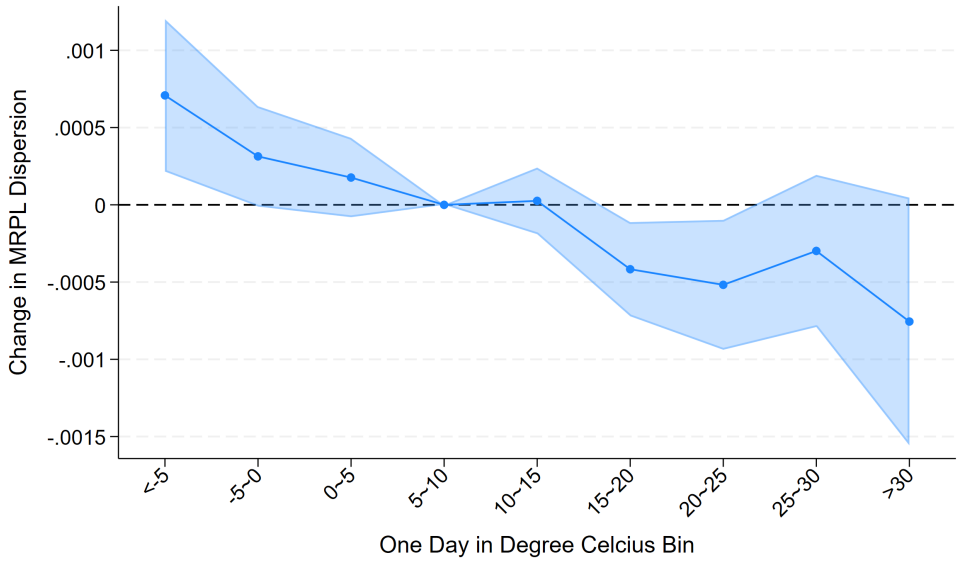
C.2 Temperature's Impact on MRPL and MRPM Dispersion

A natural question is whether temperature shocks also disperse the marginal revenue products of labor and materials. If so, the misallocation channel would extend beyond capital. Figure C.2 and Figure C.3 show that, in contrast to MRPK, neither MRPL nor MRPM dispersion exhibits a statistically significant U-shaped response to temperature. This is consistent with the model's timing: capital and adaptation are committed before temperature is realized, so temperature surprises create wedges between the ex ante capital choice and ex post productivity. Labor and materials,

by contrast, can be adjusted after temperature is observed, allowing firms to partially re-optimize and attenuating dispersion in their marginal products.

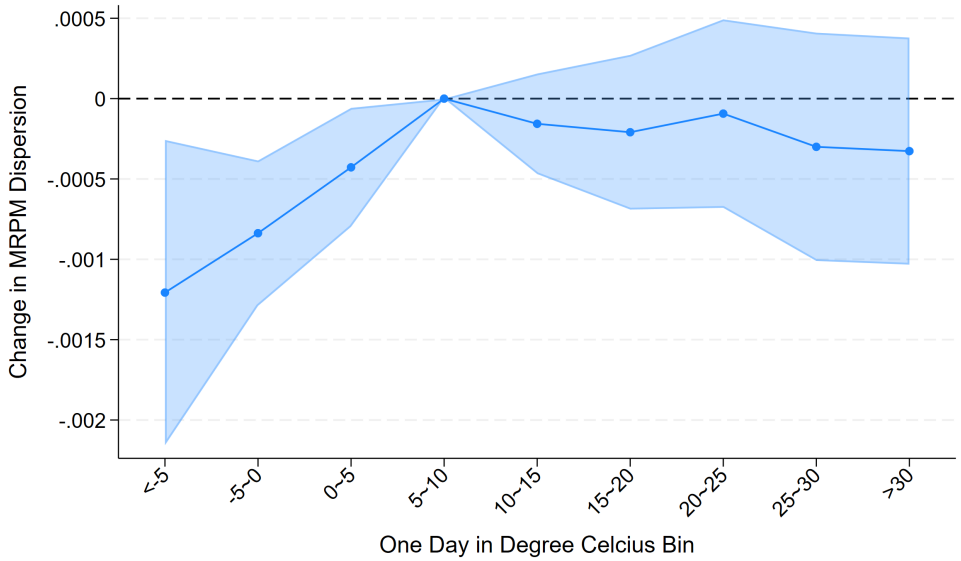
C.2.1 MRPL Dispersion

Figure C.2: Estimated impact of daily temperature shocks on annual MRPL dispersion



C.2.2 MRPM Dispersion

Figure C.3: Estimated impact of daily temperature shocks on annual MRPM dispersion

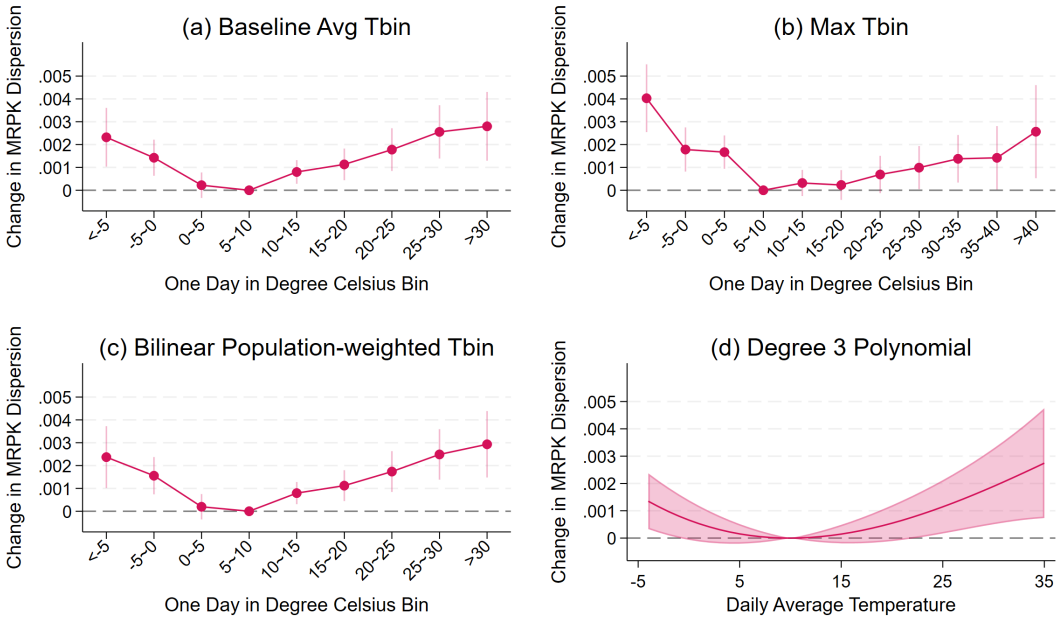


C.3 Alternative Weather Variables and Weighting

Figure C.4 demonstrates that the main results are robust to alternative constructions of the temperature variable. Panel (a) reproduces the baseline using daily mean temperature bins. Panel (b)

replaces mean with daily maximum temperature and extends the bin structure to cover the resulting warmer distribution (> 30, > 35, > 40°C). Panel (c) uses population-weighted regional temperature. Panel (d) replaces temperature bins with a cubic polynomial in daily average temperature. The U-shaped relationship between temperature and MRPK dispersion is present across all four specifications.

Figure C.4: Robustness with Alternative Weather Variables



Notes: Panel (a): baseline (daily mean temperature bins). Panel (b): daily maximum temperature bins. Panel (c): population-weighted regional temperature bins. Panel (d): cubic polynomial in daily average temperature.

C.4 Alternative Standard-Error Clustering

Figure C.5 reports alternative standard-error specifications: clustering by region, two-way clustering by region and year, and two-way clustering by region and country–year. Figure C.6 shows robustness to spatial HAC standard errors. Our results remain statistically significant even when allowing for spatial correlation up to a cutoff distance of 1,000 km.

Figure C.5: Robustness with Alternative Standard-Error Clustering

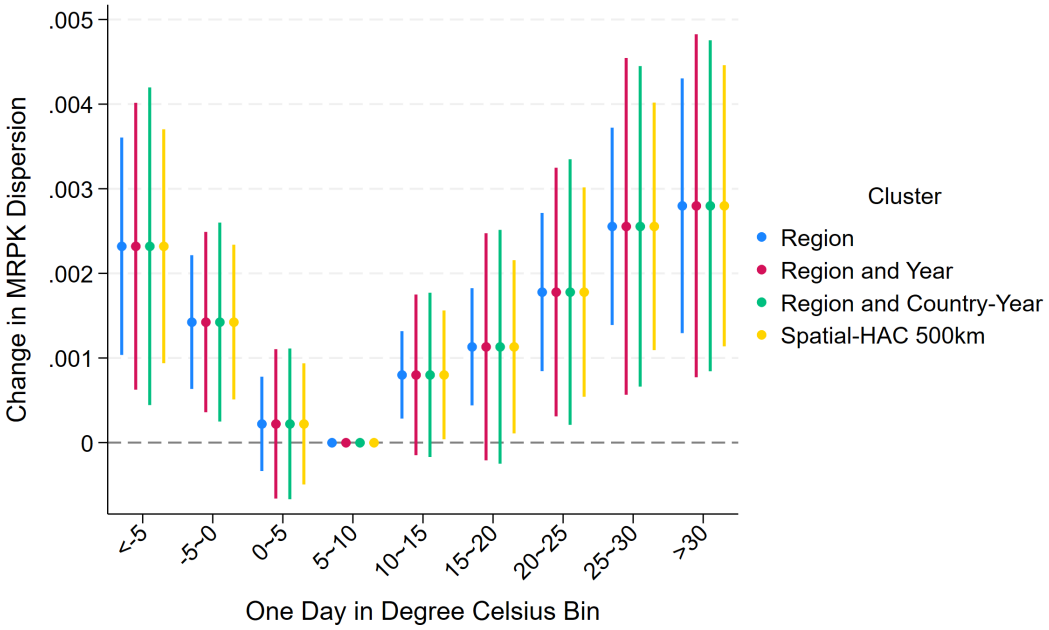
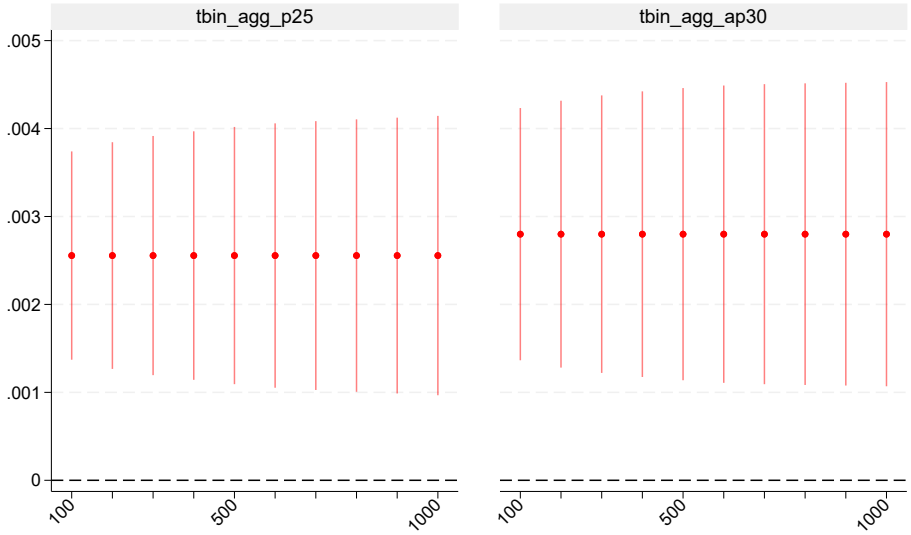


Figure C.6: Robustness with Alternative Distance Cutoffs under Spatial HAC



C.5 Alternative Region–Sector Definitions

The baseline defines region–sector cells as NUTS 3 $\times$ SIC 1-digit. To verify that results are not driven by the level of sectoral aggregation, we re-estimate the main specification under two finer definitions.

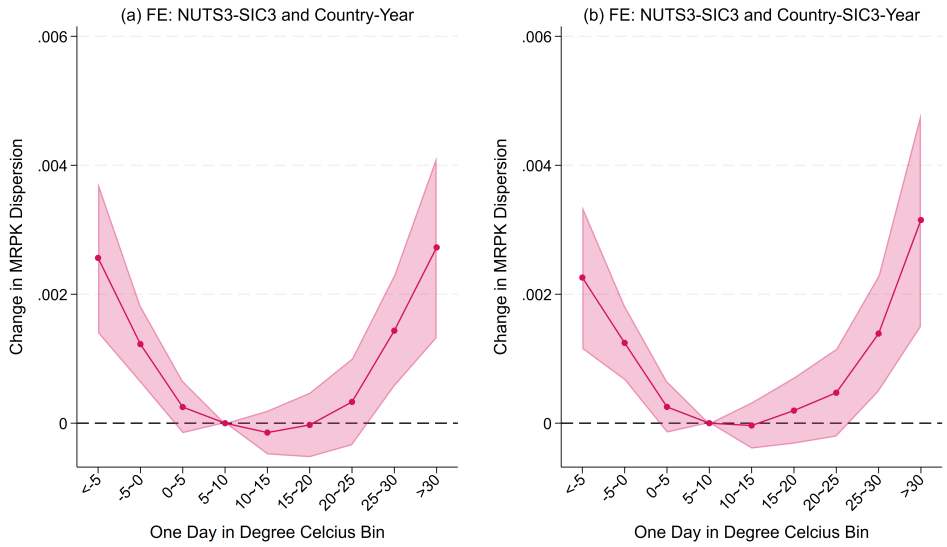
NUTS 3–SIC 2. Figure C.7 redefines the unit as NUTS 3 $\times$ SIC 2-digit, recomputes $\mathrm{Var}(\mathrm{MRPK})$, and re-estimates the baseline under alternative fixed-effect structures. The results are quantitatively similar to the baseline.

Figure C.7: Results Using NUTS 3–SIC 2 as the Region–Sector Unit, Under Alternative Fixed Effects



NUTS 3–SIC 3. For European countries, we further disaggregate to NUTS 3 $\times$ SIC 3-digit. Figure C.8 shows that the main patterns are preserved.

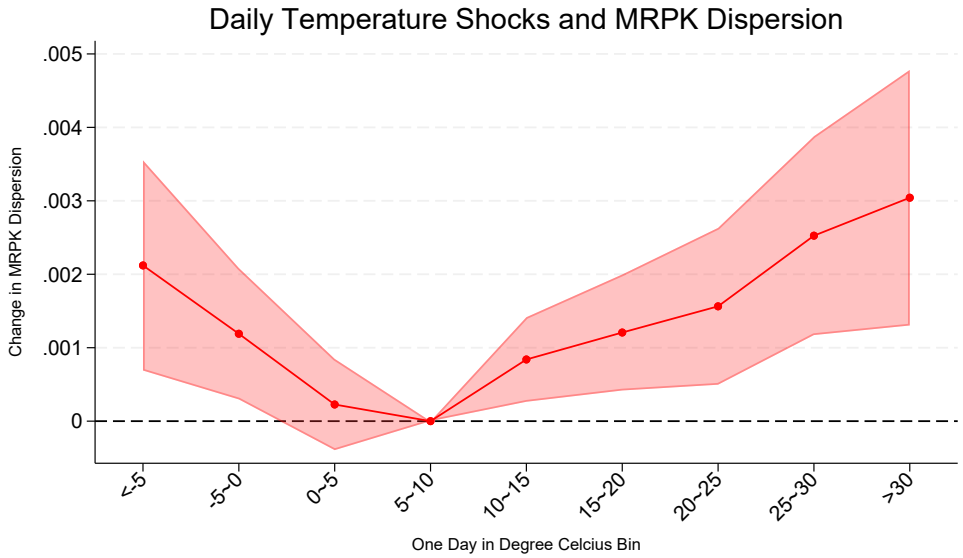
Figure C.8: Results Using NUTS 3–SIC 3 as the Region–Sector Unit, Under Alternative Fixed Effects



C.6 Alternative Winsorization

To verify that results are not driven by extreme outliers in the revenue-to-capital distribution, we winsorize MRPK at the 3% level (rather than the baseline 0.1%) before computing region–sector–year variances. Figure C.9 shows that the results are robust to this substantially more aggressive trimming.

Figure C.9: Estimated Effects of Daily Temperature Shocks on Annual MRPK Dispersion: 3% Winsorized MRPK



C.7 Alternative Production-Function Specifications

The baseline analysis measures MRPK using the revenue-to-capital ratio under Cobb–Douglas production ($\sigma_{\text{CES}} = 1$). This subsection verifies that results hold under CES production, which relaxes the unit-elasticity restriction and allows for different mappings from factor ratios to capital wedge dispersion.

C.7.1 CES with Hicks-Neutral Productivity

Consider a two-input CES production function,

$$Y_{it} = A_{it}\left[\gamma K_{it}^{\frac{\sigma-1}{\sigma}} + (1-\gamma)B_{it}L_{it}^{\frac{\sigma-1}{\sigma}}\right]^{\frac{\sigma}{\sigma-1}},$$

where A_{it} is Hicks-neutral productivity with firm-specific temperature sensitivity, $A_{it} = \tilde{A}_{it}e^{a_{it}T_{rt}}$, and $B_{it} = \tilde{B}_{it}e^{b_{nt}T_{rt}}$ is labor-augmenting productivity with a common regional-sectoral temperature component. When $\sigma \to 1$, this reduces to Cobb–Douglas.

Under monopolistic competition with firm-specific capital wedges τ_{it}^k, the ratio of the capital and labor first-order conditions yields

$$\frac{1}{\sigma}\log\frac{L_{it}}{K_{it}} = \log(1+\tau_{it}^k) + \frac{\sigma-1}{\sigma}\log B_{it} + \log r - \log w - \log\frac{\gamma}{1-\gamma}.$$

Within a region–sector–year, factor prices are common, so the within-cell variance reduces to

$$\frac{1}{\sigma^2}\operatorname{Var}\left(\log\frac{L_{it}}{K_{it}}\right) = \operatorname{Var}\left(\log(1+\tau_{it}^k)\right) + \left(\frac{\sigma-1}{\sigma}\right)^2\operatorname{Var}\left(\log\tilde{B}_{it}\right) + 2\frac{\sigma-1}{\sigma^2}\operatorname{Cov}\left(\log(1+\tau_{it}^k), \log\tilde{B}_{it}\right).$$

Under the assumption that the cross-sectional distributions of $\tilde{B}_{it}$ and its covariance with wedges

do not respond to temperature,[31] the temperature response of capital wedge dispersion is identified as

$$\frac{d\,\mathrm{Var}\big(\log(1+\tau_{it}^{k})\big)}{dT} = \frac{1}{\sigma^2}\,\frac{d\,\mathrm{Var}\Big(\log\frac{L_{it}}{K_{it}}\Big)}{dT}.$$

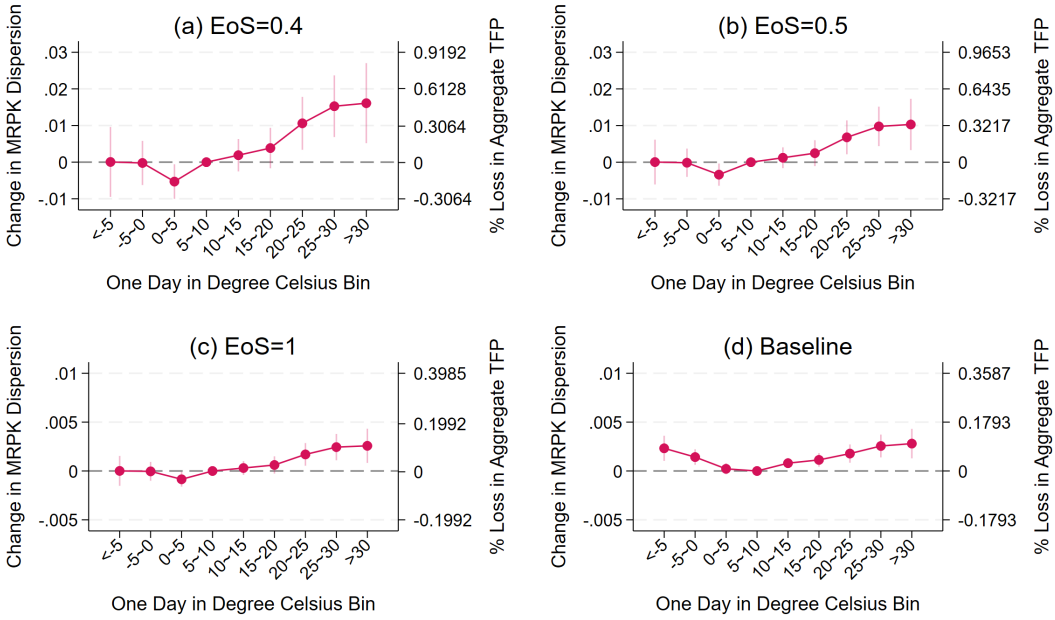
TFP losses. Following Baqaee and Farhi (2019), under CES production over capital and labor, the TFP loss implied by changes in MRPK dispersion is

$$\frac{(\sigma_n-1)\alpha_K^2+\alpha_K^2+\sigma\cdot\alpha_K(1-\alpha_K)}{2}\,\Delta\sigma^2_{mrpk},$$

where σ_n is the demand elasticity and σ is the capital–labor elasticity of substitution.

Results. Figure C.10 reports the estimation under $\sigma \in \{0.4,\ 0.5,\ 1.0\}$, where $\sigma = 0.4$ corresponds to the IV estimates of Oberfield and Raval (2021) and $\sigma = 0.5$ to the average across specifications in the micro–macro literature. The U-shaped relationship between temperature and MRPK dispersion is preserved across all values of σ.

Figure C.10: Estimated Impact of Daily Temperature Shocks on Annual MRPK Dispersion: CES with Hicks-Neutral Productivity



Notes: Panels (a)–(c) measure MRPK dispersion via $\mathrm{Var}(\log(L_{it}/K_{it}))/\sigma^2$ under $\sigma = 0.4$, 0.5, and 1.0 (Cobb–Douglas), respectively. Panel (d) reproduces the baseline using $\mathrm{Var}(\log(PY_{it}/K_{it}))$.

31. This requires that the firm-specific component of labor-augmenting productivity is orthogonal to temperature, and that temperature does not systematically shift the covariance between wedges and labor productivity within a cell.

C.7.2 CES with Labor-Augmenting Productivity and Materials

To allow for labor-augmenting productivity while still identifying capital wedge dispersion, we introduce a third factor—materials M_{it}—into the CES aggregator:

$$Y_{it} = A_{it}\left[K_{it}^{\frac{\sigma-1}{\sigma}} + (B_{it}L_{it})^{\frac{\sigma-1}{\sigma}} + M_{it}^{\frac{\sigma-1}{\sigma}}\right]^{\frac{\sigma}{\sigma-1}}.$$

The capital and materials first-order conditions do not involve B_{it}, so their ratio directly identifies capital wedge dispersion:

$$\log(1+\tau_{it}^{k}) = \frac{1}{\sigma}\log\frac{M_{it}}{K_{it}} + \log\frac{p^{m}}{r},$$

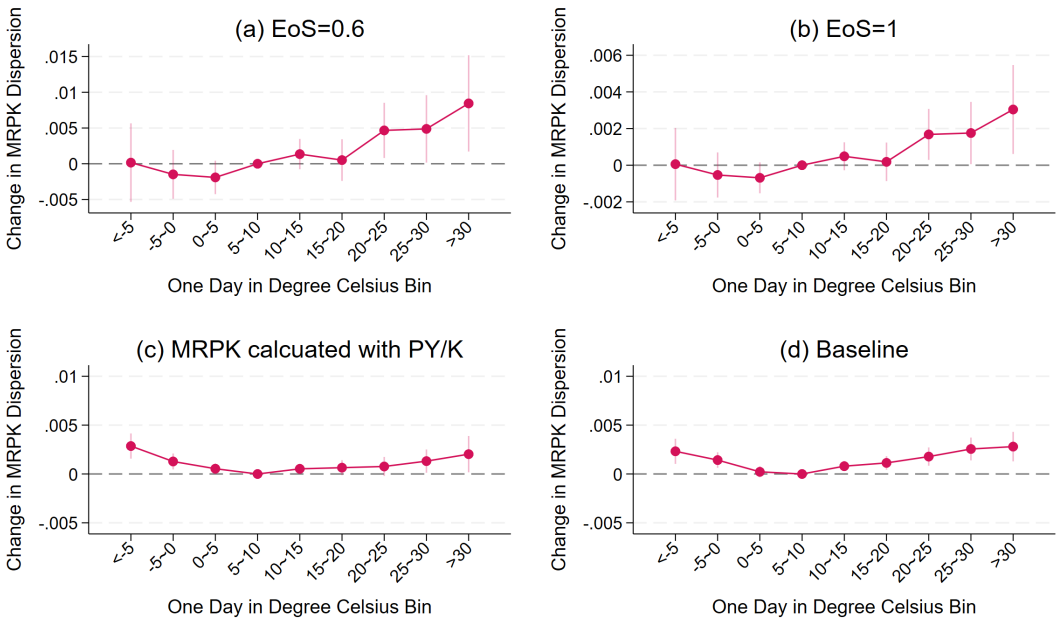
and therefore

$$\mathrm{Var}\Big(\log(1+\tau_{it}^{k})\Big) = \frac{1}{\sigma^{2}}\,\mathrm{Var}\left(\log\frac{M_{it}}{K_{it}}\right),$$

since material prices and rental rates are common within a region–sector–year. This approach eliminates labor-augmenting productivity from the identification without additional assumptions.

Results. Figure C.11 reports the results. The U-shaped pattern is again robust, confirming that the main findings do not depend on the Cobb–Douglas restriction or on the treatment of labor-augmenting productivity.

Figure C.11: Estimated Impact of Daily Temperature Shocks on Annual MRPK Dispersion: CES with Materials



Notes: Panels (a)–(c) measure MRPK dispersion via $\mathrm{Var}(\log(M_{it}/K_{it}))/\sigma^{2}$ under $\sigma = 0.4$, 0.5, and 1.0, respectively. Panel (d) reproduces the baseline using $\mathrm{Var}(\log(PY_{it}/K_{it}))$.

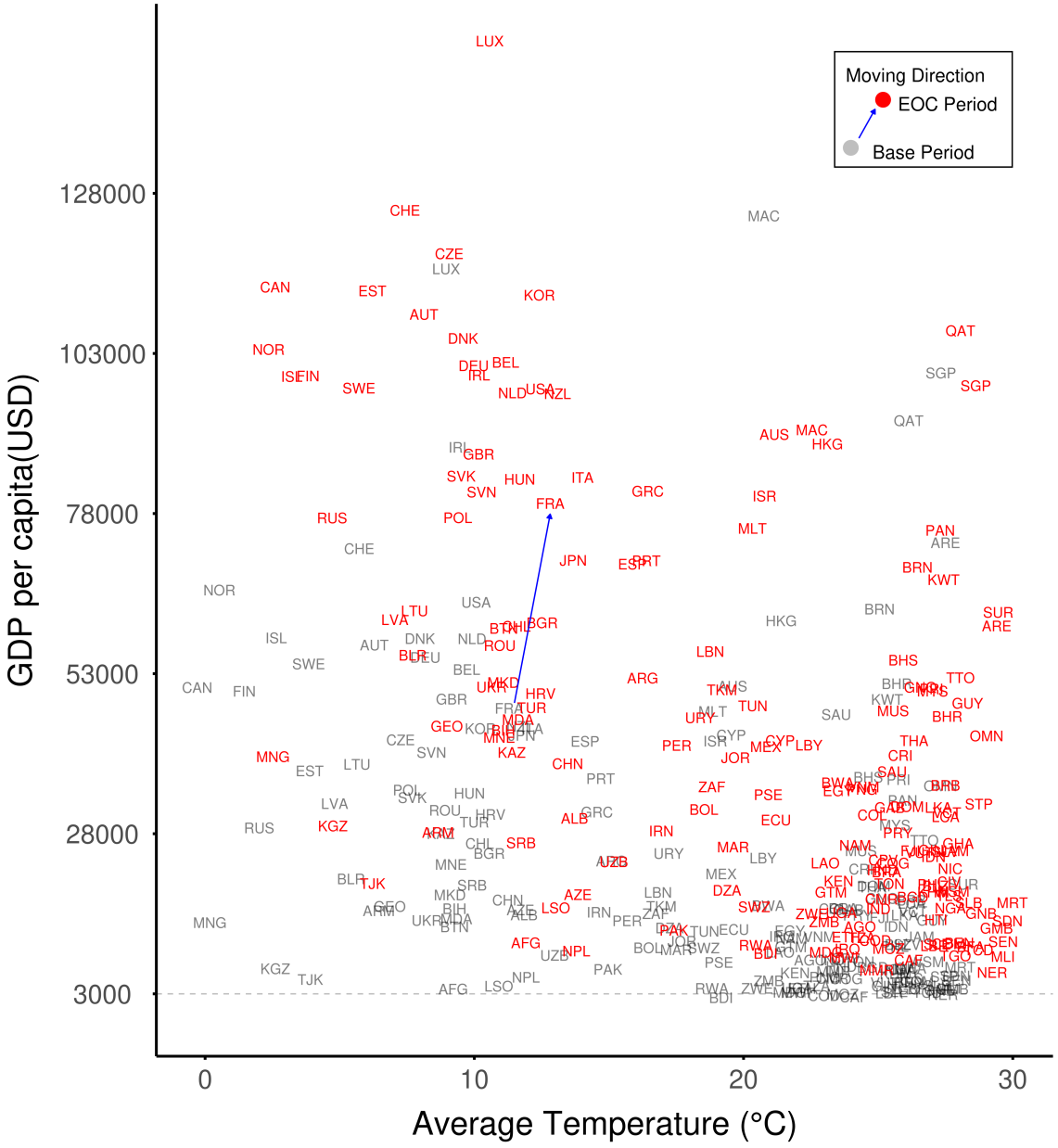
D Additional Figures for Section 4

This appendix provides additional results and figures to complement the main analysis in Section 4.

D.1 Projected Evolution of Income and Temperature under SSP3-4.5

The figure illustrates the projected evolution of income and average temperature from the 2000-2014 baseline to the end of the century (2081-2100) under the SSP3-4.5 scenarios. Among the 172 countries, All 172 countries show a rightward shift (indicating an increase in temperature), and 96% of them also show an upward shift (indicating an increase in per-capita income). In the baseline period, average temperatures are below 5°C in 11 countries, between 5-15°C in 49 countries, between 15-25°C in 62 countries, and above 25°C in 50 countries. Baseline per capita income is below $5000 in 41 countries, between $5000-$30000 in 83 countries, between $30000-$60000 in 38 countries and above $60000 in 10 countries. The blue arrow exemplifies the joint evolution of income and temperature.

Figure D.12: Joint Evolution of Income and Average Temperature from Base Period to End of Century (under SSP3-4.5)



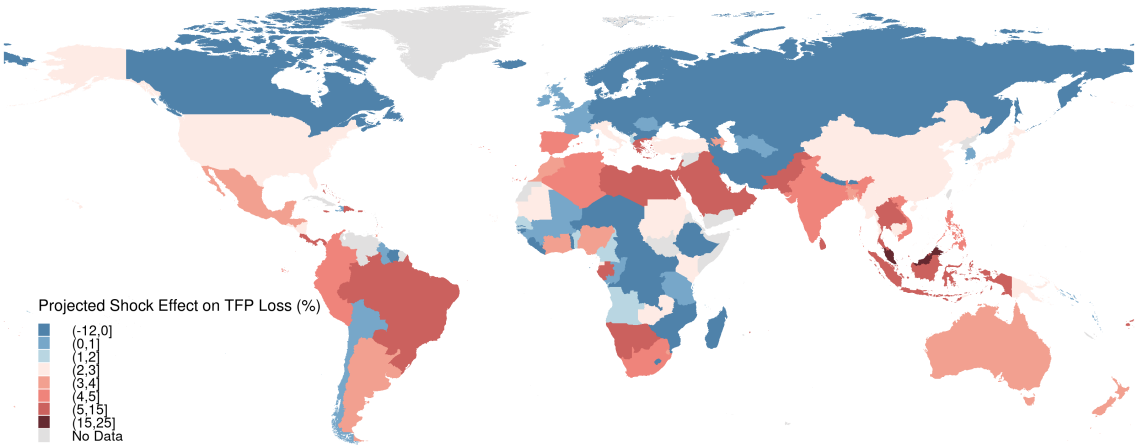
Notes: Grey texts represent the baseline period from 2000 to 2014, and the red texts represent the end of the century (2081 - 2100). End-of-century projection comes from SSP3-4.5 projection. The graph shows the joint evolution of income per capita and average temperature for each country.

D.2 Projection Components

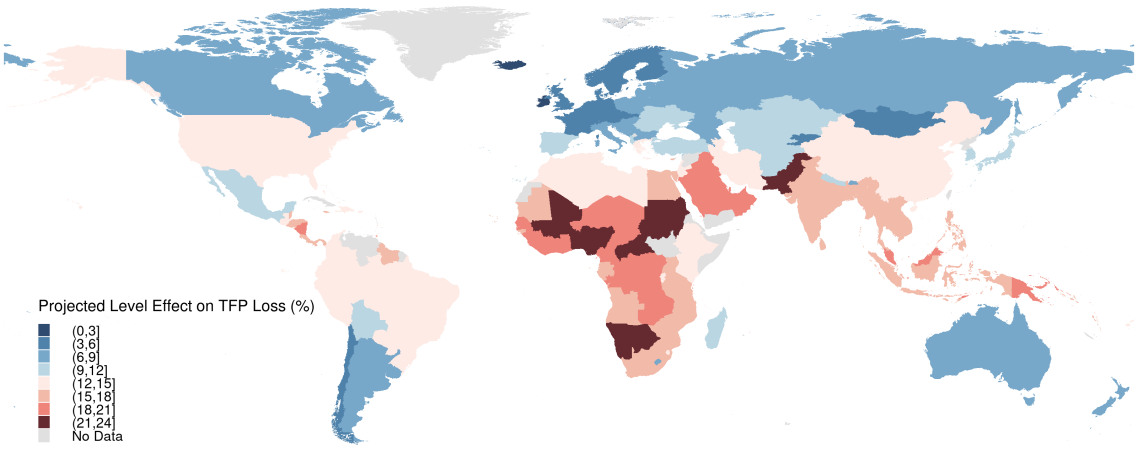
The graph shows a breakdown of the three effects contributing to the total projected TFP loss under SSP3-4.5 scenarios in Section 4.6.

Figure D.13: Three Effects Contribution to Projected TFP Loss (SSP3-4.5)

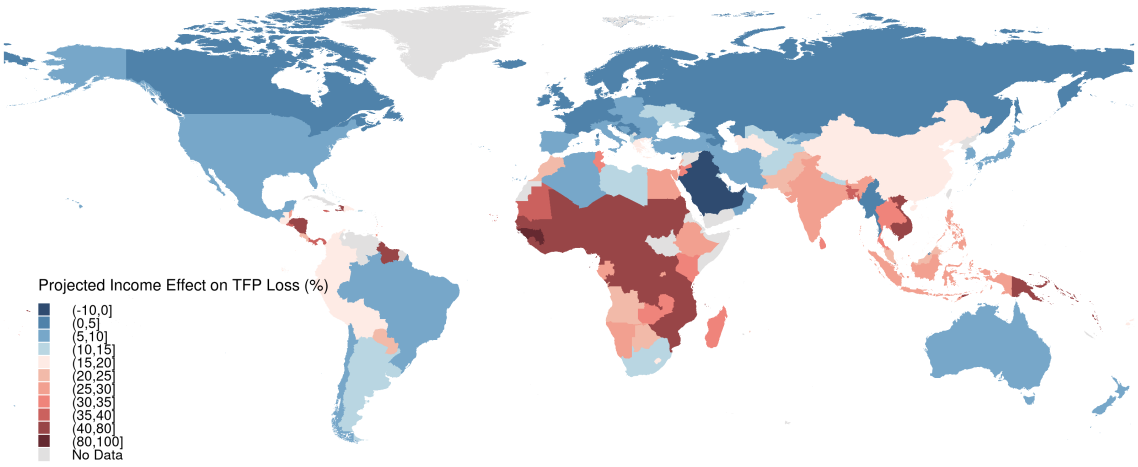
(a) Shock Effects Projection



(b) Level Effects Projection



(c) Income Effects Projection



E Firm Dynamics Model Details

This appendix provides additional details on the household problem, the timing of events, and the perturbation solution method for the model in Section 5.

E.1 Household Budget Constraint and Adaptation-Resource Pricing

The household owns all firms in the region, and all profits and revenues from tax-like wedges are rebated lump sum. At the end of period t, the household consumes C_t and sets a supply schedule R_{t+1} to meet firms' demand for adaptation resources. At the start of $t+1$, before climate shocks are realized, the predetermined quantity R_{t+1} is supplied and the contracted amount is distributed to each firm. The period-t budget constraint is

$$C_t = w_t N + w_t^R R_t + \Pi_t + S_t,$$

where w_t is the wage for unskilled labor, w_t^R is the price of adaptation resources, Π_t denotes total firm profits, and S_t denotes lump-sum rebates.

The household's optimality conditions for the supply of adaptation resources imply that the price of adaptation resources satisfies

$$w_{t+1}^R = \eta \frac{\mathbb{E}_t\left[\Lambda_{t+1} C_{t+1}\right]}{\mathbb{E}_t\left[\Lambda_{t+1}\right]}.$$

Thus, w_{t+1}^R increases with the utility-cost parameter η and with the SDF-weighted expectation of next-period consumption.

E.2 Solution via Risk-Adjusted Perturbation

We solve the model in closed form using a risk-adjusted perturbation around the homogeneous deterministic steady state (HDSS) as in David and Venkateswaran (2019). The key difficulty is that firms' Euler equations feature *risk-adjusted* expectations—products of the stochastic discount factor (SDF) and future payoffs—under non-linear temperature exposure and endogenous heterogeneity. Our approach proceeds in three steps.

Step 1: Risk-adjusted approximation of FOCs. We extend the risk-adjusted approximation in Coeurdacier, Rey, and Winant (2011) beyond log-normal environments by developing a second-order expansion of stochastic variables in conditional moments of shocks (means, variances, and covariances), and then applying it systematically to the firms' optimality conditions. As a simple illustration, the one-period risk-free return is $R_{f,t+1} = \frac{1}{\mathbb{E}_t[\Lambda_{t+1}]}$. Let $\widehat{x}_t \equiv x_t - x^{\text{HDSS}}$ denote deviations from the HDSS and let $\lambda_{t+1} \equiv \log \Lambda_{t+1}$. A second-order expansion delivers the convenient risk-adjusted representation

$$\widehat{r}_{f,t+1} \equiv \log R_{f,t+1} - \log R_f^{\text{HDSS}} \;=\; - \underbrace{\widehat{\mathbb{E}_t \lambda_{t+1}}}_{\substack{\text{Consumption} \\ \text{Smoothing}}} \; \underbrace{- \frac{1}{2} \mathbb{VAR}_t\left(\widehat{\lambda}_{t+1}\right)}_{\text{Precautionary}}$$

which makes clear that the risk-free rate falls when expected marginal utility growth rises (consumption smoothing) and when uncertainty in the pricing kernel increases (a precautionary-savings effect).

Step 2: Bilinear policy-function approximation. We approximate firms' policy rules for next-period capital and adaptation using an affine–bilinear expansion in (i) firm-level state vectors $\mathbf{x}_{it}$ (e.g., persistent and transitory productivity, wedges, and product exposure) and (ii) aggregate state vectors $\mathbf{x}_t$ (e.g., aggregate productivity, aggregate capital, and temperature moments). For example, for log capital $k_{i,t+1} \equiv \log K_{i,t+1}$,

$$k_{i,t+1} = k^{\text{HDSS}} + \mathbf{G}_i^\top \widehat{\mathbf{x}}_{it} + \mathbf{G}_a^\top \widehat{\mathbf{x}}_t + \underbrace{\widehat{\mathbf{x}}_{it}^\top \mathbf{G}_{ia}\, \widehat{\mathbf{x}}_t}_{\substack{\text{heterogeneous response to} \\ \text{aggregate shocks and uncertainty}}} + \mathbf{G}_d^\top \widehat{\mathbf{d}}_t + \mathbf{G}_\Gamma^\top \widehat{\mathbf{\Gamma}}_{micro,t},$$

and analogously for $\widetilde{\beta}_{i,t+1}$. The interaction term $\widehat{\mathbf{x}}_{it}^\top \mathbf{G}_{ia} \widehat{\mathbf{x}}_t$ is essential: it captures how a common temperature realization (or a change in forecast uncertainty) loads differently across firms through heterogeneous effective exposure and wedges, generating endogenous dispersion in firm decisions.

Step 3: Aggregation and coefficient identification. We apply the same second-order (affine-bilinear) expansion to the aggregation equations. Because the policy rules are affine-bilinear, aggregates depend on the cross-sectional distribution of $\mathbf{x}_{it}$ only through a finite set of moments, collected in $\mathbf{\Gamma}_{micro,t}$ (in the spirit of Krusell and Smith (1998)). Finally, we substitute the approximated policy rules and aggregation equations into all equilibrium conditions (firms' Euler equations, factor-market clearing, and the household pricing kernel), and solve for the unknown coefficients by matching terms of equal order (constant, linear, and bilinear). This guess-and-verify procedure yields closed-form expressions for both micro policies and macro equilibrium objects, including MRPK dispersion and the resulting aggregate TFP losses.

F Model Estimation Details

This appendix provides the full set of moment conditions used for identification, the fixed-point algorithm used for implementation, and the aggregation formulas used in the quantitative exercises.

F.1 Moment Conditions for Model Identification

This section summarizes the moment restrictions used to identify the region-level parameters and firm-level latent components.

(i) Firm-level Moment Conditions For each region, we assume the permanent component of productivity $\overline{a}_i$ and $\overline{mrpk}_i$ for each firm satisfy the standard firm fixed effect moment conditions. Given the presence of heterogeneous sensitivities, we assume the firm-level a_{it} and $mrpk_{it}$, once netted out the temperature-related and permanent components, should satisfy the Yule-Walker

conditions implied by their respective AR(1) structure.[32] Lastly, for each region r', the correlated distortion satisfy $\mathbb{E}^i[\bar{a}_i(\overline{mrpk}_i - \omega^a \bar{a}_i)|r(i) = r'] = 0$. Given β_i, Ψ_{it} and T^*, these conditions jointly identifies $\left(\omega^a_r,\ \rho_{z,r},\ \rho_{\phi^\tau,r},\ \{\bar{a}_i\}_i\right)$ for each region r. We can also recover all innovations $\varepsilon^{\phi^\tau}_{it}$, ε^z_{it} and therefore z_{it} and τ_{it} up to some unobserved random damage $\xi_{it}(T_{rt} - T^*)$.

(ii) Product sensitivity β_i. We assume intrinsic product sensitivity is constant within 3-digit category p: $\beta_i = \beta_{q(i)}$, where $q(i)$ maps firm i to its category. Define the MRPK residual after removing region–year general-equilibrium components and endogenous adaptation terms,

$$\widetilde{mrpk}_{i,t+1} \equiv mrpk_{i,t+1} - \theta_A\left(a_{t+1} + \tilde{\alpha}_K k_{t+1}\right) - \left(\tilde{\beta} + \Psi_{i,t+1}\right)\left(T_{t+1} - \mathbb{E}_t[T_{t+1}]\right).$$

Then β_p is identified by the orthogonality condition implied by Equation (22), for each category p,

$$\mathbb{E}\Big[\mathbf{1}\{q(i) = p\}\left(\widetilde{mrpk}_{i,t+1} - \beta_p(T_{t+1} - \mathbb{E}_t[T_{t+1}])\right)\left(T_{t+1} - \mathbb{E}_t[T_{t+1}]\right) \Big|\ \gamma_i, \gamma_{c(r)t}\Big] = 0. \tag{42}$$

Intuitively, after netting out endogenous adaptation and region–year aggregate components, exposure to temperature surprises should operate through intrinsic product sensitivity only, conditional on firm and country–year fixed effects. The regional average product sensitivity can also be recovered by using $\bar{\beta}_r = \mathbb{E}[\hat{\beta}_i | r = r(i)]$.

(iii) Adaptation cost $\eta_r H_r$. To identify regional variation in adaptation costs, we parametrize the inverse cost shifter as $\frac{1}{\eta_r H_r} \equiv f\left(\overline{\ln \mathrm{GDP}_r}\right)$, where $f(\cdot)$ is a third-order polynomial in $\overline{\ln \mathrm{GDP}_r}$. Given this parametrization, Equation (22) implies a set of orthogonality conditions that link temperature forecast errors to cross-firm heterogeneity in exposure and scale. Specifically, we impose the moments

$$\mathbb{E}\Bigg[\underbrace{\Big(mrpk_{it} - \rho_{\phi^\tau}\phi^\tau_{i,t-1} - \left(\widehat{\beta}_i + \Psi_{it}\right)\Big[\left(T_{rt} - \mathbb{E}_{t-1}T_{rt}\right) - \Theta\left(\overline{\beta}_i + \tilde{\beta}\right)\mathbb{VAR}_{t-1}T_{rt}\Big]\Big)}_{\text{MRPK residual}}$$
$$\cdot \underbrace{\Big(\overline{\ln \mathrm{GDP}_r}^{\,k} \cdot \left(\bar{T}_r - T^*\right) \cdot \Big[(\bar{T}_r - T^*)\widehat{\beta}_i + \bar{a}_i + \rho z_{it} - \alpha\tau_{i,t+1}\Big]\ \left(T_{rt} - \mathbb{E}_{t-1}T_{rt}\right)\Big)}_{\text{instruments for adaptation-cost shifter}} \Big|\ \gamma_i, \gamma_{rt}\Bigg] = 0, \tag{43}$$

$\forall\, k \in \{0, 1, 2, 3, 4\}$. Intuitively, after netting out the wedge dynamics and the common aggregate temperature component, the remaining cross-firm variation in MRPK responses to temperature surprises should be orthogonal to functions of regional income interacted with the model-implied drivers of endogenous adaptation, within-firm and within-region-year. These moments discipline the coefficients of $f(\overline{\ln \mathrm{GDP}_r})$, and therefore identify $\frac{1}{\eta_r H_r}$ across regions.

(iv) Bliss point T^* and random-damage dispersion σ^2_ξ. The model implies that the bliss point T^* and the dispersion of idiosyncratic climate damages σ^2_ξ can be jointly identified from region–sector–year variation in (i) TFP-growth volatility and (ii) MRPK dispersion. As in Equation (24), after netting out heterogeneous exposure and the components driven by forecast errors and ag-

32. These moment conditions are also conditional on region-year fixed effects.

gregate uncertainty (captured by some $\text{VolCorrection}_{rst}$ and $\text{MisCorrection}_{rst}$), the remaining temperature dependence is governed by the quadratic damage term $\sigma_\xi^2(T_{rt}-T^*)^2$. Define the residual volatility and residual MRPK dispersion, $\widetilde{V}_{rst}^{\Delta a} \equiv \mathbb{VAR}_{rst}^i(a_{it}-a_{i,t-1}) - \text{VolCorrection}_{rst}$, and $\widetilde{V}_{rst}^{mrpk} \equiv \mathbb{VAR}_{rst}^i\left(mrpk_{it}\right) - \text{MisCorrection}_{rst}$. Because $a_{it}-a_{i,t-1}$ loads on the idiosyncratic damage realizations in both t and $t-1$, the model predicts $\widetilde{V}_{rst}^{\Delta a}$ scales with $(T_{rt}-T^*)^2+(T_{r,t-1}-T^*)^2$, while $\widetilde{V}_{rst}^{mrpk}$ scales with $(T_{rt}-T^*)^2$. We therefore impose the following model-consistent moment conditions:

$$\mathbb{E}\Big[\Big(\widetilde{V}_{rst}^{\Delta a} - \sigma_\xi^2\big[(T_{rt}-T^*)^2+(T_{r,t-1}-T^*)^2\big]\Big)\left(T_{rt}^2+T_{r,t-1}^2\right) \,\Big|\, \gamma_{rs},\gamma_{ct}\Big] = 0, \tag{44}$$

$$\mathbb{E}\Big[\Big(\widetilde{V}_{rst}^{\Delta a} - \sigma_\xi^2\big[(T_{rt}-T^*)^2+(T_{r,t-1}-T^*)^2\big]\Big)\left(T_{rt}+T_{r,t-1}\right) \,\Big|\, \gamma_{rs},\gamma_{ct}\Big] = 0, \tag{45}$$

$$\mathbb{E}\Big[\Big(\widetilde{V}_{rst}^{mrpk} - \sigma_\xi^2(T_{rt}-T^*)^2\Big)\left(T_{rt}-T^*\right)^2 \,\Big|\, \gamma_{rs},\gamma_{ct}\Big] = 0. \tag{46}$$

Intuitively, once we purge the components of volatility and dispersion accounted for by heterogeneous exposure to temperature shocks and risk, the remaining cross-sectional volatility in productivity growth and dispersion in MRPK should be explained by random climate damages that rise with the squared distance from the bliss point. The first two moments use time-series variation in temperature levels to locate T^* (via how volatility co-moves with temperature), while the third moment disciplines the scale of the quadratic term and helps pin down σ_ξ^2.

Taken together, these moments jointly identify the common parameters $\{T^*, \sigma_\xi^2\}$, as well as the region-specific objects $\{\bar{\beta}_r,\ (\eta_r H_r)^{-1},\ \sigma^2_{\bar{\beta},r},\ \sigma^2_{\bar{a},r},\ \sigma^2_{\varepsilon^z,r},\ \sigma^2_{\varepsilon^{\phi^\tau},r},\ \rho_{\phi^\tau,r},\ \rho_{z,r},\ \omega_{a,r}\}_r$.

F.2 Implementation via a Fixed-Point Algorithm

We implement the estimator using a transparent fixed-point algorithm that circumvents the computational burden of solving the full joint GMM problem in one step. The algorithm iterates between (i) inverting the model to recover firm-level latent objects and region-level moments given a current parameter guess, and (ii) updating the parameters using the moment conditions described above.

1. **Initialization.** Start from an initial guess for regional adaptation costs and intrinsic product sensitivities, e.g. $\frac{1}{\eta_r H_r} = 0$ and $\beta_i = 0$, together with an initial guess for the common parameters $\{T^*, \sigma_\xi^2\}$. Given these values, compute the implied steady-state adaptation $\{\widetilde{\beta}_r\}_r$ and the corresponding regional sensitivity multipliers. This step enables model inversion: we recover firm-level fundamentals and construct all region–sector moments needed for the subsequent updates.

2. **Update the bliss point and random-damage dispersion $\{T^*, \sigma_\xi^2\}$.** Using the objects recovered in Step 1, construct the region–sector–year correction terms $\text{VolCorrection}_{rst}$ and $\text{MisCorrection}_{rst}$. We then implement the moment conditions in Equations (44)–(46) via simple two-way fixed-effects regressions to update $\{T^*, \sigma_\xi^2\}$.

3. **Update intrinsic product sensitivity** $\{\beta_i\}$**.** Given the updated T^*, recompute the endogenous exposure component Ψ_{it} and form the residualized return $\widetilde{mrpk}_{it}$ that nets out the region–year general-equilibrium terms and endogenous adaptation. We then estimate the moment condition in Equation (42) using a high-dimensional fixed-effects specification that allows for 3-digit-category-specific slopes, which updates $\beta_i = \beta_{q(i)}$ for all firms.

4. **Update regional adaptation costs** $\{(\eta_r H_r)^{-1}\}_r$**.** Under the fourth-order polynomial specification of $\frac{1}{\eta_r H_r} \equiv f\left(\overline{\ln \mathrm{GDP}_r}\right)$, using the updated $\{\beta_i\}$, we first net out the intrinsic temperature-shock component from $mrpk_{it}$. We then estimate the moment conditions in Equation (43) by projecting the relevant MRPK residual on $\left(\bar{T}_r - T^*\right)\left[\left(\bar{T}_r - T^*\right)\widehat{\beta}_i + \bar{a}_i + \rho z_{it} - \alpha\tau_{i,t+1}\right]\left(T_t - \mathbb{E}_{t-1}[T_t]\right)$ interacted with a polynomial in $\overline{\ln \mathrm{GDP}_r}$. This yields an updated estimate of $f(\overline{\ln \mathrm{GDP}_r})$ and hence $(\eta_r H_r)^{-1}$.[33]

5. **Iterate to convergence.** Update the parameter guesses and repeat Steps 1–4 until $\max\left\{\|\Delta\beta\|_i, \left\|\Delta(\eta H)^{-1}\right\|_r, |\Delta T^*|, |\Delta\sigma_\xi^2|\right\}$ falls below a pre-specified tolerance, ensuring convergence of both firm-level latent objects and region-level moments.

While we do not impose a formal uniqueness proof, in practice the fixed-point iteration converges quickly (typically in fewer than 20 iterations) and is robust to a wide range of reasonable initial guesses. Intuitively, temperature-related terms discipline a specific subset of equilibrium wedges and exposure objects, while the remaining components of firm dynamics are primarily pinned down by standard cross-sectional and time-series moments, which stabilizes the overall mapping from moments to parameters.

F.3 Aggregation Details

We aggregate the world economy using a Cobb–Douglas output index across countries and regions. Let

$$\log Y_t^{\mathrm{Global}} = \sum_c \omega_{ct} \log Y_{ct}, \qquad \log Y_{ct} = \sum_{r \in R(c)} \omega_{rt}^c \log Y_{rt},$$

where ω_{ct} is country c's global output share and ω_{rt}^c is region r's share of country c's output. This implies

$$\log \mathrm{TFP}_t^{\mathrm{Global}} = \sum_r \omega_{rt} \log \mathrm{TFP}_{rt}, \qquad \omega_{rt} \equiv \omega_{ct}\omega_{rt}^c.$$

33. For the small set of regions (less than 2% of observations) in which the fitted $f(\cdot)$ implies negative values, we set $(\eta_r H_r)^{-1} = 0$.